QCD Thermodynamics from Lattice Gauge Theory

Swagato Mukherjee

Department of Theoretical Physics,

Tata Institute of Fundamental Research,
Mumbai, India.

A thesis submitted for the degree of

Doctor of Philosophy

November, 2006

Declaration

I state that the work embodied in this thesis forms my own contribution to the research work carried out under the guidance of Prof. Rajiv V. Gavai. This work has not been submitted for any other degree to this or any other University or body. Whenever references have been made to previous works of others, it has been clearly indicated.

(signature of the supervisor) (signature of the candidate)

Acknowledgements

I would like to thank my thesis supervisor Prof. Rajiv V. Gavai for his patient guidance and teaching. I would also like to thank Prof. Sourendu Gupta who has taught me many things and in whose collaboration part of this thesis work was done. Collaboration and help of Dr. Rajarshi Ray is also gratefully acknowledged.

Without the support and help of all my friends, family members and the members of the theoretical physics group it would have been impossible for me to finish this thesis.

I would also like to acknowledge the partial financial support of the TIFR Alumni Association.

Contents

Synopsis

Introduction

One of the primary objectives of physics is to understand the basic structure of matter and the interactions among its constituents. It is known that hadrons, such as protons, neutrons *etc.*, account for almost all the mass of the observable luminous matter of our universe. Hadrons are strongly interacting particles. Quantum Chromodynamics (QCD) is the theory of strong interaction. Nearly massless quarks and massless gluons are the elementary degrees of freedom of QCD. The interactions among them are governed by their intrinsic colour charges. The hadrons are bound states of quarks (and/or anti-quarks). Most of the mass of hadrons arise through the interactions of gluons and quarks. Inside a hadron, the force between two quarks increases with separation. Thus an infinite amount of energy would be needed to isolate a single quark. In other words, the quark constituents of a hadron are not just bound but confined.

QCD is known to be an asymptotically free theory. This means that the strength of the interaction among the quarks and gluons decreases with decreasing distance, *i.e.* with increasing momentum transfer. This suggest that the quark confinement ought to have its inherent limits. Under extreme conditions of high density and/or temperature, when several hadrons are compressed into the the volume normally occupied by one single hadron, it seems implausible to identify a quark belonging to a certain hadron. In such a medium quarks are no longer confined within the volume of a single hadron. Thus it is expected that with increasing density and/or temperature, strongly interacting matter will undergo a transition from the hadronic phase, in which constituents are colour-neutral

bound states, to a plasma of deconfined colour-charged quarks and gluons. Such a state of matter is known as *Quark Gluon Plasma* (QGP).

Studies of QCD under extreme conditions of high temperature and/or high density are much more than of mere theoretical interest. The QGP can actually be produced in the laboratory if proper conditions are met. Behaviour of QCD under such unusual conditions can also have astrophysical and cosmological consequences. Thus, *e.g.* one may encounter very dense matter (density $\sim 1\ fm^{-3}$) in the core of the neutron stars or very hot (temperature $\sim 10^{12}\ K$) QGP-like matter immediately (few microseconds) after the Big Bang. The physics of nucleosynthesis or the inflationary universe may depend on the properties of QCD under those extreme conditions. In recent years, however, most attention has focused on the possibility of creating QGP in laboratories by colliding highly energetic nuclei such as sulphur (S), lead (Pb) and gold (Au). First such experiments were performed at the Alternating Gradient Synchrotron (AGS) in Brookhaven and the Super Proton Synchroton (SPS) at CERN, with center of mass energies of 2 GeV and 18 GeV per nucleon respectively. The Relativistic Heavy Ion Collider (RHIC), with center of mass energy 200 GeV per nucleon, is currently running at Brookhaven and providing us with vast amount of new data. A still higher energy collider, namely the Large Hadron Collider (LHC) at CERN, will have a center of mass energy of 5.5 TeV per nucleon and a dedicated heavy-ion detector ALICE. Thus a variety of predictions of hot and/or dense QCD will hopefully be checked against the data from these experiments.

While perturbative techniques have been highly successful in testing QCD experimentally for large momenta (*i.e.* small coupling), in the interesting region of the deconfining transition in QCD the coupling is large and non-perturbative methods are called for. Lattice regularization of field theories provides such a non-perturbative technique. Lattice field theory is a useful way of regularizing a continuum field theory, which is otherwise plagued by ultraviolet divergences. One formulates the theory on a discrete space-time lattice [1, 2] so that the lattice spacing 'a' serves as an ultraviolet regulator (cut-off). Numerical simulations of lattice field theories have a further advantage of obtaining the predictions of the theory from first principles. All one needs is the Lagrangian of the theory and the bare parameters. Over the past two decades or so, tremendous progress have been

made in the field of numerical study of QCD formulated on discrete space-time lattice. This approach has been very successful in providing detail information about the thermodynamic properties of QCD at finite temperature.

The study of finite temperature QCD (or any field theory) starts from the grand canonical partition function for a many-particle ensemble at temperature T

$$\mathcal{Z} = \text{Tr } e^{-\beta\left(\hat{H}-\mu\hat{N}\right)}. \tag{1}$$

Here, $\hat{H}$ is the Hamiltonian of the system, $\hat{N}$ is the operator for some conserved charge, μ is the chemical potential corresponding to that conserved charge and $\beta = 1/T$. We have chosen to work in terms of natural units, *i.e.* we have set $\hbar = c = k = 1$. This partition function can be written in terms of a path integral [2]. The goal of finite temperature lattice QCD is to obtain predictions for QGP using the path integral form of the underlying partition function [2]

$$\mathcal{Z} = \int_{bc} \mathcal{D}\psi\ \mathcal{D}\bar{\psi}\ \mathcal{D}A_\mu\ \exp\left[-\int_0^\beta d\tau \int d^3x\ \mathcal{L}\right]. \tag{2}$$

In the above equation $\mathcal{L}$ denotes the Lagrangian and τ is the Euclidean (imaginary) time. The notation 'bc' denotes collectively the boundary conditions (in the temporal direction) on the fields, anti-periodic for the quark fields ψ, $\bar{\psi}$ and periodic for the gauge fields A_μ.

Just as an ordinary integration can be performed by taking a limit of sums on discrete points, lattice QCD can be thought of as an attempt to define and perform the functional integrals in $\mathcal{Z}_{QCD}$ by discretizing the space-time (Euclidean) over which the fields are defined. Let N_s and N_τ denote the number of points in the spatial and the temporal (or equivalently the inverse temperature) direction and let a_s and a_τ be the corresponding lattice spacings. Then the volume V and the temperature T are given by

$$V = (N_s a_s)^3\,, \qquad \text{and} \qquad T = \frac{1}{N_\tau a_\tau}. \tag{3}$$

The finite lattice spacings a_i $(i = s, \tau)$ impose an ultraviolet cut-off a_i^{-1} and the finite volume V imposes an infrared cut-off. One, of course, needs to take a continuum limit, $a_i \to 0$, at the end of the calculation. As $a_i \to 0$ the number

of lattice points $N_i \to \infty$, in order to keep the volume and temperature fixed in the physical units. In addition, one also should take the thermodynamic limit, $V \to \infty$, to get the QCD thermodynamics.

In the conventional lattice QCD formulation the quark fields, $\psi(x)$, reside on the lattice site $x = (x_0, x_1, x_2, x_3)$. The gauge fields are introduced as link variables. Let $U_\mu(x) \in SU(N_c)$ be the gauge field associated with the directed link from site x to site $x + \hat{\mu}$, $\hat{\mu}$ being the unit vector in the μ-th direction. One also has $U^\dagger_\mu(x) = U_{-\mu}(x + \mu)$. A gauge invariant action can only be constructed by taking traces of closed loops of $U_\mu(x)$. One defines the smallest such square loop as a *plaquette*

$$U_{\mu\nu}(x) = U_\mu(x)U_\nu(x + \mu)U^\dagger_\mu(x + \nu)U^\dagger_\nu(x). \tag{4}$$

We define $P_{\mu\nu}(x) = 1 - \Re$ Tr $U_{\mu\nu}(x)/N_c$, where the 'Tr' denotes the trace in the colour space. We also introduce the notation for the average spatial and temporal plaquettes,

$$P_s = \sum_{x;i>j,ij=1}^{3} P_{ij}(x)/3N_s^3N_\tau, \qquad \text{and} \qquad P_\tau = \sum_{x,i=1}^{3} P_{0i}(x)/3N_s^3N_\tau \tag{5}$$

respectively.

The simplest possible lattice action for a pure $SU(N_c)$ gauge theory that can be constructed out of the plaquettes is the *Wilson action* [1, 2] —

$$S_G[U] = 6N_cN_s^3N_\tau \left[K_sP_s + K_\tau P_\tau\right], \quad \text{with} \quad K_s = \frac{1}{\xi g_s^2}, \quad K_\tau = \frac{\xi}{g_\tau^2}. \tag{6}$$

Here g_s and g_τ are the gauge couplings along the spatial and the temporal directions. The quantity $\xi = a_s/a_\tau$ is known as the *anisotropy parameter*. For $\xi = 1$, in the continuum limit of vanishing lattice spacing the above action reduces, upto $\mathcal{O}(a^2)$ errors, to the standard continuum Yang-Mills action. However, since the continuum limit correspond to the critical point of the theory a large class of actions, differing by irrelevant terms (proportional to higher powers of the lattice spacing), are expected to give the same continuum physics.

Choosing a fermionic lattice action is more difficult due to the well-known conceptual problem [2], called the *fermion doubling problem*. A "No-Go" theorem [2] tells us that either one has to sacrifice continuous chiral symmetry or

one ends up having too many (2^4) flavours in the continuum limit, unless one is willing to use non-local actions. We will confine ourselves to one oft-used choice, namely the *staggered fermion* action. The staggered fermions have a local nearest neighbour action. On an asymmetric lattice staggered fermions with quark chemical potential μ_f (corresponding to the flavour f) are defined as follows [2]—

$$S_F\left[U\right] = \sum_{f=1}^{n} \sum_{x,x'} \bar{\chi}^{(f)}(x) \left[\sum_{\nu=1}^{3} D^{(\nu)}(x,x') + \gamma_F D^{(0)}(x,x') + m_f a_s \delta_{x,x'} \right] \chi^{(f)}(x'), \quad (7)$$

where

$$\begin{aligned} D^{(\nu)}(x,x') &= \frac{1}{2}(-1)^{x_0+\cdots+x_{\nu-1}} \left[U_\nu(x)\delta_{x,x'-\hat{\nu}} - U_\nu^\dagger(x')\delta_{x,x'+\hat{\nu}} \right] \cdots (\nu = 1,2,3)\,, \\ D^{(0)}(x,x') &= \frac{1}{2} \left[e^{(\mu_f a_\tau)} U_0(x)\delta_{x,x'-\hat{0}} - e^{-(\mu_f a_\tau)} U_0^\dagger(x')\delta_{x,x'+\hat{0}} \right] \ . \end{aligned}$$

Here $\chi^{(f)}$, $\bar{\chi}^{(f)}$ are single component spinors, m_f is the bare quark mass and γ_F is an extra coupling [3] which is unity for $\xi = 1$. Gauge invariance is assured by the presence of U's in Eq. [7]. It is clear that $\chi^{(f)}$ cannot be identified with the quark fields in the continuum limit. It turns out, however, that $16n$ χ-fields on the corners of an elementary 4-d hypercube can be combined to define usual continuum quark fields of 4-component spinors, which for $m_f = 0$ have $U(4n) \times U(4n)$ symmetry in the continuum limit. For finite lattice spacing chiral symmetry is broken down to $U(n) \times U(n)$. This facilitates the investigation of the physics of spontaneous chiral symmetry breaking. The presence of discrete chiral symmetries, in addition, forbids mass counterterms for staggered fermions, thus rendering the bare quark mass a straightforward input in the calculation. The disadvantage is that the full flavour symmetry is restored only for very small lattice spacing, leaving the number of light flavours uncertain for coarser lattices.

Once the lattice actions $S_G[U]$ and $S_F[U]$ are defined, the finite temperature lattice QCD formalism can be extended for the numerical evaluation of the *equation of state* (EoS) of QCD. The energy density (ϵ) and the pressure (P) are defined as

$$\epsilon = \frac{T^2}{V} \left. \frac{\partial \ln \mathcal{Z}(V,T)}{\partial T} \right|_V , \qquad \text{and} \qquad P = T \left. \frac{\partial \ln \mathcal{Z}(V,T)}{\partial V} \right|_T , \quad (8)$$

where the partition function $\mathcal{Z}$ for the case of $SU(N_c = 3)$, which we shall be considering in the first two sections, is given by

$$\mathcal{Z}(V,T) = \int_{bc} \mathcal{D}U e^{-S_G[U]}. \tag{9}$$

The partial derivatives with respect to T and V can be written in terms of the two lattice parameters ξ and a_s, keeping N_s and N_τ fixed,

$$T\,\frac{\partial}{\partial T}\bigg|_V \equiv \xi\,\frac{\partial}{\partial \xi}\bigg|_{a_s}, \qquad \text{and} \qquad 3V\,\frac{\partial}{\partial V}\bigg|_T \equiv a_s\,\frac{\partial}{\partial a_s}\bigg|_\xi + \xi\,\frac{\partial}{\partial \xi}\bigg|_{a_s}. \tag{10}$$

Using these expressions, one obtains [4]

$$a_s^4\epsilon = -6N_c\xi^2\left[\frac{\partial K_s}{\partial \xi}D_s + \frac{\partial K_\tau}{\partial \xi}D_\tau\right], \qquad \text{and} \tag{11a}$$

$$a_s^4\Delta \equiv a_s^4(\epsilon - 3P) = 6N_c\xi a_s\left[\frac{\partial K_s}{\partial a_s}D_s + \frac{\partial K_\tau}{\partial a_s}D_\tau\right]. \tag{11b}$$

Since the functional integral formalism does not have normal ordering the energy density obtained above contains a contribution from the vacuum, similar to the zero-point energy of the continuum theory. This vacuum contribution can be eliminated by subtracting $\epsilon(T=0)$. For sufficiently large N_s, ϵ evaluated on the symmetric N_s^4 lattice is a good approximation to $\epsilon(T=0) \equiv \epsilon_{vac}$. A subtraction of the corresponding vacuum $(T=0)$ quantities lead to $D_i = \langle P_i\rangle - \langle P_0\rangle$ above, where $\langle P_0\rangle$ is the average plaquette value at $T=0$. The notation $\langle\cdot\rangle$ implies average over gauge configurations.

Now we can turn our attention to a few quantities which are relevant for lattice QCD studies at non-zero chemical potentials. For a theory with only u and d flavours the diagonal and off-diagonal *quark number susceptibilities* (QNS) are defined as

$$\chi_f = \left(\frac{T}{V}\right)\frac{\partial^2 \ln\mathcal{Z}}{\partial\mu_f^2}, \qquad \text{and} \qquad \chi_{ff'} = \left(\frac{T}{V}\right)\frac{\partial^2 \ln\mathcal{Z}}{\partial\mu_f\partial\mu_{f'}}, \tag{12}$$

respectively. Here, the partition function includes the quarks, *i.e.* ,

$$\ln\mathcal{Z}\,(T,V,\{m_f\},\{\mu_f\}) = \int \mathcal{D}U\left[\prod_{f=u,d} d\chi^{(f)}d\bar{\chi}^{(f)}\right] exp\,(-S_G[U] - S_F[U])\,. \tag{13}$$

Furthermore, if one introduces the quark chemical potential (μ_0) and the isospin (isovector) chemical potential (μ_I),

$$\mu_0 = \frac{\mu_u + \mu_d}{2}, \qquad \text{and} \qquad \mu_I = \frac{\mu_u - \mu_d}{2}, \tag{14}$$

then the corresponding susceptibilities will be

$$\frac{\chi_0}{T^2} = \frac{T}{V}\cdot\frac{\partial^2 \ln \mathcal{Z}}{\partial(\mu_0/T)^2} \equiv \frac{2(\chi_u + \chi_{ud})}{T^2}, \qquad \text{and} \tag{15a}$$

$$\frac{\chi_I}{T^2} = \frac{T}{V}\cdot\frac{\partial^2 \ln \mathcal{Z}}{\partial(\mu_I/T)^2} \equiv \frac{2(\chi_u - \chi_{ud})}{T^2}. \tag{15b}$$

Here, we have assumed degenerate (u,d)-quark masses to arrive at the second equalities (marked by $\equiv$) of the above relations. One can, further, perform Taylor series expansions of P, χ_0 and χ_I in (μ_0/T) (around $\mu_0 = 0$)—

$$\begin{aligned}
\frac{P}{T^4} &= \sum_{n=0}^{\infty} c_n(T)\left(\frac{\mu_0}{T}\right)^n, \\
\frac{\chi_0}{T^2} &= 2c_2 + 12c_4\left(\frac{\mu_0}{T}\right)^2 + 30c_6\left(\frac{\mu_0}{T}\right)^4 + \cdots, \qquad \text{and} \\
\frac{\chi_I}{T^2} &= 2c_2^I + 12c_4^I\left(\frac{\mu_0}{T}\right)^2 + 30c_6^I\left(\frac{\mu_0}{T}\right)^4 + \cdots,
\end{aligned} \tag{16}$$

where the coefficients $c_n(T)$ and $c_n^I(T)$ are defined as,

$$c_n(T) = \frac{1}{(n!)V}\cdot\frac{\partial^n \ln \mathcal{Z}}{\partial(\mu_0/T)^n}, \qquad \text{and} \qquad c_n^I(T) = \frac{1}{(n!)V}\cdot\frac{\partial^n \ln \mathcal{Z}}{\partial(\mu_0/T)^{n-2}\partial(\mu_I/T)^2}. \tag{17}$$

These coefficients can be computed on the lattice. We will use these quantities in the last two sections.

Speed of sound and specific heat in the QCD plasma

EoS of a pure $SU(3)$ gauge theory have been extensively studied using lattice QCD. It is now a well-established fact that the pressure, P, and the energy density, ϵ, deviate [5] in the high temperature phase of QCD by about 20% from their ideal gas values at a temperature of about $3T_c$, where T_c is the transition

temperature. Early expectations that ϵ would count the number of degrees of freedom in the QCD plasma through the Stefan-Boltzmann law are belied by the fact that perturbation theory has had great difficulty in reproducing these lattice results. In view of this, it is important to go beyond the EoS and study the thermodynamic fluctuation measures in a QCD plasma. In the pure gluon gas there is only one fluctuation measure, the specific heat at constant volume, C_V. Related to this is a kinetic variable, the speed of sound, C_s. These two quantities are defined as

$$C_V = \left.\frac{\partial\epsilon}{\partial T}\right|_V, \qquad \text{and} \qquad C_s^2 \equiv \left.\frac{\partial P}{\partial\epsilon}\right|_s = \left.\frac{\partial P}{\partial T}\right|_V \left(\left.\frac{\partial\epsilon}{\partial T}\right|_V\right)^{-1} = \frac{s/T^3}{C_V/T^3}, \tag{18}$$

where we have used the thermodynamic identity

$$\left.\frac{\partial P}{\partial T}\right|_V = \left.\frac{\partial S}{\partial V}\right|_T \quad \text{and} \quad \left.\frac{\partial S}{\partial V}\right|_T = s = \frac{\epsilon + P}{T}, \tag{19}$$

in conjunction with the definition of the total entropy, S, and the entropy density, s, above.

These quantities have direct physical relevance for the heavy-ion collision experiments. It has been suggested that C_V is directly related to the event-by-event transverse momentum fluctuations, which are measurable in heavy ion collision experiments. The speed of sound, on the other hand, controls the expansion rate of the fire-ball produced in the heavy-ion collisions. Thus the value of C_s is an important input parameter in the hydrodynamic studies. It has also been claimed that the ratio of the event-by-event fluctuations of entropy and energy, if it turns out to be measurable in heavy-ion collisions, provides a direct estimation of C_s. In addition to their relevance in the heavy-ion collision experiments, these quantities provide further tests of all the models and perturbative expansions which try to explain the lattice data on the EoS.

In order to make a lattice determination of C_V and C_s, first one needs the appropriate (lattice) expressions for these quantities. We have shown [6] that direct application of the derivatives in Eq. [10] to the expression for ϵ in Eq. [11a] gives an incorrect result for C_V, *i.e.*, C_V/T^3 does not give the correct ideal gas value ($4\epsilon/T^4$) in the weak coupling limit ($g \to 0$). This is because we have to work with the variables ξ and a_s, whereby the dimensions of both T and V come

from powers of a_s. Naive application of the derivative formulæ therefore see false scalings of these quantities. We have solved [6] this problem by choosing to work in terms of a dimensionless ratio so that the scaling is automatically taken care of. We define

$$\mathcal{C} = \frac{\Delta}{\epsilon}, \qquad \text{and} \qquad \Gamma = T\,\frac{\partial \mathcal{C}}{\partial T}\bigg|_V, \tag{20}$$

Then, using Eqs. [18, 20] one can proceed straightaway to write

$$\frac{C_V}{T^3} = \left(\frac{\epsilon/T^4}{P/T^4}\right)\left[\frac{s}{T^3} + \frac{\Gamma}{3}\frac{\epsilon}{T^4}\right], \quad \text{and} \quad C_s^2 = \left(\frac{P/T^4}{\epsilon/T^4}\right)\left[1 + \frac{\Gamma\epsilon/T^4}{3s/T^3}\right]^{-1}. \tag{21}$$

Expressions for ϵ and P are already known, Eqs. [11a, 11b]. We have evaluated [6] the expression for Γ in terms of the average plaquettes and covariances of plaquettes. The quantity Γ is proportional to the QCD β-function and hence goes to zero in the weak coupling ($g \to 0$) limit. This being the case, the correct ideal gas limits of ϵ, P and s ensure that C_V and C_s also reach their correct ideal gas limits. The above expressions also involve both first and second derivatives of the couplings g_i with respect to the lattice variables. To evaluate these derivatives we used the fact that in the weak coupling limit, g_i^{-2} 's can be expanded [7] around their symmetric lattice value $g^{-2}(a)$,

$$g_i^{-2}(a_s, \xi) = g^{-2}(a) + c_i(\xi) + O[g^2(a)], \tag{22}$$

where $a_s = a_\tau = a$ for $\xi \to 1$. So the first and second derivatives of g_i's with respect to ξ are given by $\partial c_i/\partial\xi$ and $\partial^2 c_i/\partial\xi^2$. The $\partial c_i/\partial\xi$ have been computed to one-loop order in the weak coupling limit for $SU(N_c)$ gauge theories [7]. Following [7], we evaluated [6] the quantities $\partial^2 c_i/\partial\xi^2$ using the weak coupling expansion upto one-loop order. For consistency, the derivatives of g_i with respect to the lattice spacing a have been evaluated using the one-loop order perturbative β-function of QCD.

Using the above mentioned formalism, in Ref. [6], we made a precise (with errors $\sim 5\%$) determination of the continuum limit of C_V and C_s in the high temperature phase of the QCD plasma. In the process we have also recomputed the EoS, *i.e.* the pressure, P, and the energy density, ϵ, by a method which has not been used earlier to obtain the continuum limit. Working at temperatures

$2T_c$ and $3T_c$, we made our continuum extrapolations by making linear fits in $a^2 \propto 1/N_\tau^2$ using lattices with large temporal extents ($N_\tau = 8, 10, 12$). While our results for ϵ, P and C_V deviate from there respective ideal gas values by about 20% even at $3T_c$, we found the the speed of sound C_s is very close to its ideal gas value at these temperatures. A more surprising finding was that the ideal gas relation $C_V/T^3 = 4\epsilon/T^4$ seems to hold, in spite of the non-ideal behaviour of these quantities. We explained [6] these apparently contradicting behaviors by arguing that, at these temperatures, the QCD plasma is very close to the conformal symmetric limit. This explains the very small values of the conformal measure $\mathcal{C}$ and hence, in turn, explains these puzzling behaviour of the QCD plasma. We had also tested the quantitative predictions of the strong-coupling expansion of the conformally symmetric $\mathcal{N} = 4$ Supersymmetric Yang-Mills theory (SYM) [8] by using our data on the entropy density.

EoS of QCD: improving the differential method

The method which we used, known as the *differential method*, to compute C_V and C_s produces negative pressure in the vicinity of T_c. This restricted us to investigate only the high temperature region. But more interesting physics is expected around the phase transition region. Hence a precise computation of these quantities close to T_c is necessary.

The negativity of pressure in the differential method was attributed solely to the use of perturbative formulae for various derivatives of the coupling. Hence it was believed that this problem could be remedied if one goes to large enough N_τ or equivalently to small enough lattice spacing. However, we found that [9] even when one determines the continuum limit of the pressure, using temporal lattices upto $N_\tau = 12$, the negative pressure problem of the differential method still persists.

The alternative technique which cures this negative pressure problem is known as the *integral method* [5]. The integral method bypasses the use of one set of derivatives by using the thermodynamic relation $F = -PV$, where F is the

free energy, and determined the other derivative (the QCD β-function) non-perturbatively. The integral method has the drawback that the relation $F = -PV$ holds only for a homogeneous system, and therefore fails across a first order phase transition. Also, avoiding derivatives has the practical drawback that fluctuation measures can only be obtained by numerical differentiation, which is prone to large errors.

In view of this situation we have proposed [9] a new variant of the differential method which gives positive pressure over the entire temperature range. In contrast to the choice of the spatial lattice spacing in the previous approach of the differential method, we choose the temporal lattice spacing to set the scale of the theory. Thus our method could be called the *t-favoured* differential method and the previous method may be called the *s-favoured* differential method. Once a choice of the scale $a = a_\tau$ is made, as opposed to the choice $a = a_s$ of the s-favoured scheme, the lattice version of the derivatives with respect to T and V change from Eq. [10] to—

$$T\,\frac{\partial}{\partial T}\bigg|_V = \xi\,\frac{\partial}{\partial \xi}\bigg|_a - a\,\frac{\partial}{\partial a}\bigg|_\xi, \qquad \text{and} \qquad V\,\frac{\partial}{\partial V}\bigg|_T = \frac{\xi}{3}\,\frac{\partial}{\partial \xi}\bigg|_a. \tag{23}$$

In [9] we have shown that the coefficients $c_i(\xi)$ remain same for both the schemes. With these information one can proceed straightaway, as in the earlier s-favoured scheme, to determine the expressions for the energy density and pressure. In the $\xi \to 1$ limit these become

$$\begin{aligned}
\frac{\epsilon}{T^4} &= 6N_cN_\tau^4\left[\frac{D_s - D_\tau}{g^2} - (c_s' D_s + c_\tau' D_\tau)\right] + 6N_cN_\tau^4\frac{B(\alpha_s)}{2\pi\alpha_s^2}\left[D_s + D_\tau\right], \qquad \text{and} \\
\frac{P}{T^4} &= 2N_cN_\tau^4\left[\frac{D_s - D_\tau}{g^2} - (c_s' D_s + c_\tau' D_\tau)\right].
\end{aligned} \tag{24}$$

Here the primes denote derivatives with respect to ξ, $B(\alpha_s)$ is the QCD β-function, with the usual definition of $\alpha_s = g^2(a)/4\pi$. Comparison of the expressions of Eq. [24] with that of the s-favoured scheme shows that the P in the t-favoured method is exactly $\epsilon/3$ of the s-favoured method. The positivity of the ϵ in the s-favoured scheme guarantees the positivity of P in the t-favoured scheme. The interaction measure Δ is same for both the t and s-favoured methods. Since Δ is always positive the expression for ϵ $(= \Delta + 3P)$ is also bound to give positive

values for the energy density. Being a differential method the t-favoured scheme can be easily extended [9] for the calculation of C_V and C_s, following exactly the same formalism developed in [6].

Using the t-favoured method we determined [9] the continuum limit of P, ϵ, C_V and C_s for the temperature range $0.9Tc \leq T \leq 3T_c$. Continuum extrapolations were performed by making linear fits in $a^2 \propto 1/N_\tau^2$, using lattices with large temporal extents $N_\tau = 8, 10, 12$. High statistics (around few hundred thousand measurements) were accumulated to get very precise (errors $\sim 5\%$) results. We have showed that this method gives positive pressure for all temperatures and N_τ used, even when the older s-favoured method gives negative pressure. Note that this is so in spite of the use of the same perturbative values for the coefficients c_i's in both cases. On the other hand in the phase transition region the t-favoured method pressure shows a steeper rise than that of the integral method pressure. Compared to the integral method the energy density in the t-favoured method is harder near T_c and agrees with that of the integral method for $T \geq 2T_c$. This indicates a difference in the latent heat determined by the two methods. Part of the difference between these two methods closer to T_c is most likely to be the use of one-loop order perturbative Karsch coefficients. Inclusion of the effects of higher order loops in the Karsch coefficient might improve the agreement. Also integral method assumes that the pressure below T_c is zero. Relaxing this assumption can restore agreement close to T_c, at the cost of the high-T region. Also the results for the integral method were obtained on coarser lattices [5] and using different renormalized coupling than what was used in our study. Surprisingly, we also found that the pressure in the t-favoured method agrees with that obtained from a dimensionally reduced theory, matched with the 4-d theory perturbatively upto order $g^6 \ln(1/g)$ [10], almost all the way down to T_c. Our continuum results C_V shows that for $T \geq 2T_c$, C_V/T^3 is far from its ideal gas value but is quite consistent with the prediction in conformal theories that $C_V/T^3 = 4\epsilon/T^4$. In the neighbourhood of T_c, C_V shows a peak-like structure. Whereas C_s is consistent with its ideal gas value (in accordance with the prediction for a conformal theory) for $T \geq 2T_c$, it decreases dramatically near T_c giving rise to a soft point in the EoS. A comparison of our continuum entropy density with its quantitative predictions [8] for a strongly coupled $\mathcal{N} = 4$ SYM shows good agreement from

$T > 1.5T_c$. This, along with our results for C_V/T^3 and C_s^2, gives a hint that the $SU(3)$ gauge theory behaves like a quasi-conformal theory for t' Hooft couplings $g^2N_c < 9$. It will be very interesting to check whether this is also true for the full QCD.

Degrees of freedom in QCD plasma: robust observables from lattice

As discussed earlier the lattice QCD studies show that the thermodynamic quantities, like pressure and energy density, deviate from their respective ideal gas (of free quarks and gluons) values by about 20% even at temperature $T = 3T_c$. Also recent results from RHIC indicate the formation of a thermalized medium endowed with large collective flow and very low viscosity. These findings suggest that close to T_c the nature of the QGP is far from a gas of free quarks and gluons, rather it is a strongly interacting system. In view of this situation, it is very important to identify the degrees of freedom of such a strongly coupled QGP.

If the relevant degrees of freedom of a strongly coupled QGP are quasi-quarks then, different conserved charges, *e.g.* baryon number (B), electric charge (Q), third component of isospin (I) *etc.* , are carried by different flavours (u, d, s) of quarks. Thus in the conventional quasi-particle models conserved charges come in strict proportion to number of u, d, s quarks. Hence conserved charges are strongly correlated with the flavours and the flavours have no correlations among themselves. Based on the above arguments, in [11], it has been suggested that the baryon-strangeness correlation

$$C_{BS} = -3\frac{\langle BS\rangle - \langle B\rangle\langle S\rangle}{\langle S^2\rangle - \langle S\rangle^2}, \tag{25}$$

can be used to probe the degrees of freedom of QGP. Here $B = (U + D - S)/3$ is the net baryon number and U, D, S are the numbers of net (quarks minus anti-quarks) up-quarks, down-quarks and strange-quarks respectively. The notation $\langle\cdot\rangle$ denotes average taken over a suitable ensemble. The quantity C_{BS} probes the linkage of the strangeness carrying excitations to baryon number and hence gives

an idea about the average baryon number of all the excitations carrying the s flavours. The ratio is normalized such that for a pure quark gas, *i.e.* where unit strangeness is carried by excitations having $B = -1/3$, $C_{BS} = 1$. A value of C_{BS} significantly different from 1 will indicate that the QGP phase may contain some other degrees of freedom apart form the quasi-quarks.

In order to uncover the nature of QGP in the vicinity of T_c many different suggestions have been made over the last decade. One such model which has generated considerable amount of interest in the recent years is the model proposed by Shuryak and Zahed [12]. This model proposed a strongly interacting chromodynamic system of quasi-particles (with large thermal masses) of quarks, anti-quarks and gluons along with their numerous (possibly coloured) bound states. In the model of [12], presence of bound states demands correlations among different flavours. Hence correlations between conserved charges and flavours depend on the mass-spectrum of the bound states and the strong correlations among them are lost. For this model $C_{BS} = 0.62$ at $T = 1.5T_c$ [11], while for a gas of hadron resonances $C_{BS} = 0.66$ [11].

By extending the idea of [11], recently in [13], C_{BS} has been calculated using lattice QCD simulations with two flavours of dynamical light quarks and three flavours (two light and one heavier) of valence quarks. The calculations of [13] found that this ratio has values which are close to their respective ideal gas values ($= 1$) even just above T_c. As the lattice study of [13] involved simulations with dynamical quarks, they were done using small lattices having temporal lattice size $N_\tau = 4$. By comparing with the results from quenched simulations it has been shown [13] that some ratios similar to C_{BS} do not depend on N_τ for temperature $T = 2T_c$. However, it is known that the contributions of the bound states of [12] become more and more important as one approaches T_c. So on the lattice it is necessary to investigate the continuum limit of C_{BS}, in order to rule out that C_{BS} has values close to the predictions of the bound state QGP model [12].

Two quantities, C_{BS} and C_{QS} (electric charge-strangeness correlation), which can directly probe the degrees of freedom in a QGP can be related to the quantities measurable on the lattice by the following way [13]

$$C_{BS} = 1 + \frac{2\chi_{us}}{\chi_s} \qquad \text{and} \qquad C_{QS} = 1 - \frac{\chi_{us}}{\chi_s}, \tag{26}$$

where χ_f is the diagonal QNS and $\chi_{ff'}$ is the off-diagonal QNS, as defined in the Introduction. A value of C_{BS} and C_{QS} significantly different from 1 will indicate that the QGP phase may contain some other degrees of freedom apart form the quasi-quarks. Similar ratios can also be formed for the light (u and d) quark sector [13]. In [14], we have made a careful investigation of the continuum limit of the ratios of off-diagonal to diagonal QNS like C_{BS}, C_{QS} *etc.* by going to large lattices with $N_\tau = 4,\ 8,\ 10,$ and 12, for the temperatures $1.1T_c \leq T \leq 2T_c$, chemical potential $\mu_f = 0$ and using quenched approximations. We have found that for this whole range of temperature the lattice results for the ratios like C_{BS}, C_{QS} *etc.* are almost independent (within $\sim 5\%$) of the lattice spacing, *i.e.* they are robust. By comparing our results with that from [13] we also found that these ratios have very mild dependence on the sea quark content of the theory. Moreover, we have found that these quantities acquire values which are very close to their respective ideal gas limits. Thus the lattice results of [13] and [14] favour a quasi-particle like picture of QGP, as opposed to the bound state model of [12].

Wroblewski parameter (λ_s) is a quantity of extreme interest due to its relation to the enhancement of strangeness production in QGP. Under certain conditions it can be shown that [15]

$$\lambda_s = \frac{2\langle s\bar{s}\rangle}{\langle u\bar{u} + d\bar{d}\rangle} = \frac{\chi_s}{\chi_u}. \tag{27}$$

In [14], we have also re-confirmed (see [13]) that λ_s is robust not only in the sense that it does not depend on the lattice spacings but also has very mild dependence on the see quark masses. The robustness of the Wroblewski parameter is very encouraging specially since in the vicinity of T_c the lattice results for this quantity almost coincide with the value extracted by fitting the experimental data of RHIC with a hadron gas fireball model.

Testing the PNJL model against the lattice data

The lattice QCD studies have established that QGP is a strongly interacting system in the vicinity of T_c, with quasi-particle like degrees of freedom. While lattice studies are based on the first principles, in view of their numerical nature

it is important to understand the underlying physics of the lattice results in terms of QCD inspired effective models. On the other hand, it is necessary to put these effective models under stringent tests against the lattice data in order to verify that these models capture the correct physics.

It is known that in the limit of infinite quark mass (m_q) the order parameter for the deconfinement transition is the thermal average of the Polyakov loop

$$L(\vec{x}) = \mathcal{P} \exp\left[i \int_0^\beta d\tau \; A_0(\vec{x}, \tau)\right], \tag{28}$$

where $A_0(\vec{x}, \tau)$ is the gauge field in the Euclidean time direction and $\mathcal{P}$ denotes path ordering. On the other hand, in the chiral limit, *i.e.* $m_q \to 0$, the order parameter for the chiral transition in QCD is the chiral condensate $\langle \bar{\psi}\psi \rangle$,

$$\psi = \begin{pmatrix} u \\ d \end{pmatrix}$$

being the two component quark field corresponding to the 'up' (u) and 'down' (d) quarks. Lattice simulations have found a simultaneous deconfinement and chiral transition at the same temperature. The primary aim of the *Polyakov-loop-extended Nambu Jona-Lasinio* (PNJL) model [18] is to explain this lattice finding, within the framework of a QCD inspired effective theory having quasi-quark excitations. To achieve this the PNJL model couples the Polyakov loop, which incorporates the physics of deconfinement, with the Nambu Jona-Lasinio (NJL) model which is supposed to give the correct chiral properties.

The Lagrangian for the NJL model is

$$\mathcal{L}_{NJL} = \bar{\psi}(i\partial\!\!\!/ - m)\psi + G\left[\left(\bar{\psi}\psi\right)^2 + \left(\bar{\psi} i\gamma_5 \vec{\tau}\psi\right)^2\right], \tag{29}$$

where $m = diag(m_u, m_d)$. In the $m_u = m_d \to 0$ limit this Lagrangian is symmetric under $SU_V(2) \times SU_A(2) \times U_V(1)$, where $SU_V(2)$ is the isospin symmetry, $U_V(1)$ is the baryonic symmetry and $SU_A(2)$ is the chiral symmetry. In the chiral limit the NJL model shows a second order phase transition belonging to the $O(4)$ class. On the other hand, an effective Lagrangian for an $SU(3)$ gauge theory can be written as [16]

$$\mathcal{L}_{SU(3)} \equiv -\mathcal{U}\left(\Phi[A], \bar{\Phi}[A], T\right) = -\frac{b_2(T)}{2}\Phi\bar{\Phi} - \frac{b_3}{6}\left(\Phi^3 + \bar{\Phi}^3\right) + \frac{b_4}{4}\left(\bar{\Phi}\Phi\right)^2, \tag{30}$$

with $\Phi = \text{Tr } L/N_c$ and $\bar{\Phi} = \text{Tr } L^\dagger/N_c$. Here 'Tr ' denote traces in the colour space. This model has a $Z(3)$ symmetry and shows a first order phase transition which is similar to a deconfinement phase transition found in lattice QCD simulations.

The PNJL is a synthesis of these two models [17], namely

$$\mathcal{L}_{PNJL} = \bar{\psi}(i\not{D} - m)\psi + G\left[\left(\bar{\psi}\psi\right)^2 + \left(\bar{\psi}i\gamma_5\vec{\tau}\psi\right)^2\right] - \mathcal{U}\left(\Phi[A], \bar{\Phi}[A], T\right). \quad (31)$$

A mean field analysis of this model can be performed by treating $\langle\bar{\psi}\psi\rangle$, Φ and $\bar{\Phi}$ as classical fields. Using the mean field analysis at finite temperature and non-zero quark chemical potential $\mu_0 = (\mu_u + \mu_d)/2$ (or baryon chemical potential, $\mu_b = 3\mu_0$), in [18] thermodynamic quantities like pressure, energy density *etc.* were calculated and compared with the lattice results. This work found that, indeed, PNJL model shows a coincidence of the onset of chiral restoration and deconfinement in agreement with the lattice simulations. Moreover, in [18] it was found that the pressure (for $\mu_0 = 0$) calculated from the PNJL model agrees with the lattice data. However, the quark number density $n_0 = \partial \ln \mathcal{Z}/\partial\mu_0$, though reproducing the qualitative features of the lattice data, quantitatively deviates from the lattice results for larger values of μ_0. Later, in [19], c_n (see the Introduction section), were analyzed within the PNJL model. It was found that while both the lattice and PNJL model have the same qualitative features for c_{2n} for $n = 0, 1, 2, 3$, the quantitative agreements are not so good.

In view of these results it is very important to perform more stringent tests on the PNJL model, specially in presence of non-zero chemical potentials. In order to do so, we have extended [20] the PNJL model for non-zero isospin chemical potential $\mu_I = (\mu_u - \mu_d)/2$. We have calculated the coefficients c_{2n}^I (see the Introduction section for definitions) for $n = 0, 1, 2, 3$, for which lattice data are available. This also allowed us to calculate the diagonal QNS $[\chi_u/T^2 = (c_2^I + c_2)/2]$ and the off-diagonal QNS $[\chi_{ud}/T^2 = (c_2^I - c_2)/2]$. Since the off-diagonal QNS measures the correlation among the u and d flavours, this quantity provide a direct understanding of the extent to which the PNJL model captures the underlying physics of lattice QCD. We found [20] that though the PNJL model failed to reproduce the lattice data for the diagonal QNS, the qualitative features were more or less the same. On the other hand, for the off-diagonal QNS the PNJL model was unable to reproduce even the qualitative features of the lattice results.

The PNJL model predicts the correct sign for the χ_{ud}, but for large temperature χ_{ud} do not approach zero. Instead it tends to saturate at some relatively large negative value which is far from the lattice result. This implies that the flavour-mixing in the PNJL model is much larger.

In an attempt to pin point the problem in PNJL model, further, we modified the NJL part of the PNJL model by using the NJL Lagrangian proposed in [21]. This Lagrangian has two parts. One, $\mathcal{L}_1$, has the $SU_V(2)\times SU_A(2)\times U_V(1)\times U_A(1)$ symmetry, while the other, $\mathcal{L}_2$, breaks the $U_A(1)$ axial symmetry. The second term can be interpreted as an interaction induced by instantons and reflects the $U_A(1)$-anomaly of QCD. This term has the structure of a 't-Hooft determinant in the flavour space, leading to flavour-mixing. By adjusting the relative strength of $\mathcal{L}_1$ and $\mathcal{L}_2$ one can explicitly control the amount of flavour-mixing in the NJL sector. This modified NJL Lagrangian reduces to the standard NJL Lagrangian of Eq. [29] when the strength of the $\mathcal{L}_1$ and $\mathcal{L}_2$ becomes equal. We recalculated [20] the diagonal and off-diagonal QNS by coupling this modified form of the NJL model with the Polyakov loop model for different amount of flavour-mixing. We found no dependence of χ_{ud} on the amount of flavour-mixing in the NJL sector, both above and below T_c. This motivated us to conclude that in the PNJL model, at the mean field level, the form of the interaction between the gauge fields Φ, $\bar{\Phi}$ and the chemical potentials μ_f is insufficient to capture the underlying physics of the lattice results. This is a very critical drawback of the PNJL model as the lattice results of [14] show that correlation among the flavours in the off-diagonal QNS is largely governed by the interaction of the quarks with the gauge fields and is almost independent of the presence of the quarks loops.

Bibliography

[1] K. Wilson, *Phys. Rev.* D 10, 2445 (1970). ii, iv

[2] M. Creutz, Quarks, *Gluon and Lattices*, Cambridge University Press (1985); I. Montvay and G. Münster, *Quantum Fields on a Lattice*, Cambridge University Press (1997); H. J. Rothe, *Lattice Gauge Theories: An Introduction*, World Scientific (1998). ii, iii, iv, v

[3] F. Karsch and I. Stamatescu, *Phys. Lett.* B 227, 153 (1989). v

[4] J. Engels *et al.* , *Nucl. Phys.* B 205 [FS5], 545 (1982). vi

[5] G. Boyd *et al.* , *Phys. Rev. Lett.* 75, 4169 (1995); *Nucl. Phys.* B 469, 419 (1996). vii, x, xii

[6] R. V. Gavai, S. Gupta and S. Mukherjee, *Phys. Rev.* D 71, 074013 (2005). viii, ix, x, xii

[7] F. Karsch, *Nucl. Phys.* B 205 [FS5], 285 (1982). ix

[8] S. S. Gubser, I. R. Klebanov and A. A. Tseytlin, *Nucl. Phys.* B 534, 202 (1998). x, xii

[9] R. V. Gavai, S. Gupta and S. Mukherjee, PoS LAT2005 173 (2005); hep-lat/0506015. x, xi, xii

[10] K. Kajantie *et al.* , *Phys. Rev.* D 67, 105008 (2003). xii

[11] V. Koch, A. Majumder and J. Randrup, *Phys. Rev. Lett.* 95, 182301 (2005). xiii, xiv

[12] E. Shuryak and I. Zahed, *Phys. Rev.* D 70, 054507 (2004); *Phys. Rev.* C 70, 021901 (2004). xiv, xv

[13] R. V. Gavai and S. Gupta, *Phys. Rev.* D 73, 014004 (2006). xiv, xv

[14] S. Mukherjee, *Phys. Rev.* D 74, 054508 (2006). xv, xviii

[15] R. V. Gavai and S. Gupta, *Phys. Rev.* D 65, 094515 (2002). xv

[16] R. D. Pisarski, *Phys. Rev.* D 62, 111501 (2000). xvi

[17] K. Fukushima, *Phys. Lett.* B 591, 277 (2004). xvii

[18] C. Ratti, M. A. Thaler and W. Weise, *Phys. Rev.* D 73, 014019 (2006). xvi, xvii

[19] S. K. Ghosh, T. K. Mukherjee, M. G. Mustafa and R. Ray, *Phys. Rev.* D 73, 114007 (2006). xvii

[20] S. Mukherjee, M. G. Mustafa and R. Ray, *Phys. Rev.* D 75, 094015 (2007). xvii, xviii

[21] M. Frank, M. Buballa and M. Oertel, *Phys. Lett.* B 562, 221 (2003). xviii

Chapter 1

Introduction

It has been established [1] that almost the entire mass of the visible matter in our universe consists of baryonic particles. Baryons are strongly interacting particles. Quantum ChromoDynamics (QCD) is the theory of strong interaction. The basic degrees of freedom of QCD are quarks and gluons. Quarks and gluons carry colour charges, analogous to the electric charge of an electron. However, experimental searches [2] looking for the existence of isolated free quarks have produced negative results. This experimental fact has motivated the hypothesis of confinement. An important open problem regarding QCD is the phenomenon of confinement [3]. Confinement is the phenomenon where the elementary particles (fields) present in the Lagrangian of the theory are absent in its physical spectrum. In the case of QCD it means that quarks, gluons and in general all colour-charged objects cannot exist as separate asymptotic objects, rather they exist only as bound states (hadrons and glueballs) which are colour neutral.

However, at energy densities large compared to the natural scale ($\Lambda_{QCD}^4 \sim 200\ MeV/fm^3$) quarks and gluons may not remain confined inside the volume of a hadron [4]. At such high energy densities the average separation, d, between the quarks and gluons may become $d \ll \Lambda_{QCD}^{-1} \sim 1\ fm \sim (volume\ of\ a\ hadron)^{1/3}$. The strength of interaction between these closely packed quarks and gluons is weak due to the asymptotic freedom of QCD [5], which says that the QCD coupling decreases as the distance between quarks and gluons decreases or as the exchanged momentum between them increases. Such high energy densities (or small separation) can be reached at high temperature and/or densities. Thus it

is expected that with increasing temperature and/or density, strongly interacting matter will undergo a transition from the hadronic phase, in which constituents are colour-neutral bound states, to a plasma of deconfined colour-charged quarks and gluons. Such a state of matter is known as Quark Gluon Plasma (QGP) [6].

Quark-hadron transition may have taken place during the evolution of early universe. QGP-like matter may have been present immediately (at $\sim 10^{-5}$ *sec*) after the Big Bang. At these stages our universe was very hot (temperature $\gtrsim 10^{12}$ K), but close to net-baryon free. Cosmological QCD transition may have some important consequences regarding the initial condition of the Big Bang Nucleosynthesis, small scale structure and composition of Cold Dark Matter, damping of gravitational waves *etc.* [7]. Another example where such extreme conditions may arise are the compact stellar objects, such as the core of a neutron star, where densities can be as high as $10^{16} - 10^{17}$ g/cm^3 [4]. Quark matter may also be found in such a situation, which in turn may have experimentally verifiable implications on the cooling of those objects [8]. On the other hand, there is a good possibility that this new form of matter might be produced in the laboratory through the collisions of ultra-relativistic heavy nuclei [9]. Many experimental signatures of the possible formation of QGP in heavy-ion collision experiments have been proposed [10]. First such heavy-ion collision experiments were performed at Alternating Gradient Synchrotron (AGS) [11] in Brookhaven and Super Proton Synchroton (SPS) [12] at CERN, with center of mass energies per nucleon ($\sqrt{s}/A$) of $\sqrt{s}/A = 2$ GeV and $\sqrt{s}/A = 18$ GeV respectively. Relativistic Heavy Ion Collider (RHIC), with $\sqrt{s}/A = 200$ GeV, is currently running at Brookhaven and providing us with vast amount of new data [13]. A still higher energy collider, namely the Large Hadron Collider (LHC) at CERN, will have $\sqrt{s}/A = 5.5$ TeV and a dedicated heavy-ion detector ALICE [14]. Thus a variety of predictions of hot and/or dense QCD will hopefully be checked against the data from these experiments.

Perturbative techniques have been highly successful [15] in testing QCD for large momenta exchanges, *i.e.* for small couplings. The motivation for considering QGP as a weakly coupled system is the asymptotic freedom [5], which suggest that the effective QCD coupling used in thermodynamic calculations should be small if either the temperature T or the baryon chemical potential μ_B is high enough.

For instance, if the temperature is the largest scale in the problem then the QCD coupling $\alpha_s(\bar{\mu}) \equiv g^2/4\pi \propto 1/\ln(\bar{\mu}/\Lambda_{QCD})$, with typically $\bar{\mu} = 2\pi T$. For $T > \Lambda_{QCD} \sim 200\ MeV$ the coupling is reasonably small, $\alpha_s < 0.3$. Extensive weak-coupling calculations have been performed to study the bulk thermodynamic properties of QGP [16]. For example, at zero chemical potential the perturbative expansion of pressure is—

$$\frac{P}{T^4} = c_0 + c_2 g^2 + c_3 g^3 + (c_4' \ln g + c_4)\, g^4 + c_5 g^5 + (c_6' \ln g + c_6)\, g^6 + \cdots, \quad (1.1)$$

where the coefficient

$$c_0 = \left[2(N_c^2 - 1) + 2N_c N_f \left(\frac{7}{4}\right)\right] \frac{\pi^2}{90}, \quad (1.2)$$

is the Stefan-Boltzmann constant corresponding to the ideal (non-interacting) gas. The coefficient c_2 [17] arises from the lowest-order (two-loop diagrams) perturbative corrections to the pressure of an ideal gas. The computation of the coefficient c_3 [18] requires a resummation of plasmon ring diagrams in the infrared limit. The coefficient c_4' has been computed in Ref. [19] and c_4 [20] is due to three-loop diagrams. The coefficient c_5 [21, 22] arises from correction to the three-loop diagrams due to Debye screening of chromo-electric gluons. The coefficient c_6' can also be computed perturbatively [23] using four-loop diagrams. c_6 is genuinely non-perturbative and can only be computed using some non-perturbative technique. This is where the perturbative expansion of the pressure in QGP breaks down due to severe infra-red divergences, known as the *Linde problem* [24]. At zero temperature and large chemical potentials the expansion in known upto $\mathcal{O}(g^4)$ [25, 26], and at high temperatures but finite chemical potentials upto $\mathcal{O}(g^6 \ln g)$ [27, 28]. Very recently perturbative expansion, valid for all values of T and μ, of QGP pressure have been computed [29] upto $\mathcal{O}(g^4)$.

The perturbative series of Eq. [1.1] has poor convergence properties. The second order terms $\sim c_2 g^2$ gives a negative contribution to Stefan-Boltzmann pressure (c_0), which is less than 10% of c_0 at $T \sim 10^3 \Lambda_{\overline{MS}}$ and at most 40% of c_0 at $T \sim \Lambda_{\overline{MS}}$ ($\sim T_c$, the transition temperature). However, the next contribution $\sim c_3 g^3$ is positive and so large that the pressure overshoots c_0 even upto $T \sim 10^3 \Lambda_{\overline{MS}}$. The terms of order g^4 are again small, but also positive, such that, to

$\mathcal{O}(g^4)$ the pressure is larger than c_0. The terms of $\mathcal{O}(g^5)$ are negative and so large in magnitude, that the pressure even vanishes at $T \sim \Lambda_{\overline{MS}}$. The convergence of these expansions are reasonably good only for coupling constants as low as $\alpha_s < 0.05$, corresponding to temperature as high as $\gtrsim 10^5 \Lambda_{\overline{MS}}$. Thus, naive perturbation theory is clearly not applicable for temperatures of order T_c. Even the results of improved perturbation techniques, such as dimensional reduction [16, 23, 30], Hard Thermal Loop (HTL) resummations [16, 31, 32] *etc.* , show that they are applicable only for temperatures $\gtrsim 3T_c$. Hence, to study the properties of QCD for $T \lesssim 3T_c$ non-perturbative techniques are essential.

Lattice regularization of field theories provide such a non-perturbative technique. Lattice field theory is a useful way of regularizing a continuum field theory, which is otherwise plagued by ultraviolet divergences. One formulates the theory on a discrete space-time lattice [33, 34] so that the lattice spacing 'a' serves as an ultraviolet regulator (cut-off). Numerical simulations of lattice field theories have a further advantage of obtaining the predictions of the theory from first principles. All one needs is the Lagrangian of the theory and the bare parameters. Over the past two decades or so, tremendous progress has been made in the field of numerical study of QCD formulated on discrete space-time lattice. This approach has been very successful in providing detail information about the thermodynamic properties of QCD at finite temperature.

1.1 Basics of finite temperature lattice QCD

The study of finite temperature QCD (or any field theory) starts with the grand canonical partition function for a many-particle ensemble at temperature T

$$\mathcal{Z} = \mathrm{Tr}\ e^{-\beta\left(\hat{H}-\mu\hat{N}\right)}. \tag{1.3}$$

Here, $\hat{H}$ is the Hamiltonian of the system, $\hat{N}$ is the operator for some conserved charge (*e.g.* baryon number, electric charge *etc.*), μ is the chemical potential corresponding to that conserved charge and $\beta = 1/T$. We have chosen to work in terms of natural units, *i.e.* we have set $\hbar = c = k_B = 1$. The above partition

function can be written in terms of a path integral [34]—

$$\mathcal{Z} = \int_{bc} \mathcal{D}\psi\ \mathcal{D}\bar{\psi}\ \mathcal{D}A_\mu\ \exp\left[-\int_0^\beta d\tau \int d^3x\ \mathcal{L}\right]. \tag{1.4}$$

In the above equation $\mathcal{L}$ denotes the Lagrangian and τ is the inverse temperature, *i.e.* the Euclidean (imaginary) time. The notation 'bc' denotes collectively the boundary conditions on the fields, anti-periodic for the quark fields ψ, $\bar{\psi}$ and periodic for the gauge fields A_μ. The thermal expectation value of a physical observable $\mathcal{O}$, defined by

$$\langle \mathcal{O} \rangle = \frac{1}{\mathcal{Z}} \mathrm{Tr}\ \left[\mathcal{O} e^{-\beta(\hat{H}-\mu\hat{N})}\right], \tag{1.5}$$

then takes the following form in the functional integral approach

$$\langle \mathcal{O} \rangle = \frac{\int_{bc} \mathcal{D}\psi\ \mathcal{D}\bar{\psi}\ \mathcal{D}A_\mu\ \mathcal{O} \exp\left[-\int_0^\beta d\tau \int d^3x\ \mathcal{L}\right]}{\int_{bc} \mathcal{D}\psi\ \mathcal{D}\bar{\psi}\ \mathcal{D}A_\mu\ \exp\left[-\int_0^\beta d\tau \int d^3x\ \mathcal{L}\right]}. \tag{1.6}$$

The primary goal of finite temperature Lattice QCD (LQCD) is to obtain predictions for QGP using the path integral form of the underlying QCD partition function [34]. Just as an ordinary integration can be performed by taking a limit of sums on discrete points, LQCD can be thought of as an attempt to define and perform the functional integrals in $\mathcal{Z}$ and $\langle \mathcal{O} \rangle$ by discretizing the space-time (Euclidean) over which the fields are defined. Let N_s and N_τ denote the number of points in the spatial and the temporal (or equivalently the inverse temperature) direction and let a_s and a_τ be the corresponding lattice spacings. Then the volume V and the temperature T are given by

$$V = (N_s a_s)^3, \qquad \text{and} \qquad T = \frac{1}{N_\tau a_\tau}. \tag{1.7}$$

The finite lattice spacings a_i $(i = s, \tau)$ impose ultraviolet cut-offs a_i^{-1} and the finite volume V imposes an infrared cut-off.

In the LQCD formulation the quark fields, $\psi(x)$, reside on the lattice site $x = (x_0, x_1, x_2, x_3)$. The gauge fields are introduced as directed link variables. Let $U_\mu(x) \in SU(N_c)$ be the gauge field associated with the directed link from site x to site $x + \hat{\mu}$, $\hat{\mu}$ being the unit vector in the μ-th direction (see Fig. [1.1a]

for a simplified illustration). Unitarity of U's also demands $U_\mu^\dagger(x) = U_{-\mu}(x+\mu)$. Under a local gauge transformation $V(x) \in SU(N_c)$ the fields transform as

$$\begin{aligned} \psi(x) &\longrightarrow \psi'(x) = V(x)\psi(x), \qquad \text{and} \\ U_\mu(x) &\longrightarrow U'_\mu(x) = V(x)U_\mu(x)V^\dagger(x+\hat{\mu}). \end{aligned} \tag{1.8}$$

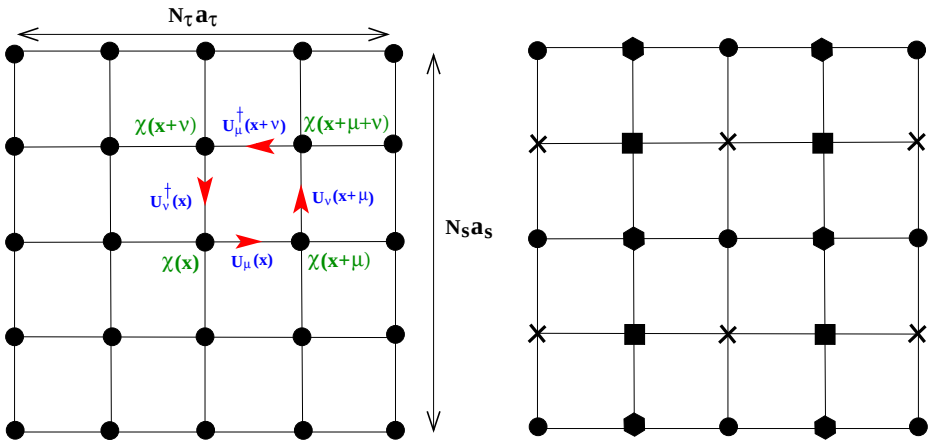

(a) (b)

Figure 1.1: (a) Illustration of the setup of (2-d) lattice gauge theory. The gauge fields (U) reside on the links, while the matter fields (in this case the staggered fermion fields, χ) reside on the sites. (b) Distributing 2^d degrees of freedom on a two dimensional ($d = 2$) lattice.

1.1.1 The Wilson gauge action

The above gauge transformation of the gauge variables implies that a gauge invariant action can only be constructed by taking traces of closed loops of $U_\mu(x)$. One calls the smallest such square loop as a *plaquette*

$$U_{\mu\nu}(x) = U_\mu(x)U_\nu(x+\mu)U_\mu^\dagger(x+\nu)U_\nu^\dagger(x) \tag{1.9}$$

(see Fig. [1.1a] for a simplified illustration). We define $P_{\mu\nu}(x) = 1 - \Re\,\mathrm{Tr}\, U_{\mu\nu}(x)/N_c$, where the 'Tr' denotes the trace in the colour space. We also introduce the notation for the average spatial and temporal plaquettes,

$$P_s = \sum_{x;j>i,ij=1}^{3} P_{ij}(x)/3N_s^3N_\tau, \qquad \text{and} \qquad P_\tau = \sum_{x,i=1}^{3} P_{0i}(x)/3N_s^3N_\tau \tag{1.10}$$

respectively.

The simplest possible lattice action for a pure $SU(N_c)$ gauge theory that can be constructed out of the plaquettes is the *Wilson action* [33, 35, 36]—

$$\begin{aligned} S_G[U] &= 6N_cN_s^3N_\tau\left[K_sP_s + K_\tau P_\tau\right], \qquad \text{with} \\ K_s &= \frac{1}{\xi g_s^2}, \qquad \text{and} \qquad K_\tau = \frac{\xi}{g_\tau^2}. \end{aligned} \tag{1.11}$$

Here, g_s and g_τ are the gauge couplings along the spatial and the temporal directions [37]. The quantity $\xi = a_s/a_\tau$ is known as the *anisotropy parameter*.

In the $\xi \to 1$ limit, expanding the Wilson action for small lattice spacings $a_s = a_\tau = a \to 0$ and using the fact that $U_\mu(x) \sim e^{-igA_\mu(x)}$ (g is the gauge coupling) for $a \to 0$, one obtains [34] the continuum Yang-Mills action

$$S_{YM} = -\frac{1}{4}\int_0^\beta d\tau \int d^3x F^b_{\mu\nu}F_b^{\mu\nu} + \mathcal{O}(a^2). \tag{1.12}$$

The correction to the continuum action is of order $\mathcal{O}(a^2)$. However, since the continuum limit corresponds to the critical point of the theory a large class of actions, differing by irrelevant terms (proportional to higher powers of the lattice spacing), are expected to give the same continuum physics. This fact is used to construct *improved actions* [38]. A construction principle behind an improved action is to add further terms to S_G in Eq. [1.11] in order to eliminate corrections of order $\mathcal{O}(a^2)$. Repeating this procedure, one can systematically eliminate discretization error upto a given power of a. Extending the same procedure one can also eliminate the all corrections, leading to the so-called *perfect actions* [39]. It is also worth noting that it is not necessary to add a gauge fixing term $S_{gauge-fixing}$ with the latticized gauge action S_G. This is because on a finite-size lattice the integration over the gauge fields becomes convergent [33].

1.1.2 The staggered fermion action

The naive discretization of the fermionic part of the QCD action is not particularly suitable because of the so-called *fermion doubling problem* [34] on the lattice. Extra doubler states originate due to the periodicity of the fermionic dispersion

relation within the Brillouin zone. One obtains one extra doubler state per space-time dimension, such that there are in total $2^4 = 16$ fermion species instead of a single one. The doubling phenomenon must occur in any lattice regularizations which respects the usual hermiticity, locality and translational invariance requirements. This follows from the 'No Go' theorem [40] which states that, under the above assumptions, one cannot solve the fermion doubling problem without breaking chiral symmetry for the vanishing fermion mass. This suggest that one may get rid of the doubling problem at the expense of explicit breaking of the chiral symmetry on the lattice. This leads to the so-called *Wilson fermion* prescription [34].

As the fermion doubling problem owes its existence to the fact that the fermionic dispersion relation vanishes at the corners of the Brillouin zone, one possibility of eliminating the unwanted fermion modes is by reducing the Brillouin zone, *i.e.* by doubling the effective lattice spacing. The *staggered fermion* formulation [41] achieves this by distributing the fermionic degrees of freedom over the lattice in such a way that the effective lattice spacing for each type of quark is twice the fundamental lattice spacing.

Let us consider a d-dimensional space-time lattice and subdivide it into elementary d-dimensional hypercubes of unit length. At each site within a given hypercube place a different (fermionic) degree of freedom, and repeat this structure periodically throughout the lattice. Then the effective lattice spacing have been doubled for each degree of freedom. In Fig. [1.1b] this has been for shown the case of a 2-dimensional lattice. Since there are 2^d sites within a hypercube but only $2^{d/2}$ components of a Dirac field (in even space-time dimensions), one needs $2^{d/2}$ different fermionic fields to reduce the Brillouin zone by a factor of half. In 4 space-time dimensions such a prescription may therefore be appropriate for describing $2^2 = 4$ different species of fermions. Thus staggered fermions do not solve the doubling problem completely, rather the number of doubler states are reduced to 4. These 4 different fermions are interpreted as the 4 degenerate flavours of quarks and the standard staggered fermion action is interpreted as describing QCD with $N_f = 4$ flavours. In numerical simulations with staggered fermions the standard practice is to use the so-called *fourth-root trick* [42], *i.e.* use

different staggered fermions for each flavour and take the fourth-root of the staggered fermion determinant corresponding to each flavour. The advantage of the staggered fermion prescription is that, even for non-zero lattice spacings $a \neq 0$, it preserves a $U(1) \times U(1)$ subgroup of the original $U(4) \times U(4)$ chiral symmetry [43]. The chiral condensate is thus an order parameter for the chiral symmetry restoration at the QCD transition. The presence of discrete chiral symmetries, in addition, forbids mass counterterms for staggered fermions [44, 45, 46], thus rendering the bare quark mass a straightforward input in the calculation.

In terms of the spin-diagonal basis the the action for staggered fermion on an anisotropic lattice is defined as [47, 43, 48, 49]—

$$S_F[U] = \sum_{x,x'} \bar{\chi}(x) \left[\sum_{\nu=1}^{3} D^{(\nu)}(x,x') + \gamma_F D^{(0)}(x,x') + m_f a_s \delta_{x,x'} \right] \chi(x'), \quad (1.13)$$

where

$$D^{(\nu)}(x,x') = \frac{1}{2}(-1)^{x_0+\cdots+x_{\nu-1}} \left[U_\nu(x)\delta_{x,x'-\hat{\nu}} - U_\nu^\dagger(x')\delta_{x,x'+\hat{\nu}} \right], \quad (1.14a)$$

$$D^{(0)}(x,x') = \frac{1}{2} \left[e^{(\mu a_\tau)} U_0(x)\delta_{x,x'-\hat{0}} - e^{-(\mu a_\tau)} U_0^\dagger(x')\delta_{x,x'+\hat{0}} \right]. \quad (1.14b)$$

Here $\chi(x)$, $\bar{\chi}(x)$ are one-component spinors and m_f is the bare quark mass. The anisotropic lattice introduces an extra coupling γ_F [48], which is unity for $\xi = 1$. Gauge invariance is assured by the presence of U's in Eq. [1.13]. μ is the quark chemical potential. It is known [49] that the naive way of introducing the chemical potential on the lattice leads to quadratic divergences even for free fermions. Though there are many ways of introducing the chemical potential on the lattice [50], we have chosen to work with the prescription of Ref. [49]

1.1.3 Continuum limit

In order to extract the continuum physics from LQCD calculations, one has to extrapolate the results to the case of vanishing lattice spacing $a \to 0$. (Here, and in the following discussion we assume that $\xi = 1$, *i.e.* one is working with an isotropic lattice having $a_s = a_\tau = a$.) Any quantity which has a dimension in units of a will give zero or infinity when extrapolated to $a \to 0$. Hence such a continuum extrapolation is meaningful only after converting a to some physically

relevant dimensional quantity, which is expected to remain fixed as $a \to 0$. For our case this quantity is the temperature T. For $N_c = 3$, the temperature can be related to the the bare coupling $\beta = 2N_c/g^2$ through the two-loop renormalization group equation—

$$a\Lambda_L \simeq \left(\frac{6b_0}{\beta}\right)^{-\frac{b_1}{2b_0^2}} \exp\left(-\frac{\beta}{12b_0}\right), \tag{1.15}$$

and the relation $T = 1/aN_\tau$. Here,

$$b_0 = \frac{1}{16\pi^2}\left(11 - \frac{2}{3}N_f\right), \quad \text{and} \quad b_1 = \left(\frac{1}{16\pi^2}\right)^2\left[102 - \left(10 + \frac{8}{3}\right)N_f\right] \tag{1.16}$$

are the two universal (independent of the renormalization scheme) coefficients and Λ_L is a scale parameter which can be related to the scale parameter in other regularization schemes, *e.g.* to $\Lambda_{\overline{MS}}$.

In Ref. [51] it has been shown that it is advantageous to use a renormalized β [52] (since it gives better scaling of $T_c/\Lambda_{\overline{MS}}$ with N_τ) in Eq. [1.15], instead of the bare β. Hence in this thesis, to determine the coupling β we always use the method suggested in Ref. [51], where the one-loop order renormalized couplings have been evaluated by using V-scheme [52], taking care of the scaling violations due to finite lattice spacing errors using the method of Ref. [53]. Using this method a precise determination of the transition temperature (T_c) for the pure $SU(3)$ gauge theory has been made in Ref. [51]. Through out this thesis (except in Chapter [5]) we will use this value for T_c, namely $T_c = 285 \pm 10\ MeV$.

Following the above discussion one can choose a β for each N_τ, keeping T fixed. Using these β as the input, one can perform numerical simulations for different N_τ, keeping the aspect ratio N_s/N_τ fixed. This ensures simulations at different lattice spacings $a = 1/(TN_\tau)$, keeping the temperature T and volume $V = (aN_s)^3 = [(N_s/N_\tau)/T]^3$ fixed. Results of these simulations at different a can then be extrapolated, using some fitting function, to $a \to 0$ to extract the continuum physics. Since both the Wilson gauge action and the unimproved staggered fermion action have $\mathcal{O}(a^2)$ cut-off errors, in the present case, the fitting function is conveniently chosen as $c_0 + c_2 a^2$ [*i.e.* $c_0 + c_2/(T^2N_\tau^2)$], c_0 and c_2 being some constants. Thus for our present purpose continuum extrapolation will simply mean extrapolation to $N_\tau \to \infty$, by fitting with $a + b/N_\tau^2$, for a fixed temperature and aspect ratio.

Finally, not only one is interested in the continuum limit at finite volume V, one would also like to extrapolate to the thermodynamic limit $V = (aN_s)^3 = [(N_s/N_\tau)/T]^3 \to \infty$. This is done by taking the continuum limit at fixed T for different aspect ratios N_s/N_τ, and extrapolating those results to $(N_s/N_\tau) \to \infty$.

1.1.4 Equation of state from LQCD

Once the lattice actions are defined, the finite temperature LQCD formalism can be extended for the numerical evaluation of the *Equation of State* (EoS) of QCD. The energy density (ϵ) and the pressure (P) are defined as

$$\epsilon = \frac{T^2}{V}\left.\frac{\partial \ln \mathcal{Z}(V,T)}{\partial T}\right|_V, \qquad \text{and} \qquad P = T\left.\frac{\partial \ln \mathcal{Z}(V,T)}{\partial V}\right|_T. \tag{1.17}$$

For simplicity, here, we will restrict ourselves to the case of pure $SU(N_c)$ gauge theory. So in the present case the partition function $\mathcal{Z}$ is given by

$$\mathcal{Z}(V,T) = \int_{bc} \mathcal{D}U e^{-S_G[U]}. \tag{1.18}$$

The two most popular methods that have been used for the determination of the EoS from LQCD are— the *differential method* [36] and the *integral method* [54].

1.1.4.1 Differential method

In order to distinguish between T and V derivatives, the differential method formulate the theory on a 3+1 dimensional anisotropic lattice having different lattice spacings in the spatial (a_s) and the temporal (a_τ) directions. In the differential method one trades the variables $\{T, V\}$ in terms of the anisotropy parameter ξ and a scale a, defined as—

$$\xi = \frac{a_s}{a_\tau}, \qquad \text{and} \qquad a = a_s. \tag{1.19}$$

The partial derivatives with respect to T and V can be written in terms of the two lattice parameters ξ and a, keeping N_s and N_τ fixed,

$$T\left.\frac{\partial}{\partial T}\right|_V \equiv \xi\left.\frac{\partial}{\partial \xi}\right|_a, \qquad \text{and} \qquad 3V\left.\frac{\partial}{\partial V}\right|_T \equiv a\left.\frac{\partial}{\partial a}\right|_\xi + \xi\left.\frac{\partial}{\partial \xi}\right|_a. \tag{1.20}$$

Using these expressions and the definitions of Eqs. [1.17, 1.18, 1.11], one obtains [36]

$$a^4\epsilon = -6N_c\xi^2\left[\frac{\partial K_s}{\partial\xi}D_s + \frac{\partial K_\tau}{\partial\xi}D_\tau\right], \tag{1.21a}$$

$$a^4P = -2N_c\xi^2\left[\frac{\partial K_s}{\partial\xi}D_s + \frac{\partial K_\tau}{\partial\xi}D_\tau\right] - 2N_c\xi a\left[\frac{\partial K_s}{\partial a}D_s + \frac{\partial K_\tau}{\partial a}D_\tau\right], \tag{1.21b}$$

$$a^4\Delta \equiv a^4(\epsilon - 3P) = 6N_c\xi a\left[\frac{\partial K_s}{\partial a}D_s + \frac{\partial K_\tau}{\partial a}D_\tau\right]. \tag{1.21c}$$

The quantity Δ, the so-called *interaction measure*, is the trace anomaly of the energy-momentum tensor of QCD, generated by the conformal invariance breaking of QCD at the quantum level. Since the functional integral formalism does not have normal ordering the energy density obtained above contains a contribution from the vacuum, similar to the zero-point energy of the continuum theory. This vacuum contribution can be eliminated by subtracting $\epsilon(T=0)$. For sufficiently large N_s, ϵ evaluated on the symmetric N_s^4 lattice is a good approximation to $\epsilon(T=0) \equiv \epsilon_{vac}$. Its subtraction leads to $D_i = \langle P_i\rangle - \langle P_0\rangle$ above, where $\langle P_0\rangle$ is the average plaquette value at $T=0$.

The above expressions also involve derivatives of the couplings g_i (see Eq. [1.11]) with respect to the lattice variables. In the weak coupling limit, g_i^{-2} 's can be expanded [56] around their symmetric lattice value $g^{-2}(a)$,

$$g_i^{-2}(a,\xi) = g^{-2}(a) + c_i(\xi) + O[g^2(a)], \tag{1.22}$$

with the condition $c_i(\xi=1)=0$. The quantities $c_i(\xi)$'s are known as the *Karsch coefficients*. The computation of the first derivatives of the couplings requires $b(a) = a\partial g^{-2}/\partial a$. With the usual definition of the one-loop order perturbative QCD β-function—

$$B(\alpha_s) = \frac{\mu}{2}\frac{\partial\alpha_s}{\partial\mu} = -\frac{33-2N_f}{12\pi}\alpha_s^2 + \cdots, \qquad \text{where} \qquad \alpha_s = g^2/4\pi, \tag{1.23}$$

one finds $b(a) = B(\alpha_s)/2\pi\alpha_s^2$ ($N_f = 0$ for the present case). Then,

$$a\frac{\partial K_s}{\partial a} = \frac{B(\alpha_s)}{2\pi\alpha_s^2\xi}, \tag{1.24a}$$

$$K_s' = -\frac{g_s^{-2}}{\xi^2} + \frac{c_s'}{\xi}, \tag{1.24b}$$

$$a\frac{\partial K_\tau}{\partial a} = \frac{\xi B(\alpha_s)}{2\pi\alpha_s^2}, \tag{1.24c}$$

$$K_\tau' = g_\tau^{-2} + \xi c_\tau', \tag{1.24d}$$

where primes denote derivative with respect to ξ. The quantities c_s' and c_τ' have been computed to one-loop order in the weak coupling limit for $SU(N_c)$ gauge theories [37].

Putting all these together, in the isotropic ($\xi \to 1$) limit one obtains [36]—

$$\frac{\epsilon}{T^4} = 6N_cN_\tau^4\left[\frac{D_s - D_\tau}{g^2} - (c_s'D_s + c_\tau'D_\tau)\right], \tag{1.25a}$$

$$\frac{P}{T^4} = 2N_cN_\tau^4\left[\frac{D_s - D_\tau}{g^2} - (c_s'D_s + c_\tau'D_\tau)\right] - 2N_cN_\tau^4\frac{B(\alpha_s)}{2\pi\alpha_s^2}\left[D_s + D_\tau\right], \tag{1.25b}$$

$$\frac{\Delta}{T^4} = 6N_cN_\tau^4\frac{B(\alpha_s)}{2\pi\alpha_s^2}\left[D_s + D_\tau\right]. \tag{1.25c}$$

1.1.4.2 Integral method

In computations on coarse lattices, it was found [57] that the differential method yielded negative pressure near the transition temperature, T_c. At that time it was argued that this problem is solely due to the use of perturbative formulae for various derivatives of the coupling. To cure this problem about a decade back a new method, called the *integral method*, was employed [54, 55] to determine the EoS of QCD matter. The integral method is formulated on an isotropic lattice, *i.e.* where $a_s = a_\tau = a$, and uses the fact that for a homogeneous system the pressure is given by (see Eq. [1.17])

$$P = \frac{T}{V}\cdot\ln\mathcal{Z}(T,V). \tag{1.26}$$

Hence, the task is to evaluate the partition function $\mathcal{Z}$. For an isotropic lattice ($\xi = 1$) the Wilson action is of the form $S_G[U] = N_s^3N_\tau\cdot\beta(P_s + P_\tau)$, with

$\beta = 2N_c/g^2$ and $g_s = g_\tau = g$ (see Eq. [1.11]). Then Eq. [1.18] immediately tells us that

$$\ln \mathcal{Z}|_\beta - \ln \mathcal{Z}|_{\beta_0} = -N_s^3 N_\tau \int_{\beta_0}^{\beta} d\beta' \left[\langle P_s(\beta')\rangle + \langle P_\tau(\beta')\rangle\right]. \tag{1.27}$$

This in turn gives us the pressure upto an additive constant—

$$\left.\frac{P}{T^4}\right|_\beta - \left.\frac{P}{T^4}\right|_{\beta_0} = -N_\tau^4 \int_{\beta_0}^{\beta} d\beta' \left[\langle P_s(\beta')\rangle + \langle P_\tau(\beta')\rangle\right]. \tag{1.28}$$

Below T_c ($\sim 200\ MeV$) the pressure, $P \sim \exp(-m_g/T)$, will be dominated by the lightest glueball states, which has mass $m_g \sim 1\ GeV$. This makes pressure rather small for temperatures $\lesssim T_c$. Motivated by this fact, the additive constant in the above equation is usually chosen to be zero at some coupling β_0 corresponding to temperature $\lesssim T_c$. Making this choice and doing the usual vacuum subtraction, as in the earlier case, one finally gets

$$\frac{P(\beta)}{T^4} = -N_\tau^4 \int_{\beta_0}^{\beta} d\beta' \left[D_s(\beta') + D_\tau(\beta')\right], \tag{1.29}$$

where β_0 correspond to some temperature $\lesssim T_c$.

Once the pressure is known, one can use the thermodynamic identity that for a homogeneous system the entropy density (s) is given by

$$\left.\frac{\partial P}{\partial T}\right|_V = \left.\frac{\partial S}{\partial V}\right|_T = s = \frac{\epsilon + P}{T}, \tag{1.30}$$

S being the total entropy, to arrive at the relation—

$$\frac{\Delta}{T^4} = \frac{\epsilon - 3P}{T^4} = T \left.\frac{\partial\left(P/T^4\right)}{\partial T}\right|_V. \tag{1.31}$$

Using the relation that for an isotropic lattice

$$T \left.\frac{\partial}{\partial T}\right|_V \equiv -a\frac{\partial}{\partial a}, \tag{1.32}$$

it is easy to see form Eqs. [1.31, 1.29]

$$\frac{\Delta}{T^4} = N_\tau^4 \left(a\frac{\partial\beta}{\partial a}\right)\left[D_s + D_\tau\right] = 6N_c N_\tau^4 \frac{B(\alpha_s)}{2\pi\alpha_s^2}\left[D_s + D_\tau\right]. \tag{1.33}$$

Once both P and Δ are known the energy density can easily be computed form the relation $\epsilon = 3P + \Delta$. One can use a non-perturbative β-function, $B(\alpha_s)$, to determine Δ [55]. Thus, no perturbative coupling is needed to compute the EoS of QCD using the integral method.

1.1.5 Taylor expansion in chemical potential

In presence of the quark chemical potential, μ, the fermion determinant, $\det M$, becomes complex [49, 50]. Since a complex $\det M$ cannot be interpreted as the probability with which important sampling can be performed, a direct Monte Carlo simulations of LQCD is not possible at $\mu \neq 0$. However, several techniques have been invented [58, 59] to study LQCD at non-zero μ. One such method is the Taylor expansion in chemical potential [60, 58, 59]. In this method any quantity of interest is Taylor expanded in the chemical potential around $\mu = 0$. As, in that case, the coefficients of the Taylor expansion are defined at $\mu = 0$, they can be extracted from the usual LQCD simulations at $\mu = 0$. These coefficients can then be used to construct the Taylor series in μ, to get an idea about the behaviour of the quantity at small but non-zero chemical potential. For example, for a theory with two flavours, the Taylor expansion of pressure can be written as [61, 62]—

$$P\left(T, \mu_f, \mu_{f'}\right) = \sum_{n=0}^{\infty} \sum_{j=0}^{n} \chi_{j,n-j}(T) \cdot \frac{\mu_f^j \mu_{f'}^{n-j}}{j!(n-j)!}, \tag{1.34}$$

where,

$$\chi_{j,n-j} = \left(\frac{T}{V}\right) \frac{\partial^n \ln \mathcal{Z}}{\partial \mu_{f'}^{(n-j)} \partial \mu_f^j}\bigg|_{\mu_f = \mu_{f'} = 0}. \tag{1.35}$$

Here, μ_f is the quark chemical potential corresponding to the flavour f. All the odd-order terms of the above expansion are zero due to CP symmetry. The lowest (2-nd) order coefficients are known as the *Flavour Diagonal Quark Number Susceptibility* (FDQNS) and the *Flavour Off-Diagonal Quark Number Susceptibility* (FODQNS), defined as [63]

$$\chi_f = \left(\frac{T}{V}\right) \frac{\partial^2 \ln \mathcal{Z}}{\partial \mu_f^2}\bigg|_{\{\mu_f\}=0}, \qquad \text{and} \qquad \chi_{ff'} = \left(\frac{T}{V}\right) \frac{\partial^2 \ln \mathcal{Z}}{\partial \mu_f \partial \mu_{f'}}\bigg|_{\{\mu_f\}=0}, \tag{1.36}$$

respectively.

Furthermore, if one introduces the *average quark chemical potential* (μ_0) and the *isospin/isovector chemical potential* (μ_I),

$$\mu_0 = \frac{\mu_u + \mu_d}{2}, \qquad \text{and} \qquad \mu_I = \frac{\mu_u - \mu_d}{2}, \tag{1.37}$$

then the corresponding susceptibilities will be [64]

$$\frac{\chi_0}{T^2} = \left(\frac{T}{V}\right)\frac{\partial^2 \ln \mathcal{Z}}{\partial(\mu_0/T)^2} \equiv \frac{2(\chi_u + \chi_{ud})}{T^2}, \quad \text{and} \tag{1.38a}$$

$$\frac{\chi_I}{T^2} = \left(\frac{T}{V}\right)\frac{\partial^2 \ln \mathcal{Z}}{\partial(\mu_I/T)^2} \equiv \frac{2(\chi_u - \chi_{ud})}{T^2}. \tag{1.38b}$$

Here, we have assumed degenerate (u, d)-quark masses to arrive at the second equalities (marked by $\equiv$) of the above relations. One can, further, perform Taylor series expansions of P, χ_0 and χ_I in (μ_0/T), around $\mu_0 = 0$, [64]—

$$\frac{P}{T^4} = \sum_{n=0}^{\infty} c_n(T)\left(\frac{\mu_0}{T}\right)^n, \tag{1.39a}$$

$$\frac{\chi_0}{T^2} = 2c_2 + 12c_4\left(\frac{\mu_0}{T}\right)^2 + 30c_6\left(\frac{\mu_0}{T}\right)^4 + \cdots, \tag{1.39b}$$

$$\frac{\chi_I}{T^2} = 2c_2^I + 12c_4^I\left(\frac{\mu_0}{T}\right)^2 + 30c_6^I\left(\frac{\mu_0}{T}\right)^4 + \cdots, \tag{1.39c}$$

where the coefficients $c_n(T)$ and $c_n^I(T)$ are defined as—

$$c_n(T) = \frac{1}{(n!)V}\cdot\frac{\partial^n \ln \mathcal{Z}}{\partial(\mu_0/T)^n}, \quad \text{and} \tag{1.40a}$$

$$c_n^I(T) = \frac{1}{(n!)V}\cdot\frac{\partial^n \ln \mathcal{Z}}{\partial(\mu_0/T)^{n-2}\partial(\mu_I/T)^2}. \tag{1.40b}$$

These coefficients can not only be computed from LQCD [64, 65], but also within the framework of improved perturbation theory [66, 67]. We will use these quantities in Chapter 4 and Chapter 5.

1.1.6 Brief outline of the thesis

In this thesis we have studied, using LQCD, different thermodynamic properties of QCD. In Chapter [2] we go beyond the EoS to study the fluctuation measures, like the specific heat at constant volume (C_V) and the speed of sound (C_s). We have found appropriate lattice expressions for these quantities and made precise determination of their continuum values for a Gluon Plasma at relatively high temperatures [68]. Based on our data, we also discuss the significance of conformal symmetry breaking in QCD. In Chapter [3] we propose an improvement of the differential method [69] for the computation of EoS using LQCD. Using

this improved method we compute EoS of a pure $SU(3)$ gauge theory both above and below the transition temperature. We have extended this method for the computation of C_V and C_s. We also make comparison of our results with the predictions of the perturbation theory and AdS/CFT correspondence. After gaining some insight about the bulk thermodynamic properties QGP, in Chapter [4] we investigate the degrees of freedom which give rise to such properties of QGP. In order to do so, we study different correlations between conserved charges and flavours [70]. Our studies in Chapter [4] have shown that the FODQNS plays an important role in capturing the underlying physics of the lattice results. In view of this, we calculated those in a the QCD inspired effective model, namely the Polyakov-loop Nambu Jona-Lasinio (PNJL) model, and compare with the available LQCD data [71]. These stringent tests of the PNJL model is the topic of Chapter [5]. Finally, in Chapter [6], we summarize all our works pertaining to this thesis and conclude.

Chapter 2

Speed of sound and specific heat in QCD plasma

2.1 Introduction

EoS of pure $SU(3)$ gauge theory has been extensively studied using lattice QCD. It is now a well-established fact that the pressure, P, and the energy density, ϵ, deviate [55] in the high temperature phase of QCD by about 20% from their ideal gas values at a temperature of about $3T_c$, where T_c is the transition temperature. Early expectations that ϵ would count the number of degrees of freedom in the QCD plasma through the Stefan-Boltzmann law are belied by the fact that perturbation theory has had great difficulty in reproducing these lattice results (see the discussion in Chapter [1]). In view of this, it is important to go beyond the EoS and study the thermodynamic fluctuation measures in a gluonic plasma. In the pure gluon gas there is only one fluctuation measure, the specific heat at constant volume (C_V). Related to this is a kinetic variable, the speed of sound (C_s).

The specific heat is a direct measure of fluctuations. It was suggested in Ref. [72] that event-by-event temperature fluctuation in the heavy-ion collision experiments can be used to measure C_V. Also it has been argued in Ref. [73] that C_V is directly related to the event-by-event transverse momentum fluctuations. In fact, recently there have been attempts to measure this quantity in the RHIC experiments [74].

The speed of sound, on the other hand, controls the expansion rate of the fire-ball produced in the heavy-ion collisions and hence plays a crucial role in the hydrodynamic studies of QGP. Elliptic flow is one of the most important quantity that has been suggested for the signature of QGP formation in the heavy-ion collision experiments. It has been shown [75, 76, 77, 78, 79] that elliptic flow is sensitive to the value of C_s.

In recent years, event-by-event fluctuations of quantities have been of immense interest as signatures of quark-hadron phase transition. In order to use fluctuations as a probe of the plasma phase, one has to identify observables whose fluctuations survive the freeze-out of the fireball. The evolution of these fluctuations is sensitive to the values of C_s, as shown in Ref. [80] for the case of net baryon number fluctuation. In Ref. [81] it has been claimed that, within the regime of thermodynamics, the ratio of the event-by-event fluctuations of entropy and energy is given by

$$R_e = \frac{(\delta S)^2 / S^2}{(\delta E)^2 / E^2} = \frac{1}{(1 + C_s^2)^2}, \tag{2.1}$$

and hence provides an estimate of the speed of sound, if R_e turns out to be measurable in heavy-ion collisions. It has also been suggested that using the idea of conical flow an average value of C_s can be extracted from the RHIC data on di-hadron azimuthal correlations [82].

In this chapter we propose a method to obtain C_V and C_s from LQCD simulations. After introducing the method, in this chapter we determine the continuum limit of these quantities in pure $SU(3)$ gauge theory.

2.2 Formalism

The specific heat at constant volume (C_V) and the speed of sound (C_s) are defined as

$$C_V = \left.\frac{\partial \epsilon}{\partial T}\right|_V, \qquad \text{and} \tag{2.2a}$$

$$C_s^2 \equiv \left.\frac{\partial P}{\partial \epsilon}\right|_s = \left.\frac{\partial P}{\partial T}\right|_V \left(\left.\frac{\partial \epsilon}{\partial T}\right|_V\right)^{-1} = \frac{s/T^3}{C_V/T^3}, \tag{2.2b}$$

where we have used the thermodynamic identity of Eq. [1.30].

In order to make a lattice determination of C_V and C_s, first one needs the appropriate lattice expressions for these quantities. It turns out [68] that a naive application of the temperature derivative of Eq. [1.20] to the expression for ϵ in Eq. (1.21a) gives an incorrect lattice expression for C_V. Below we, first, demonstrate this fact and then propose a modification to get the appropriate lattice expression for C_V.

To lighten the subsequent formulæ we define the following functions (see Eq. [1.21])—

$$F(\xi, a) = \frac{\Delta a^4}{6N_c\xi} = a\left[\frac{\partial K_s}{\partial a}D_s + \frac{\partial K_\tau}{\partial a}D_\tau\right], \quad \text{and} \tag{2.3a}$$

$$G(\xi, a) = \frac{-\epsilon a^4}{6N_c\xi} = \xi\left[\frac{\partial K_s}{\partial \xi}D_s + \frac{\partial K_\tau}{\partial \xi}D_\tau\right]. \tag{2.3b}$$

2.2.1 Naive derivative

Applying the lattice version of the temperature derivative of Eq. [1.20] on the expression of ϵ in Eq. [2.3] one gets

$$a^4 T\left(\frac{\partial \epsilon}{\partial T}\right)_V = -6N_c\xi\left(G + \xi G'\right), \tag{2.4}$$

where, as before, the prime denotes derivative with respect to ξ. Form the above definition of G it is easy to see that

$$G' = \left(K_s' D_s + K_\tau' D_\tau\right) + \xi\left(K_s'' D_s + K_\tau'' D_\tau\right) + \xi\left(K_s' D_s' + K_\tau' D_\tau'\right). \tag{2.5}$$

Since the plaquettes do not explicitly depend on ξ or a, we can easily take the derivatives above—

$$D_i' = D_i\left\langle S_G'\right\rangle - \left\langle (P_i - P_0) S_G'\right\rangle = -6N_c N_\tau N_s^3\left(K_s'\sigma_{s,i} + K_\tau'\sigma_{\tau,i}\right), \tag{2.6a}$$

$$\begin{aligned}\frac{\partial D_i}{\partial a} &= D_i\left\langle\frac{\partial S_G}{\partial a}\right\rangle - \left\langle (P_i - P_0)\left(\frac{\partial S_G}{\partial a}\right)\right\rangle \\ &= -6N_c N_\tau N_s^3\left[\frac{\partial K_s}{\partial a}\sigma_{si} + \frac{\partial K_\tau}{\partial a}\sigma_{\tau i}\right].\end{aligned} \tag{2.6b}$$

where $\sigma_{s,i} = \langle D_s D_i \rangle - \langle D_s \rangle \langle D_i \rangle$ and $\sigma_{\tau,i} = \langle D_\tau D_i \rangle - \langle D_\tau \rangle \langle D_i \rangle$ are the variances and covariances of the plaquettes.

Besides the derivatives of the plaquettes (D_i 's), one also requires the derivatives of the couplings K_i 's. The first derivatives of the couplings are given by Eq. [1.24]. Using Eqs. [1.22, 1.23], one can also compute all possible second derivatives—

$$
\begin{aligned}
a\frac{\partial K_s'}{\partial a} &= -\frac{B(\alpha_s)}{2\pi\alpha_s^2\xi^2}, && \text{(2.7a)}\\
K_s'' &= \frac{2g_s^{-2}}{\xi^3} - \frac{2c_s'}{\xi^2} + \frac{c_s''}{\xi}, && \text{(2.7b)}\\
a^2\frac{\partial^2 K_s}{\partial a^2} &= -\frac{B(\alpha_s)}{2\pi\alpha_s^2\xi} = -a\frac{\partial K_s}{\partial a}, && \text{(2.7c)}\\
a\frac{\partial K_\tau'}{\partial a} &= \frac{B(\alpha_s)}{2\pi\alpha_s^2}, && \text{(2.7d)}\\
K_\tau'' &= 2c_\tau' + \xi c_\tau'', && \text{(2.7e)}\\
a^2\frac{\partial^2 K_\tau}{\partial a^2} &= -\frac{\xi B(\alpha_s)}{2\pi\alpha_s^2} = -a\frac{\partial K_\tau}{\partial a}. && \text{(2.7f)}
\end{aligned}
$$

Putting all these pieces together, in the isotropic limit $\xi \to 1$, one gets

$$
\begin{aligned}
\frac{C_V}{T^3} &= 6N_cN_\tau^4\left[\frac{D_s - D_\tau}{g^2} - (c_s'D_s + c_\tau'D_\tau)\right]\\
&- 6N_cN_\tau^4\left[\frac{D_s + D_\tau}{g^2} - c_s'D_s + 3c_\tau'D_\tau + c_s''D_s + c_\tau''D_\tau\right]\\
&+ 36N_c^2N_\tau^5N_s^3\left[\frac{\sigma_{s,s} + \sigma_{\tau,\tau} - 2\sigma_{s,\tau}}{g^4} + \frac{2(c_\tau'\sigma_{\tau,\tau} + c_s'\sigma_{s,\tau} - c_s'\sigma_{s,s} - c_\tau'\sigma_{s,\tau})}{g^2}\right]\\
&+ 36N_c^2N_\tau^5N_s^3\left[{c_s'}^2\sigma_{s,s} + {c_\tau'}^2\sigma_{\tau,\tau} + 2c_s'c_\tau'\sigma_{s,\tau}\right]. \qquad \text{(2.8)}
\end{aligned}
$$

A correct expression for C_V must satisfy the proper ideal gas limit, *i.e.* one must get the relation $C_V/T^3 = 4\epsilon/T^4$ in the ideal gas limit. In the ideal gas limit $T \to \infty$, which in turn means that $g(T) \to 0$ by asymptotic freedom. Since the renormalized coupling goes to zero, one also expects that the bare coupling g also goes to zero in the ideal gas limit. Hence one can take the ideal gas limit of the above expression by sending the bare coupling $g \to 0$. It is known [83] that in the weak-coupling limit ($g \to 0$) the dominant contribution to all plaquettes varies as

g^2. Hence, in the $g \to 0$ limit $D_i \sim g^2$ and $\sigma_{i,j} \sim g^4$. Based on these information it is clear that the above expression does not satisfy the correct ideal gas limit, *i.e.* $C_V/T^3 \neq 4\epsilon/T^4$ as $g \to 0$ (see Eq. [1.25a] for the expression of ϵ/T^4).

2.2.2 Correct expressions

The reason behind the failure of the naive application of the temperature derivative is as follows— for an anisotropic lattice one has two dimensional variables a_s and a_τ. For convenience, one trades these two dimensional variables in terms of a dimensionless variable ξ and a dimensional variable a. Hence the dimensions of both T and V come from powers of a alone. Application of the temperature derivative, which contains only the dimensionless variable ξ (see Eq. [1.20]), therefore sees inadequate scalings of T and V. Thus if one chooses a quantity which is dimensionless in units of a, like the partition function $\mathcal{Z}$, then derivative of that quantity will not see any false dimensional scaling coming from powers of a. For this purpose we choose the dimensionless quantity

$$\mathcal{C} = \frac{\Delta}{\epsilon} = -\frac{F}{G}. \tag{2.9}$$

We also define

$$\Gamma = T \left.\frac{\partial \mathcal{C}}{\partial T}\right|_V . \tag{2.10}$$

Then, using Eqs. [2.2, 2.10] one can proceed straightaway to write

$$\frac{C_V}{T^3} = \left(\frac{\epsilon/T^4}{P/T^4}\right)\left[\frac{s}{T^3} + \frac{\Gamma}{3}\frac{\epsilon}{T^4}\right], \qquad \text{and} \tag{2.11a}$$

$$C_s^2 = \left(\frac{P/T^4}{\epsilon/T^4}\right)\left[1 + \frac{\Gamma\epsilon/T^4}{3s/T^3}\right]^{-1}. \tag{2.11b}$$

In order to complete these expressions, one needs to express Γ in terms of quantities computable on the lattice. From Eqs. [2.10, 2.9] one finds that

$$\Gamma = -\frac{T}{G}\left.\frac{\partial F}{\partial T}\right|_V + \frac{TF}{G^2}\left.\frac{\partial G}{\partial T}\right|_V . \tag{2.12}$$

Again from the form of the lattice derivative, Eq. [1.20], it is clear that one needs to find the quantities—

$$F' = a\left[\frac{\partial K'_s}{\partial a}D_s + \frac{\partial K'_\tau}{\partial a}D_\tau\right] + a\left[\frac{\partial K_s}{\partial a}D'_s + \frac{\partial K_\tau}{\partial a}D'_\tau\right], \tag{2.13}$$

and G', which is given by Eq. [2.5]. With the help of Eq. [2.6, 2.7] it is easy to see that in the $\xi \to 1$ limit—

$$\begin{aligned} F' &= \frac{B(\alpha_s)}{2\pi\alpha_s^2}\left[D_\tau - D_s\right] \\ &- 6N_cN_\tau N_s^3\frac{B(\alpha_s)}{2\pi\alpha_s^2}\left[\frac{\sigma_{\tau,\tau}-\sigma_{s,s}}{g^2} + c'_s\sigma_{s,s} + c'_\tau\sigma_{\tau,\tau} + (c'_s+c'_\tau)\sigma_{s,\tau}\right], \qquad (2.14a) \\ G' &= \frac{D_s+D_\tau}{g^2} - c'_sD_s + 3c'_\tau D_\tau + c''_sD_s + c''_\tau D_\tau \\ &- 6N_cN_\tau N_s^3\left[\frac{\sigma_{s,s}+\sigma_{\tau,\tau}-2\sigma_{s,\tau}}{g^4} + \frac{2(c'_\tau\sigma_{\tau,\tau}+c'_s\sigma_{s,\tau}-c'_s\sigma_{s,s}-c'_\tau\sigma_{s,\tau})}{g^2}\right] \\ &- 6N_cN_\tau N_s^3\left[{c'_s}^2\sigma_{s,s} + {c'_\tau}^2\sigma_{\tau,\tau} + 2c'_sc'_\tau\sigma_{s,\tau}\right]. \qquad (2.14b) \end{aligned}$$

As argued earlier, $D_i \sim g^2$ and $\sigma_{i,j} \sim g^4$ in the limit $g \to 0$. Thus $F,\ F' \to 0$ but G and G' remain finite, and as a result $\Gamma \to 0$ in this limit. As can be seen form Eq. [2.11], $\Gamma \to 0$ means that $C_V/T^3 = (\epsilon s)/(PT^3)$ and $C_s^2 = P/\epsilon$. Since the in the ideal gas limit $\epsilon = 3P$ and $s/T^3 = 4P/T^4$, in the same limit $C_V/T^3 \to 4\epsilon/T^4$ and $C_s^2 \to 1/3$. This shows that these expressions reproduce the correct ideal gas limits.

2.2.3 Second order derivatives of Karsch coefficients

As can be seen form the above expressions, in order to compute C_V and C_s on the lattice second derivatives of the Karsch coefficients $c_i(\xi)$ are needed. The first order derivatives $c'_i(\xi)$ have been computed to one-loop order in the weak coupling limit for $SU(N_c)$ gauge theories [37]. We have computed these second order derivatives $c''_i(\xi)$ [68].

For an $SU(N_c)$ gauge theory the expressions for $c_s(\xi)$ and $c_\tau(\xi)$ in the weak-

coupling limit are [37]

$$c_s(\xi) = 4N_c\left[\frac{N_c^2-1}{24N_c^2}\left(I_1(\xi)-\frac{3}{4}\right)-\frac{5}{288}I_{2a}(\xi) + \frac{1}{48}I_3(\xi)+\frac{1}{128}I_4(\xi)+\frac{11}{12}FIN(\xi)+0.010245\right], \tag{2.15a}$$

$$c_\tau(\xi) = 4N_c\left[\frac{N_c^2-1}{24N_c^2}\left(\frac{1}{3\xi^2}I_1(\xi)+\frac{1}{\xi}I_5(\xi)-\frac{1}{2}\right)+\frac{1}{64}I_3(\xi)-\frac{5}{576}I_{2a}(\xi) + \frac{1}{256\xi^2}I_4(\xi)-\frac{1}{48\xi^2}I_6(\xi)-\frac{1}{192\xi^2}I_7(\xi)+\frac{11}{12}FIN(\xi)+0.010245\right]. \tag{2.15b}$$

Here $b^2 = \sin^2 x_1 + \sin^2 x_2 + \sin^2 x_3$, and

$$I_1(\xi) = \xi\left(\frac{2}{\pi}\right)^3\int d^3x b(\xi^2+b^2)^{-1/2}, \tag{2.16a}$$

$$I_{2a}(\xi) = \xi\left(\frac{2}{\pi}\right)^3\int d^3x b^{-1}(\xi^2+2b^2)(\xi^2+b^2)^{-3/2}, \tag{2.16b}$$

$$I_{2b}(\xi) = \xi^3\left(\frac{2}{\pi}\right)^3\int d^3x \left[b(\xi^2+b^2)^{1/2}\left(b+(\xi^2+b^2)^{1/2}\right)^2\right]^{-1}, \tag{2.16c}$$

$$I_3(\xi) = \xi\left(\frac{2}{\pi}\right)^3\int d^3x \sin^2 x_1 \sin^2 x_2 \frac{\xi^2+2b^2}{b^3(\xi^2+b^2)^{3/2}}, \tag{2.16d}$$

$$I_4(\xi) = \xi\left(\frac{2}{\pi}\right)^3\int d^3x \sin^2 2x_1 \frac{\xi^2+2b^2}{b^3(\xi^2+b^2)^{3/2}}, \tag{2.16e}$$

$$I_5(\xi) = \xi^2\left(\frac{2}{\pi}\right)^3\int d^3x (\xi^2+b^2)^{-1/2}\left[b+(\xi^2+b^2)^{1/2}\right]^{-1}, \tag{2.16f}$$

$$I_6(\xi) = \xi^3\left(\frac{2}{\pi}\right)^3\int d^3x b^{-1}(\xi^2+b^2)^{-3/2}\cos^2 x_1, \tag{2.16g}$$

$$I_7(\xi) = \xi^3\left(\frac{2}{\pi}\right)^3\int d^3x b^{-1}(\xi^2+b^2)^{-3/2}. \tag{2.16h}$$

Limits of all the above integrals are $[0, \pi/2]$. Also—

$$DIV(\xi) = \frac{1}{(2\pi)^4}\int\int_{-\pi/2}^{\pi/2}\int d^3x \int_{-\pi\xi/2}^{\pi\xi/2} dx_4 \left[b^2+\xi^2\sin^2(x_4/\xi)\right]^{-2}, \tag{2.17a}$$

$$FIN(\xi) = DIV(\xi) - DIV(1). \tag{2.17b}$$

The integral $DIV(\xi)$ is infrared divergent. However, what actually needed here is $FIN(\xi)$. $FIN(\xi)$ is not divergent as it is constructed by subtracting the

	Integrals	1-st derivatives	2-nd derivatives
I_1	0.750000	0.440133	-0.518412
I_{2a}	0.929600	0.208546	-0.663270
I_{2b}	0.119734	0.190133	0.030921
I_3	0.103289	0.033774	-0.088777
I_4	0.478934	0.065779	-0.262319
I_5	0.250000	0.309867	-0.101321
I_6	0.206578	0.238384	-0.146561
I_7	0.309867	0.411188	-0.159106
FIN	0.0	0.003166	-0.014471

Table 2.1: Values of the integrals $I_x(\xi)$'s and $FIN(\xi)$ and their derivatives with respect to ξ at $\xi = 1$.

integral $DIV(1)$, having the same infrared divergence as that of $DIV(\xi)$. The derivatives of $FIN(\xi)$ are just the derivatives of $DIV(\xi)$ which are not divergent. We have calculated $FIN''(1)$ by direct numerical integration and also by taking a derivative of $FIN'(\xi)$, at $\xi = 1$, numerically. We found that values obtained from both the methods are consistent.

The numerical values of all these above integrals and their derivatives with respect to ξ, at $\xi = 1$, are tabulated in Table [2.1]. Using these values we obtain ξ derivatives of the Karsch coefficients at $\xi = 1$

$$c_s' = 4N_c\left[\frac{N_c^2-1}{32N_c^2}0.586844 + 0.000499\right], \tag{2.18a}$$

$$c_s'' = 4N_c\left[\frac{1-N_c^2}{32N_c^2}0.691216 - 0.005649\right], \tag{2.18b}$$

$$c_\tau' = 4N_c\left[\frac{1-N_c^2}{32N_c^2}0.586844 + 0.005306\right], \tag{2.18c}$$

$$c_\tau'' = 4N_c\left[\frac{N_c^2-1}{32N_c^2}1.038595 - 0.001044\right]. \tag{2.18d}$$

While the $c_i''(\xi)$'s are computed by us, our values for all the integrals and their first derivatives as well as the regular Karsch coefficients match with their respective values mentioned in Ref. [37].

2.2.4 On the method

The formalism outlined in the previous section is based on the differential method. As discussed in Chapter [1], this method requires the use of perturbative couplings. On the other hand, the integral method evades this problem relying on the assumption of homogeneity (see Chapter [1] for details). If the EoS were to be evaluated by the integral method then C_V and C_s can only be evaluated by numerical differentiation, which is prone to large errors [84]. Moreover, since the pure gauge phase transition in QCD is of first order, the system is not homogeneous at T_c and the method may not be applicable there. Thus one makes an unknown systematic error in integrating through T_c. This is in addition to a small systematic error due to setting $P = 0$ just below T_c and the numerical integration errors.

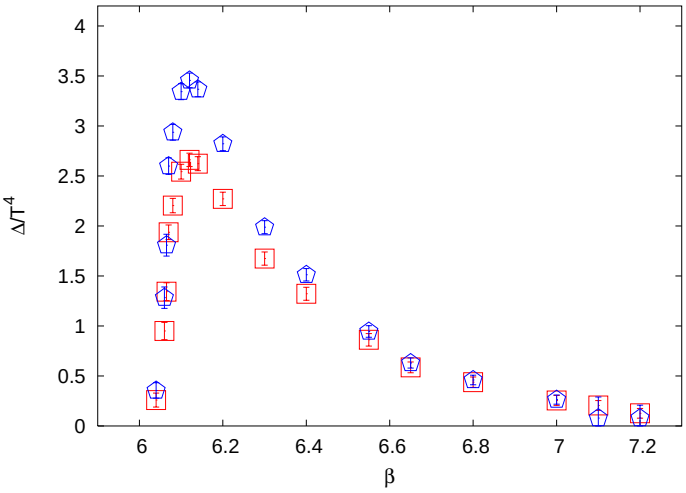

Figure 2.1: Δ/T^4 as a function of the bare coupling β using a non-perturbative (squares) [55] and the one-loop order perturbative (pentagons) β-function, $B(\alpha_s)$. The results agree for $\beta \geq 6.5$. The plaquette values for $N_\tau = 8$ given Ref. [55] have been used in this analysis.

Two methods must agree if one uses sufficiently small lattice spacings, *viz.* when the use of perturbative couplings is justified, in the differential method computation. A reanalysis of the data of Ref. [55] showed that the two methods agreed to within 5% (*i.e.* within statistical errors) for $T \geq 2T_c$ [51] already for $N_\tau = 8$, *i.e.* for $a = 1/16T_c$. In fact a criterion for the agreement is straightforward, and follows from the fact the expression for Δ/T^4 (see Eqs. [1.25c, 1.33]) is common to both the methods. Since the integral method does not need the Karsch coefficients, it allows one to use a non-perturbatively determined β-function $B(\alpha_s)$. On the other hand, the differential method requires, for internal consistency, that the Karsch coefficients and $B(\alpha_s)$ be obtained at the same order, *i.e.* at one-loop order in the present state of the art.

Thus, a comparison between the values of Δ/T^4 extracted for a given N_τ using the two techniques would reveal at what T the two methods become identical. Then, using asymptotic scaling, one could also give the minimum value of N_τ which would be required for the same level of agreement as a function of T. Such a comparison is shown in Fig. [2.1], which demonstrates that a bare coupling of $\beta \geq 6.55$ already suffices.

2.3 Simulation details

The simulations have been performed using the Cabbibo-Marinari pseudo-heatbath [85] algorithm with Kennedy-Pendleton updating [86] of three $SU(2)$ subgroups on each sweep. Plaquettes were measured on each sweep. For each simulation we discarded around 5000 initial sweeps for thermalization. We found that integrated autocorrelation time for the plaquettes never exceeded 3 sweeps. In Table [2.2] we give the details of our runs. All errors were calculated by the jack-knife method, where the length of each deleted block was chosen to be at least six times the maximum integrated autocorrelation time of all the simulations used for that calculation.

T/T_c	β	Asymmetric Lattice		Symmetric Lattice	
		size	stat.	size	stat.
2.0	6.0625	4×8^3	60000	22^4	38000
		$\times 10^3$	56000		
		$\times 12^3$	50000		
		$\times 14^3$	51000		
		$\times 16^3$	51000		
	6.5500	8×18^3	1100000	12^4	800000
				16^4	626000
				18^4	802000
				22^4	552000
				32^4	330000
	6.7500	10×22^3	1100000	22^4	969000
	6.9000	12×26^3	1040000	26^4	550000
	7.0000	14×30^3	425000	30^4	146000
3.0	6.3384	4×10^3	220000	22^4	75000
		$\times 12^3$	200000		
		$\times 16^3$	200500		
		$\times 20^3$	210000		
		$\times 22^3$	150000		
	7.0500	10×32^3	560000	32^4	146000
	7.2000	12×38^3	315000	38^4	58000

Table 2.2: The coupling (β), lattice sizes ($N_\tau \times N_s^3$), statistics and symmetric lattice sizes (N_s^4) are given for each temperature. Statistics means number of sweeps used for measurement of plaquettes after discarding for thermalization.

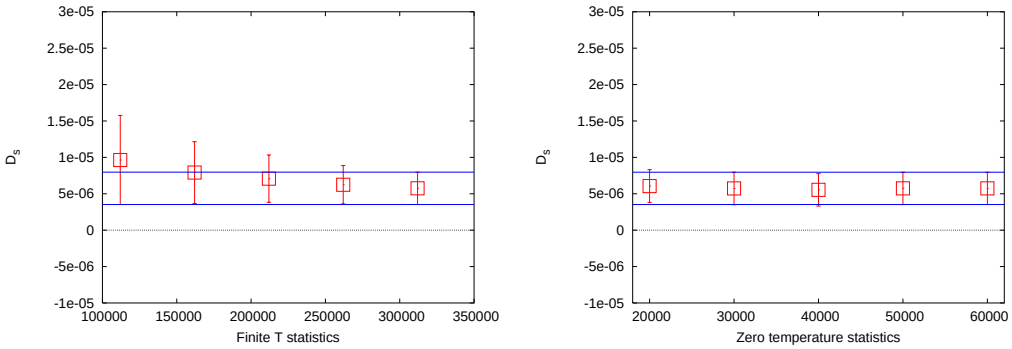

(a) (b)

Figure 2.2: Stability of D_s against the statistics in $T > 0$ (a) and $T = 0$ (b) simulations. The coupling corresponds to $3T_c$ on a 12×38^3 lattice and the corresponding $T = 0$ simulation was performed on a 38^4 lattice. In both the figures we have also plotted the 1-σ error band of the final errors.

2.3.1 Stability against statistics

Of all the quantities which go into determining the equation of state, *viz.* D_s, D_τ and $(D_s - D_\tau)$, we found that D_s was the smallest. Hence control over the errors of D_s was the most stringent requirement on the amount of statistics needed. In Fig. [2.2] we show the stability of D_s against the finite temperature and zero temperature statistics for the case where we have minimum statistics, *viz.* for the $3T_c$ run on the 12×38^3 lattice and the run at the same coupling on the 38^4 lattice. Note that the plaquette values are of the order of unity, and the first four digits cancel in computing D_s. Thus, the control over errors shown in Fig. [2.2] was due to reducing the errors in the plaquette variables to a few parts per million.

2.3.2 Volume dependence

We checked the stability of D_s against the spatial size of the $T > 0$ lattice. Fig. [2.3a] displays the dependence of D_s on N_s for $N_\tau = 4$ when the temperature is $2T_c$ and the symmetric lattice size is 22^4. We have also shown a fit to a constant using the data on the three largest lattices. These fits pass through the data collected on the $N_s = (T/T_c)N_\tau + 2$ lattice. We have checked that this condition holds for $3T_c$ also. This observation is consistent with the results of earlier investigation of

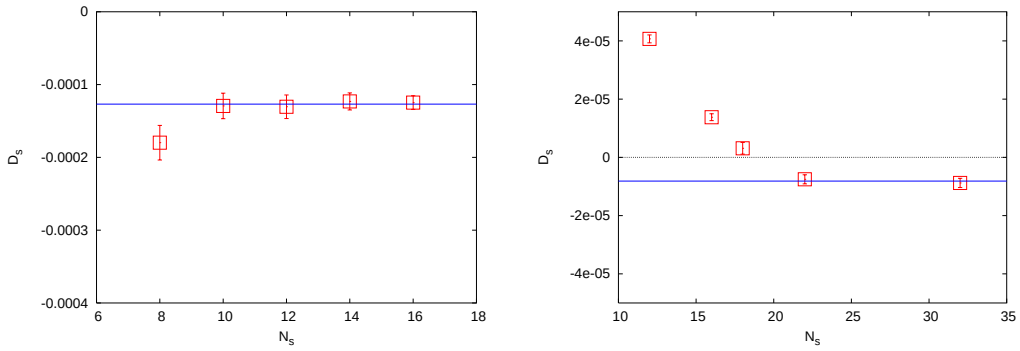

(a) (b)

Figure 2.3: (a) Dependence of D_s against the spatial size, N_s, of the $T > 0$ lattice for $2T_c$ and 22^4 lattice for the $T = 0$ computation. We have shown a fit to a constant through the three largest lattices. (b) Dependence of D_s on N_s for the $T = 0$ lattice when the $2T_c$ computation is performed on an 8×18^3 lattice. A fit to a constant with the two largest sizes is also shown.

finite size effects for $T > 0$ [87] and motivated our choice of $N_s = (T/T_c)N_\tau + 2$.

We also investigated the dependence of D_s on the size of the symmetric N_s^4 lattice used for the $T = 0$ subtraction. Fig. [2.3b] exhibits the dependence of D_s on N_s for a run at $2T_c$ on a 8×18^3 lattice. D_s is seen to be constant for $N_s \geq 22$. In view of this we have used 22^4 as our minimum $T = 0$ lattice size, and scaled this up with changes in the lattice spacing.

2.3.3 Plaquette covariances

N_τ	$V\sigma_{s,s}$	$V\sigma_{\tau,\tau}$	$V\sigma_{s,\tau}$
10	0.08 ± 0.1	0.08 ± 0.1	0.04 ± 0.07
12	0.1 ± 0.2	0.1 ± 0.3	0.1 ± 0.2
14	0.1 ± 0.2	0.1 ± 0.2	0.1 ± 0.2

Table 2.3: Contributions of different covariances, with their respective errors, are tabulated for different N_τ at $2T_c$. This shows all the contributions are negligible.

We evaluated the contributions of the terms containing different covariances of

the plaquettes and found them to be negligible, as shown in Table [2.3]. It is worth noting that a previous computation close to T_c, but in $SU(2)$ pure gauge theory, found significantly larger and clearly non-vanishing variances of the plaquettes [88]. This suggests that the variance terms might make significant contributions to the specific heat and speed of sound closer to the softest point of the EoS.

2.4 Results

Following the observation illustrated in Fig. [2.1], all our continuum extrapolations have been done with lattice spacings which are smaller than that at $\beta = 6.55$. For $T = 2T_c$ this leaves three values of N_τ from which a continuum extrapolation linear in $a^2 \propto 1/N_\tau^2$ can be performed (as discussed in Chapter [1]). However, at $T = 3T_c$, the continuum extrapolation has been performed with two values of N_τ. This completely fixes the two parameters of the linear extrapolation and the error in the continuum extrapolated value is by definition zero. In this case the error in the continuum value was estimated by three methods. Two of these consisted of first making the best fit using two parameters, and then keeping one fixed while allowing the other to vary in order to make an estimate of the error in that parameter. We also made extrapolations using the upper end of one error bar and the lower end of the other. This last procedure gave the maximum errors in the continuum extrapolated values, and we choose to quote this, since it is the most conservative error estimate.

As mentioned in Chapter [1], the energy density (ϵ) and pressure (P) can be computed using Eq. [1.25]. In Fig. [2.4] we present our continuum extrapolations for ϵ and P using the differential method, which have not been used earlier to obtained the continuum results for the EoS. At $3T_c$ the continuum limit values of ϵ/T^4 and P/T^4 differ from their respective ideal gas values ($8\pi^2/15$ and $8\pi^2/45$) by about 24%, and by about 40% at $2T_c$. This is consistent with previous measurements of the equation of state at these temperatures. At $2T_c$ our results differ from the ideal gas value by almost 7-σ.

Similar continuum extrapolation of C_V/T^3 and C_s^2 are shown in Fig. [2.5]. Fig. [2.6] shows the continuum extrapolated results for these quantities. Continuum extrapolated values of different quantities for two temperatures are tabulated in

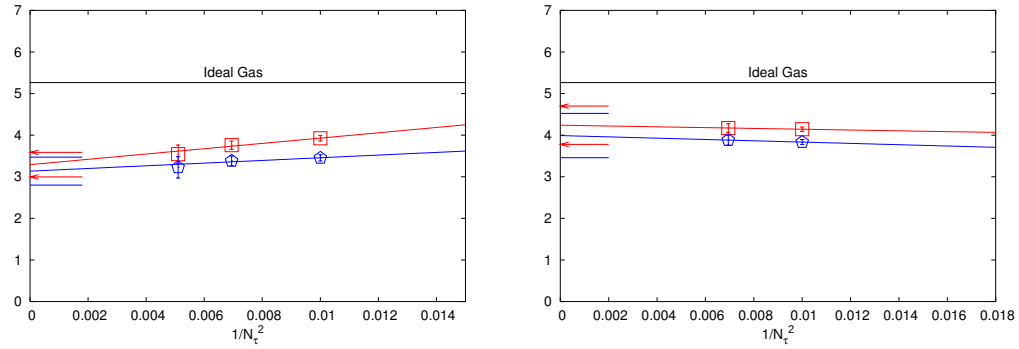

(a) (b)

Figure 2.4: Dependence of ϵ/T^4 (squares) and $3P/T^4$ (pentagons) on $1/N_\tau^2$ for $T = 2T_c$ (a) and $T = 3T_c$ (b). The 1-σ error band of the continuum values has been indicated by arrows (for ϵ/T^4) and lines (for $3P/T^4$).

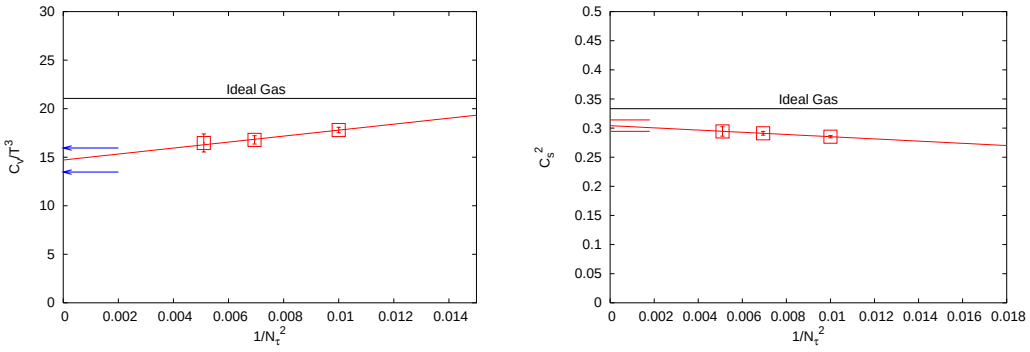

(a) (b)

Figure 2.5: Dependence of C_V/T^3 (a) and C_s^2 (b) on $1/N_\tau^2$ at $T = 2T_c$. The 1-σ error band of the continuum values has been indicated by the arrows.

T/T_c	ϵ/T^4	P/T^4	s/T^3	C_V/T^3	C_s^2
2.0	3.3 (3)	1.0 (1)	4.2 (3)	15 (1)	0.30 (1)
3.0	4.2 (5)	1.3 (2)	5.6 (6)	18 (2)	0.30 (2)

Table 2.4: Continuum values of some quantities at the two temperatures we have explored. The numbers in brackets are the error on the least significant digit.

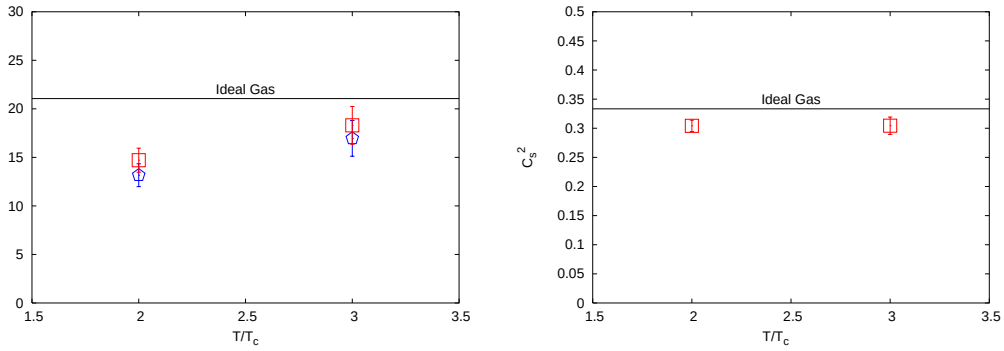

(a) (b)

Figure 2.6: (a) We show the continuum values of $4\epsilon/T^4$ (pentagons) and C_V/T^3 (squares) against T/T_c. (b) We show the temperature dependence of the continuum extrapolated values of C_s^2.

Table [2.4]. It can be seen that although ϵ/T^4 and P/T^4 differ significantly from their ideal gas values, C_s^2 is quite close to 1/3, being within 2-3 σ. Similarly, it can be seen that C_V/T^3 is completely compatible with $4\epsilon/T^4$. However, its deviation from the ideal gas value is seen to be more significant.

2.5 Discussion

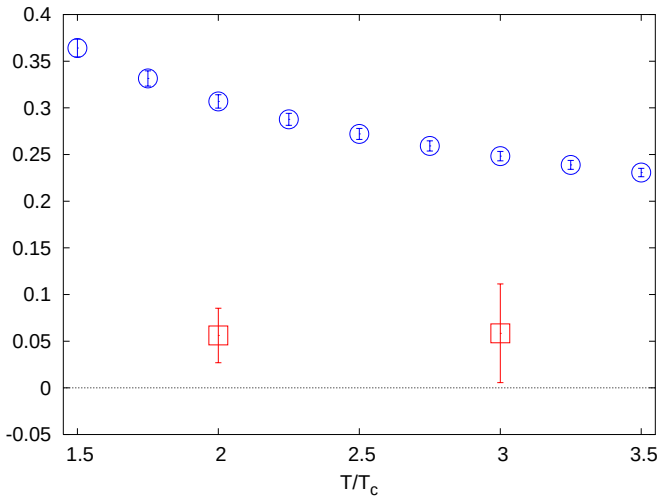

Figure 2.7: Continuum values of the conformal measure, $\mathcal{C}$, (squares) and the negative of the one-loop order β-function (circles) evaluated at the scale $2\pi T$

It is quite remarkable that while ϵ, P and C_V deviate significantly from their respective ideal gas values, C_s is pretty close to its ideal gas limit. Moreover, the ideal gas relation $C_V/T^3 = 4\epsilon/T^4$ seems to hold even for $T \sim 2T_c$. Below, we will try to give a possible explanation for this apparently contradictory behaviour of QCD plasma.

It is common knowledge that QCD generates a scale (Λ_{QCD}), microscopically, and thus breaks conformal invariance. The strength of the breaking of this symmetry at any scale is parametrized by the β-function. At finite temperature there is a scale, T, which appears in, for example, ϵ as a factor of T^4. However, the strength of the breaking of conformal symmetry must be measured as always, through the trace of the stress-tensor. After subtracting the ultraviolet divergent ($T = 0$) pieces, this is given by the so-called interaction measure, $\Delta = \epsilon - 3P$. Thus the ratio $\mathcal{C} = \Delta/\epsilon$, which we call the *conformal measure*, parametrizes the departure from conformal invariance at the long-distance scale. Note that in any conformal invariant theory in $d+1$ dimensions one has $\epsilon = d \cdot P$, *i.e.* $\mathcal{C} = \Gamma = 0$, and hence, by Eq. [2.11], $C_s^2 = 1/d$ and $C_V/T^3 = (d+1)\epsilon/T^4$. We show our continuum results for $\mathcal{C}$ in Fig. [2.7]. As the generation of a scale and the consequent breaking of conformal invariance at short distances in QCD is quantified by the β-function of QCD and at long distance in the finite temperature plasma by the conformal measure $\mathcal{C}$, in the same figure we also compare these two quantities. The smallness of the conformal measure $\mathcal{C}$ suggest that the plasma phase is not far from the conformal symmetric limit, in which $C_s^2 = 1/3$ and $C_V/T^3 = 4\epsilon/T^4$ (for $3+1$ dimensions).

2.6 Summary

In this chapter we have extended the differential method for the computation of the specific heat at constant volume and the speed of sound, and computed them in the continuum limit of the pure gluon plasma. We have limited our computations to lattice spacings where the method is guaranteed to work because of the observed scaling of results with the correct QCD beta function, as shown in Fig. [2.1]. The main advantage of this method is the relatively noise-free determination of C_s and C_V. In the process we have also recomputed the EoS,

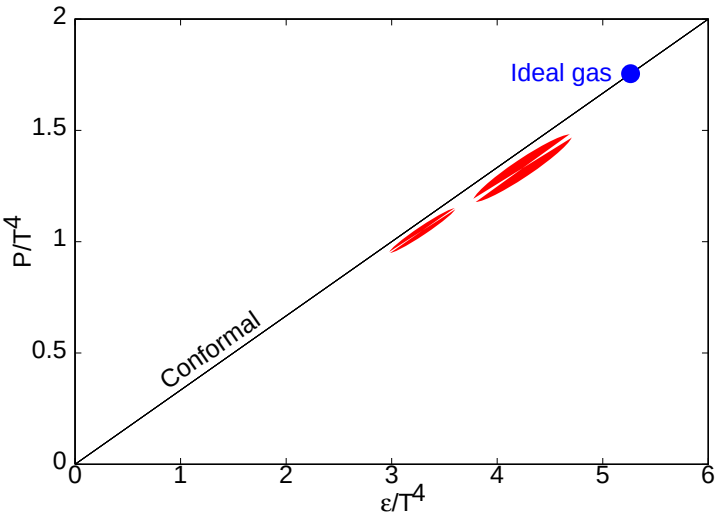

Figure 2.8: The equation of state of QCD matter. The diagonal line denotes possible EoS for theories with conformal symmetry. The circle on the diagonal denotes the ideal gluon gas, whose EoS in this form is temperature independent. The ellipses denote 66% error bounds on the measured EoS. The ratio of the axes is a measure of the covariance in the measurements of ϵ/T^4 and P/T^4, which is about 90%. The wedges piercing these ellipses have average slope C_s^2, and the opening half-angle of these wedges indicate the error in C_s^2.

i.e. the pressure P and the energy density ϵ by a method which has not been used earlier to obtain the continuum limit. Based on our results we have also argued that the plasma phase is not far from the conformal symmetric limit.

A partial summary of our results is illustrated by plotting the equation of state as P/T^4 against ϵ/T^4, as in Fig. [2.8]. In this plot, the ideal gas for fixed number of colours is represented by a single point, and theories with conformal symmetry by the line $\epsilon = 3P$. Pure gauge QCD lies close to the conformal line at high temperature, as shown. One expects the EoS to drop well below this line near T_c, since the theory then contains massive hadrons (glueballs in pure gluon QCD) with masses in excess of T_c. Thus one expects the origin to be approached almost horizontally as $T \to 0$. We will present data closer to, and below, T_c in the next chapter.

Chapter 3

EoS of QCD: improving the differential method

3.1 Introduction

In the previous chapter we used the differential method to determine the specific heat at constant volume (C_V) and the speed of sound (C_s). Since the differential method is known to produce negative pressure in the vicinity of the transition temperature (T_c) [57], we had to restrict our investigation to the high temperature region where the method gives correct results (see Chapter [2] for details). But more interesting physics is expected around the phase transition region. Hence a precise computation of these quantities close to T_c is necessary. A computation of C_V and C_s close to T_c using the differential method is thus desirable. But in order to do so, first, one has to improve the differential method so that it can be used in the vicinity of T_c.

The negativity of pressure in the differential method has been attributed solely to the use of perturbative formulae for various derivatives of the coupling. Hence it was believed that this problem could be remedied if one goes to small enough lattice spacing. However, we found that [69] even when one determines the continuum limit of the pressure, using temporal lattices upto $N_\tau = 12$, the negative pressure problem of the differential method still persists. One does not have this negative pressure problem in the integral method. However, as discussed in Chapter [2], the integral method has the practical drawback that a fluctuation

measure like C_V can only be obtained by numerical differentiation, which is prone to large errors.

In view of this, in this chapter we propose a new variant of the differential method which gives positive pressure over the entire temperature range. We choose the temporal lattice spacing to set the scale of the theory, in contrast to the choice of the spatial lattice spacing in the approach of Ref. [36] (see Chapter [1] for the details). This change of scale is analogous to the use of different renormalization schemes. As a consequence, our method could be called the *t-favoured scheme* [69] and the method of Ref. [36] may be called the *s-favoured scheme*. This choice of scale has already been used in Ref. [89]. What we show here is that with this choice one gets a positive pressure for the entire temperature range, even when one uses one-loop order perturbative couplings. Since the operator expressions are derived with an asymmetry between the two lattice spacings a_s and a_τ, the s-favoured and t-favoured schemes give different expressions for the pressure. In that sense the use of t-favoured scheme is tantamount to the use of improved operators. Being a differential method the t-favoured scheme can be easily extended for the calculation of C_V and C_s, following exactly the same formalism developed in Chapter [2] and Ref. [68].

3.2 Formalism

From the relations of Eq. [1.7], one can write the lattice version of the temperature and the volume derivatives as

$$T\,\frac{\partial}{\partial T}\bigg|_V = -a_\tau\,\frac{\partial}{\partial a_\tau}\bigg|_{a_s}, \qquad \text{and} \qquad 3V\,\frac{\partial}{\partial V}\bigg|_T = a_s\,\frac{\partial}{\partial a_s}\bigg|_{a_\tau}. \tag{3.1}$$

In the t-favoured scheme one trades the thermodynamic variables $\{T, V\}$ in favour of the the lattice variables $\{\xi, a\}$, where the the anisotropy parameter ξ and the scale a are given by the relations

$$\xi = \frac{a_s}{a_\tau}, \qquad \text{and} \qquad a = a_\tau. \tag{3.2}$$

With these choices, the partial derivatives with respect to T and V now become

$$T\,\frac{\partial}{\partial T}\bigg|_V = \xi\,\frac{\partial}{\partial \xi}\bigg|_a - a\,\frac{\partial}{\partial a}\bigg|_\xi, \qquad \text{and} \qquad 3V\,\frac{\partial}{\partial V}\bigg|_T = \xi\,\frac{\partial}{\partial \xi}\bigg|_a. \tag{3.3}$$

One obtains the second expression by writing $a_s = a\xi$ and taking a partial derivative keeping a fixed. For the first expression, one takes a derivative with respect to a and then introduces constraints on the differentials $d\xi$ and da in order to keep a_s fixed. This choice of scale $a = a_\tau$ seems to be natural, since most numerical work at finite temperature sets the scale by $T = 1/N_\tau a_\tau$. For example, continuum limits are taken at fixed physics by keeping T fixed while increasing N_τ, *i.e.* decreasing a_τ. This is done not only when isotropic lattices are used, but also when the simulation is performed with anisotropic lattices [90].

In the s-favoured scheme [36], by contrast, the scale of the theory is set by the spatial lattice spacing, $a = a_s$, at every ξ and only after taking the $\xi \to 1$ limit this natural choice of scale emerges. The corresponding derivatives in this case are given in Eq. [1.20].

3.2.1 Energy density and pressure

The energy density (ϵ) and pressure (P) are given by Eq. [1.17], where the gauge action S_G and the corresponding partition function $\mathcal{Z}$ are given Eq. [1.11] and Eq. [1.18]. One can then proceed, as in the s-favoured case presented in Chapter [1], by using the derivatives of Eq. [3.3] to derive lattice expressions for ϵ, P and Δ in the t-favoured scheme—

$$a^4\epsilon = -\frac{6N_c}{\xi^2}\left[K_s' D_s + K_\tau' D_\tau\right] + \frac{6N_c a}{\xi^3}\left[\frac{\partial K_s}{\partial a} D_s + \frac{\partial K_\tau}{\partial a} D_\tau\right], \tag{3.4a}$$

$$a^4 P = -\frac{2N_c}{\xi^2}\left[K_s' D_s + K_\tau' D_\tau\right], \tag{3.4b}$$

$$a^4\Delta = \frac{6N_c a}{\xi^3}\left[\frac{\partial K_s}{\partial a} D_s + \frac{\partial K_\tau}{\partial a} D_\tau\right]. \tag{3.4c}$$

Here, as before, the primes denote derivatives with respect to ξ. One can further use the expressions in Eq. [1.24] for the derivatives of the couplings K_i 's and take the isotropic limit $\xi \to 1$ to arrive at

$$\frac{\epsilon}{T^4} = 6N_c N_\tau^4\left[\frac{D_s - D_\tau}{g^2} - (c_s' D_s + c_\tau' D_\tau)\right] + 6N_c N_\tau^4 \frac{B(\alpha_s)}{2\pi\alpha_s^2}\left[D_s + D_\tau\right], \tag{3.5a}$$

$$\frac{P}{T^4} = 2N_c N_\tau^4\left[\frac{D_s - D_\tau}{g^2} - (c_s' D_s + c_\tau' D_\tau)\right], \tag{3.5b}$$

$$\frac{\Delta}{T^4} = 6N_c N_\tau^4 \frac{B(\alpha_s)}{2\pi\alpha_s^2}\left[D_s + D_\tau\right]. \tag{3.5c}$$

On comparing these expressions with those obtained using the s-favoured differential method in Eq. [1.25], one can easily see that the new expression for pressure is exactly 1/3 of the old expression for the energy density. Since the energy density in the s-favoured scheme comes out to be non-negative, our new expression for the pressure is therefore expected to give non-negative pressure. The expression for the interaction measure is same for both the cases. Since both the pressure and the interaction measure are non-negative in the t-favoured formalism, the energy density must also be non-negative.

3.2.2 Specific heat and speed of sound

As argued in Chapter [2], a direct application of the lattice version of the temperature derivative on the expression of the energy density produces incorrect expression for the specific heat at constant volume and it can be most easily be obtained by working with the conformal measure $\mathcal{C} = \Delta/\epsilon$. In that case the specific heat (C_V) and the speed of sound (C_s) are given by Eq. [2.11]. To compute C_V and C_s one needs the lattice expression for $\Gamma = T\left(\partial\mathcal{C}/\partial T\right)_V$. To this end we introduce the two functions

$$X(\xi,a) = \frac{\Delta a^4\xi^3}{6N_c} = a\left[\frac{\partial K_s}{\partial a}D_s + \frac{\partial K_\tau}{\partial a}D_\tau\right], \tag{3.6a}$$

$$Y(\xi,a) = \frac{-\epsilon a^4\xi^3}{6N_c} = \xi\left[K_s'D_s + K_\tau'D_\tau\right] - X(\xi,a). \tag{3.6b}$$

Since $\mathcal{C} = -X/Y$, one finds that

$$\Gamma = -\mathcal{C}\frac{T}{X}\left.\frac{\partial X}{\partial T}\right|_V + \mathcal{C}\frac{T}{Y}\left.\frac{\partial Y}{\partial T}\right|_V. \tag{3.7}$$

Form Eq. [3.3] it is clear that we need the following derivatives—

$$\xi\frac{\partial X}{\partial \xi} = \xi a\left[\frac{\partial K_s'}{\partial a}D_s + \frac{\partial K_\tau'}{\partial a}D_\tau\right] + \xi a\left[\frac{\partial K_s}{\partial a}D_s' + \frac{\partial K_\tau}{\partial a}D_\tau'\right], \tag{3.8a}$$

$$\begin{aligned} a\frac{\partial X}{\partial a} &= a\left[\frac{\partial K_s}{\partial a}D_s + \frac{\partial K_\tau}{\partial a}D_\tau\right] + a^2\left[\frac{\partial^2 K_s}{\partial a^2}D_s + \frac{\partial^2 K_\tau}{\partial a^2}D_\tau\right] \\ &+ a^2\left[\frac{\partial K_s}{\partial a}\frac{\partial D_s}{\partial a} + \frac{\partial K_\tau}{\partial a}\frac{\partial D_\tau}{\partial a}\right], \end{aligned} \tag{3.8b}$$

and

$$\xi\frac{\partial Y}{\partial \xi} = \xi\left[K'_s D_s + K'_\tau D_\tau\right] + \xi^2\left[K''_s D_s + K''_\tau D_\tau\right] + \xi^2\left[K'_s D'_s + K'_\tau D'_\tau\right] - \xi\frac{\partial X}{\partial \xi}, \tag{3.9a}$$

$$a\frac{\partial Y}{\partial a} = \xi a\left[\frac{\partial K'_s}{\partial a}D_s + \frac{\partial K'_\tau}{\partial a}D_\tau\right] + \xi a\left[K'_s\frac{\partial D_s}{\partial a} + K'_\tau\frac{\partial D_\tau}{\partial a}\right] - a\frac{\partial X}{\partial a}. \tag{3.9b}$$

Using the expressions for the derivatives of the plaquettes from Eq. [2.6] and the derivatives of the couplings form Eqs. [1.24, 2.7], in the $\xi \to 1$ limit one finally gets

$$\begin{aligned} T\left.\frac{\partial X}{\partial T}\right|_V &= \frac{B(\alpha_s)}{2\pi\alpha_s^2}\left[D_\tau - D_s\right] + 6N_cN_\tau N_s^3\left[\frac{B(\alpha_s)}{2\pi\alpha_s^2}\right]^2\left[\sigma_{ss} + \sigma_{\tau\tau} + 2\sigma_{s\tau}\right]. \\ &- 6N_cN_\tau N_s^3\frac{B(\alpha_s)}{2\pi\alpha_s^2}\left[\frac{\sigma_{\tau\tau} - \sigma_{ss}}{g^2} + c'_s\sigma_{ss} + c'_\tau\sigma_{\tau\tau} + (c'_s + c'_\tau)\sigma_{s\tau}\right], \end{aligned} \tag{3.10a}$$

$$\begin{aligned} T\left.\frac{\partial Y}{\partial T}\right|_V &= \frac{D_s + D_\tau}{g^2} - c'_s D_s + 3c'_\tau D_\tau + c''_s D_s + c''_\tau D_\tau - \frac{B(\alpha_s)}{2\pi\alpha_s^2}\left[D_\tau - D_s\right] - T\left.\frac{\partial X}{\partial T}\right|_V \\ &- 6N_cN_\tau N_s^3\left[\frac{\sigma_{s,s} + \sigma_{\tau,\tau} - 2\sigma_{s,\tau}}{g^4} + \frac{2(c'_\tau\sigma_{\tau,\tau} + c'_s\sigma_{s,\tau} - c'_s\sigma_{s,s} - c'_\tau\sigma_{s,\tau})}{g^2} + {c'_s}^2\sigma_{s,s}\right. \\ &+ \left.{c'_\tau}^2\sigma_{\tau,\tau} + 2c'_sc'_\tau\sigma_{s,\tau} - \frac{B(\alpha_s)}{2\pi\alpha_s^2}\left(\frac{\sigma_{\tau\tau} - \sigma_{ss}}{g^2} + c'_s\sigma_{ss} + c'_\tau\sigma_{\tau\tau} + (c'_s + c'_\tau)\sigma_{s\tau}\right)\right] \end{aligned} \tag{3.10b}$$

As discussed in Section [2.2], taking an ideal gas limit means sending the bare coupling $g \to 0$ and in that limit $D_i \propto g^2$ and $\sigma_{ij} \propto g^4$ [83]. Hence in this limit, X and its temperature derivative are negligible compared to Y and its temperature derivative, and consequently $\Gamma \to 0$ in this limit. It was shown in Section [2.2], that once $\Gamma \to 0$ the correct ideal gas limit of C_V and C_s are automatically reproduced, *i.e.* $C_V/T^3 \to 4\epsilon/T^4$ and $C_s^2 \to 1/3$. Note that in any conformal invariant theory in $d+1$ dimensions one has $\epsilon = dP$, *i.e.* $\mathcal{C} = \Gamma = 0$, and hence by Eq. [2.11] one has $C_s^2 = 1/d$ and $C_V/T^3 = (d+1)\epsilon/T^4$.

3.2.3 Equivalence of the Karsch coefficients in the t-favoured and s-favoured schemes

As can be seen from the Eq. [1.22], the Karsch coefficients $c_i(\xi)$'s are differences between the isotropic and anisotropic couplings. Hence they do not depend on the

scale a of the isotropic lattice, but only depend on a parameter which quantifies the difference between the isotropic and the anisotropic lattice, *i.e.* the anisotropy parameter ξ. Thus a change of scale from a_s to a_τ do not change the Karsch coefficients. Below, we derive this equality explicitly for the derivatives of the Karsch coefficients, which we actually need.

Let us assume that the one-loop order perturbative expansions for g_i^2 's, around the isotropic lattice coupling g, have the following forms [56]

$$g_i^{-2}(a_s,\xi) = g^{-2}(a_s) + c_i(\xi) + \mathcal{O}[g^2(a_s)], \tag{3.11a}$$
$$g_i^{-2}(a_\tau,\xi) = g^{-2}(a_\tau) + \alpha_i(\xi) + \mathcal{O}[g^2(a_\tau)]. \tag{3.11b}$$

Our aim here is to show that $[\partial c_i(\xi)/\partial\xi]_{a_s} = [\partial\alpha_i(\xi)/\partial\xi]_{a_\tau}$. In order to do so we make a Taylor series expansion of $g_i(a_s,\xi)$ around $a_s = a_\tau$, at any fixed $\xi \neq 1$

$$g_i^{-2}(a_s,\xi) = g_i^{-2}(a_\tau,\xi) + \sum_{n=1}^{\infty} \frac{(a_s-a_\tau)^n}{n!} \left[\left. \frac{\partial^n g_i^{-2}(x,\xi)}{\partial x^n} \right|_\xi \right]_{x=a_\tau}. \tag{3.12}$$

So by applying ξ derivative, at constant a_s, on the above relation

$$\left. \frac{\partial g_i^{-2}(a_s,\xi)}{\partial\xi} \right|_{a_s} = \left. \frac{\partial g_i^{-2}(a_\tau,\xi)}{\partial\xi} \right|_{a_s} + \sum_{n=1}^{\infty} \frac{n a_s^n}{n!\xi^2} \left(1-\frac{1}{\xi}\right)^{n-1} \left. \frac{\partial^n g_i^{-2}(a_\tau,\xi)}{\partial a_\tau^n} \right|_\xi + \sum_{n=1}^{\infty} \frac{a_s^n}{n!} \left(1-\frac{1}{\xi}\right)^n \frac{\partial}{\partial\xi} \left[\left. \frac{\partial^n g_i^{-2}(a_\tau,\xi)}{\partial a_\tau^n} \right|_\xi \right]_{a_s}. \tag{3.13}$$

Keeping in mind that though $[\partial g(a_s)/\partial\xi]_{a_s} = 0$, but $[\partial g(a_\tau)/\partial\xi]_{a_s} = [\partial g(a_s/\xi)/\partial\xi]_{a_s} \neq 0$, it follows that

$$\begin{aligned} \left. \frac{\partial g_i^{-2}(a_\tau,\xi)}{\partial\xi} \right|_{a_s} &= \left. \frac{\partial g^{-2}(a_\tau)}{\partial\xi} \right|_{a_s} + \left. \frac{\partial\alpha_i(\xi)}{\partial\xi} \right|_{a_s} \\ &= \frac{\partial}{\partial\xi} \left[g^{-2}(a_s) + \sum_{n=1}^{\infty} \frac{(a_\tau-a_s)^n}{n!} \frac{\partial^n g^{-2}(a_s)}{\partial a_s^n} \right]_{a_s} + \left. \frac{\partial\alpha_i(\xi)}{\partial\xi} \right|_{a_s} \\ &= -\sum_{n=1}^{\infty} \frac{n a_s^n}{n!\xi^2} \left(\frac{1}{\xi}-1\right)^{n-1} \frac{\partial^n g^{-2}(a_s)}{\partial a_s^n} + \left. \frac{\partial\alpha_i(\xi)}{\partial\xi} \right|_{a_s}. \end{aligned} \tag{3.14}$$

On substituting Eq. [3.14] in Eq. [3.13] and using relations mentioned in Eq. [3.11]

to calculate the various derivatives one gets

$$\begin{aligned}\left.\frac{\partial c_i(\xi)}{\partial \xi}\right|_{a_s} &= -\sum_{n=1}^{\infty} \frac{n a_s^n}{n!\xi^2}\left(\frac{1}{\xi}-1\right)^{n-1} \frac{\partial^n g^{-2}(a_s)}{\partial a_s^n} + \left.\frac{\partial \alpha_i(\xi)}{\partial \xi}\right|_{a_s} \\ &+ \sum_{n=1}^{\infty} \frac{n a_s^n}{n!\xi^2}\left(1-\frac{1}{\xi}\right)^{n-1} \left.\frac{\partial^n g^{-2}(a_\tau)}{\partial a_\tau^n}\right|_{\xi} \\ &+ \sum_{n=1}^{\infty} \frac{a_s^n}{n!}\left(1-\frac{1}{\xi}\right)^{n} \frac{\partial}{\partial \xi}\left[\frac{\partial^n g^{-2}(a_\tau)}{\partial a_\tau^n}\right]_{a_s}. \end{aligned} \tag{3.15}$$

Hence by taking $\xi \to 1$ limit, *i.e.* when $a_s = a_\tau$, one gets

$$\left.\frac{\partial c_i(\xi)}{\partial \xi}\right|_{a_s} = \left.\frac{\partial \alpha_i(\xi)}{\partial \xi}\right|_{a_s} \tag{3.16}$$

Since a variable transformation from $\{a_s, \xi\}$ to $\{a_\tau, \xi\}$ gives $\xi\,(\partial/\partial\xi)_{a_s} \equiv \xi\,(\partial/\partial\xi)_{a_\tau} - a_\tau\,(\partial/\partial a_\tau)_{\xi}$, using it on Eq. [3.16] one conclusively proves that

$$\left.\frac{\partial c_i(\xi)}{\partial \xi}\right|_{a_s} = \left.\frac{\partial \alpha_i(\xi)}{\partial \xi}\right|_{a_\tau} \tag{3.17}$$

Since the derivatives of the Karsch coefficients remain same for both the schemes one can use their known values, *viz.* values of first derivatives from Ref. [37] and that for the second derivatives form Chapter [2] [68].

3.2.4 On the method

Since the Karsch coefficients are same for both the t-favoured and the s-favoured schemes, from Eq. [1.22] it is clear that the anisotropic coupling constants $g_i(a, \xi)$ are different for the two schemes due to the scale dependence of the isotropic coupling constant $g(a)$. Therefore the expressions for ϵ and P are different (see Eqs. [1.25, 3.5]) at finite (but small) lattice spacing in the two different approaches. Since the s-favoured and t-favoured schemes are different due to the scale dependence of the isotropic coupling constant $g(a)$, the difference between the expressions in both the schemes goes as $\ln a$, compared to the $1/a^2$ cut-off dependence of the lattice Wilson action. So it is expected that the continuum limit results from both the methods will match only for very large temporal lattice size N_τ. Thus, the difference between the two methods is tantamount to improving the

operators. Moreover, for the usual choice of scale setting by $T = 1/N_\tau a_\tau$, our approach corresponds to the natural choice of scale in Eq. [1.22].

Following the observation that the expression for Δ/T^4 is identical (see Eqs. [1.33, 3.5c]) for both integral method and t-favoured scheme, the criterion for agreement between these two methods is exactly the same as the criterion for the agreement between the s-favoured scheme and the integral method (see Chapter [2] for detail discussion). Since the expression for Δ/T^4 is also same for the t-favoured and the s-favoured scheme, the analysis of Chapter [2] can be directly applied to the present case. So from those analysis we can conclude that a bare coupling of $\beta \geq 6.55$ should suffice to give an agreement between the t-favoured scheme and the integral method. For $\beta \leq 6.55$ use of one-loop order perturbative Karsch coefficients may give rise to some systematic effects. A comparison with the non-perturbatively determined Karsch coefficients [89, 91] shows that the difference between the perturbative and non-perturbative values are significant. For example, while at around $\beta = 6.55$ the one-loop order perturbative and non-perturbative c_i' differ by $\sim 20\%$, around $\beta = 6$ this difference increases to $\sim 80\%$.

In the present work we show that within the framework of differential method it possible to get a positive pressure for all temperatures if one uses the improved operators of the t-favoured scheme. This is so in spite of the use of one-loop order perturbative Karsch coefficients. Although one has to keep in mind that the use of one-loop order perturbative Karsch coefficients [37, 68] may give some systematic effects if the lattice spacing not small enough. For consistency, we also use one-loop order perturbative β-function (Eq. [1.23]).

3.3 Simulation details

Our simulations have been performed using the Cabbibo-Marinari [85] pseudo-heatbath algorithm with Kennedy-Pendleton [86] updating of three $SU(2)$ subgroups on each sweep. Plaquettes were measured on each sweep. For each simulation we discarded around 5000 initial sweeps for thermalization. We found that the maximum value for the integrated autocorrelation time for the plaquettes is about 12 sweeps for the $T = 0$ run at $\beta = 6$ and the minimum is 3 sweeps for the $T = 3T_c$ run for $N_\tau = 12$. Table [3.1] lists the details of these runs. All errors

T/T_c	β	Asymmetric Lattice		Symmetric Lattice	
		size	stat.	size	stat.
	6.0000	8×18^3	1565000	22^4	253000
0.9	6.1300	10×22^3	725000	22^4	543000
	6.2650	12×26^3	504000	26^4	256000
	6.1250	8×18^3	1164000	22^4	253000
1.1	6.2750	10×22^3	547000	22^4	280000
	6.4200	12×26^3	212000	26^4	136000
	6.2100	8×18^3	1903000	22^4	301000
1.25	6.3600	10×22^3	877000	22^4	217000
	6.5050	12×26^3	390000	26^4	240000
	6.3384	8×18^3	1868000	22^4	544000
1.5	6.5250	10×22^3	1333000	22^4	605000
	6.6500	12×26^3	882000	26^4	335000
	6.5500	8×18^3	2173000	22^4	534000
2.0	6.7500	10×22^3	1671000	22^4	971000
	6.9000	12×26^3	1044000	26^4	553000
	6.9500	8×26^3	1300000	26^4	433000
3.0	7.0500	10×32^3	563000	32^4	148000
	7.2000	12×38^3	317000	38^4	60000

Table 3.1: The coupling (β), lattice sizes ($N_\tau \times N_s^3$), statistics and symmetric lattice sizes (N_s^4) are given for each temperature. Statistics means number of sweeps used for measurement of plaquettes after discarding for thermalization.

were calculated by the jack-knife method, where the length of each deleted block was chosen to be at least six times the maximum integrated autocorrelation time of all the simulations used for that calculation.

As discussed in Chapter [2], at sufficiently high temperatures, finite size effects are under control if one chooses $N_s = (T/T_c)N_\tau + 2$ for the asymmetric $(N_\tau \times N_s^3)$ lattice. We have chosen the sizes of the lattices used at finite T based on this investigation. Close to T_c the most stringent constraint on allowed lattice sizes comes from the A_1^{++} screening mass determined in Ref. [92]. Among the temperature values we investigated, this screening mass is smallest at $1.1T_c$ where it is a little more than $2T$. The choice of $N_s = 2N_\tau + 2$ satisfies this constraint sufficiently. At $T = 0$ the constraints are simpler because glueball masses are larger, and also smoother functions of β. For the symmetric (N_s^4) lattices we have chosen $N_s = 22$ as the minimum lattice size and scaled this up with changes in the lattice spacing in accordance with the analysis done in Chapter [2].

3.4 Results

As discussed in Chapter [1], we have performed continuum extrapolations by linear fits in $a^2 \propto 1/N_\tau^2$ at all temperatures using the three values $N_\tau = 8$, 10, and 12. In Fig. [3.1a] we show our data on P/T^4 at finite lattice spacings and the continuum extrapolations for different temperatures, both above and below T_c. We draw attention to the fact that the pressure is positive on each of the lattices we have used, and also in the continuum limit. It is interesting to note that the slope of the continuum extrapolation changes sign at T_c; its relevance to the continuum physics is however unclear. This is also true of the continuum extrapolation for ϵ/T^4 as shown in Fig. [3.1b]. The extrapolations of both P/T^4 and ϵ/T^4 between $1.1T_c$ and $3T_c$ are similar to those shown and have therefore been left out of the figure to avoid repetition.

Similar continuum extrapolations are shown for C_V/T^3 and C_s^2 in the two panels of Fig. [3.2]. In all cases, the continuum extrapolations are smooth, and well fitted by a straight line in the range of N_τ used in this study. Also for C_V/T^3 the slope of the continuum extrapolation flips sign at T_c. This does not happen for C_s^2. Since this is the derivative of the energy density with respect to the pressure, the slope of this quantity depends on the slopes of the continuum extrapolations of ϵ/T^4 and P/T^4.

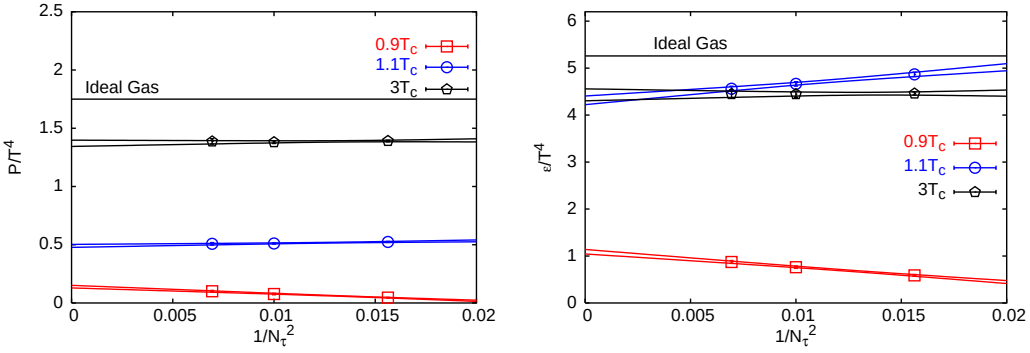

(a) (b)

Figure 3.1: (a) We show the dependence of P/T^4 on $1/N_\tau^2$ for different temperature values. (b) We show the same for ϵ/T^4. The 1-σ error band of the continuum extrapolations have been indicated by the lines.

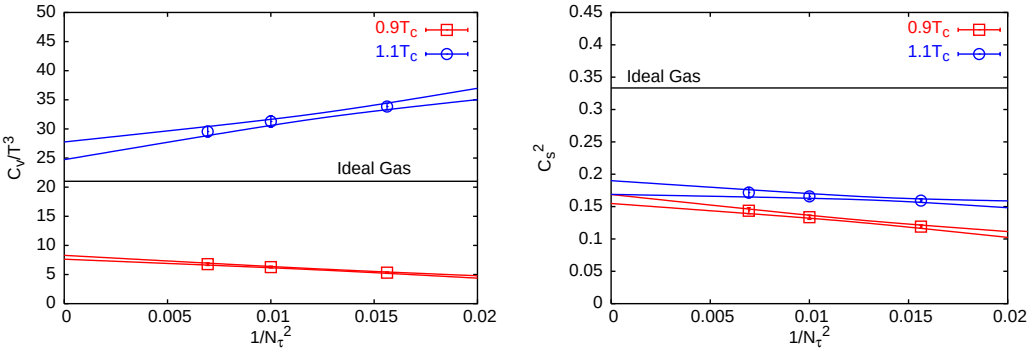

(a) (b)

Figure 3.2: (a) We show the dependence of C_V/T^3 on $1/N_\tau^2$ for different values of temperature. (b) We show the same for C_s^2. The 1-σ error band of the continuum extrapolations have been indicated by the lines.

In the various panels of Fig. [3.3] we show a comparison between the continuum results for different quantities obtained using the t-favoured scheme, s-favoured scheme and the integral method. While the results of the t-favoured and the s-favoured schemes are obtained from the analysis of our data, the results of the integral method are taken form Ref. [55].

First we note that unlike the s-favoured differential method, the t-favoured differential method yields a positive pressure (Fig. [3.3a]) at all T. There is apparent agreement between the integral and the t-favoured operator method for

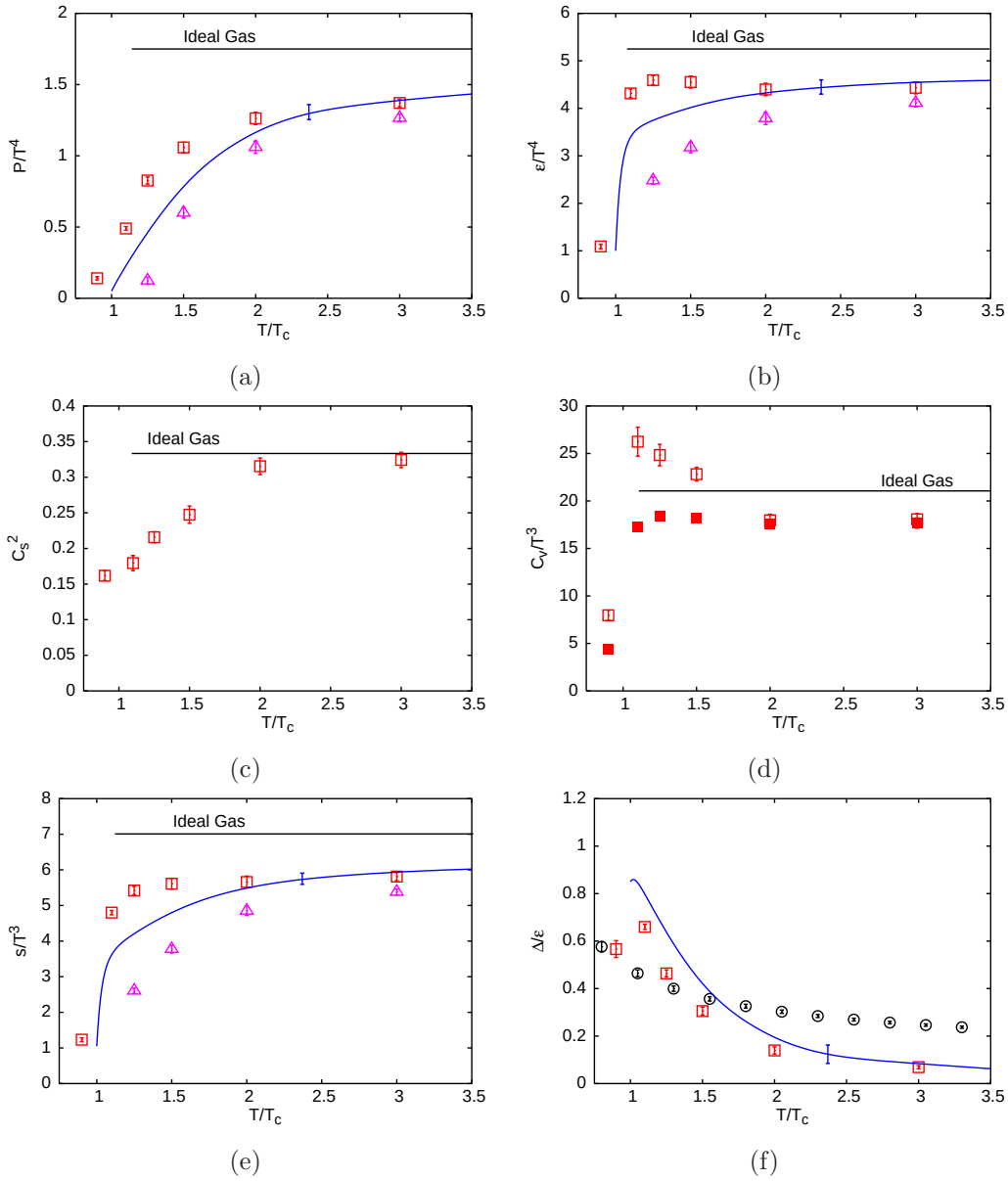

Figure 3.3: We show comparisons between the continuum results of different thermodynamic quantities for the t-favoured scheme (boxes), the s-favoured scheme (triangles) and the integral method (line). In panel (d) we show a comparison between our continuum results for C_V/T^3 (open boxes) and continuum $4\epsilon/T^4$ (filled boxes). In panel (f) we show the continuum values of the conformal measure $\mathcal{C}$, (boxes) and the negative of the one-loop order β-function (circles) evaluated at the scale $2\pi T$. The data for the integral method has been taken form Ref. [55].

$T \geq 2T_c$, both differing from the ideal value by about 20%. Only at these temperatures the coupling β becomes ≥ 6.55 for all the lattices (see Table [3.1]) that has been used to extract the continuum values in the t-favoured scheme. Hence, from our earlier discussion it is clear that an agreement between the two methods is expected to take place at these temperatures. There can be several causes for the difference between these two methods closer to T_c— (i) The use of one-loop order perturbative Karsch coefficients in the t-favoured scheme is probably the primary cause for this difference. Use of larger lattices (*i.e.* larger β) or inclusion of the effects of higher order loops in the Karsch coefficients is expected to improve the agreement. (ii) Another possible source of disagreement is that the results for the integral method shown here were obtained on coarser lattices [55] than the ones used in this study. (iii) The integral method assumes that the pressure below some β_0, corresponding to some temperature $T < T_c$, is zero. By changing β_0 one can change the integral method pressure by a temperature independent constant. This may restore the agreement close to T_c, although in that case the agreement at the high-T region may get spoiled. (iv) Also different schemes have been used to define the renormalized coupling in the two cases. This can also make some contribution to the different results of the two methods.

The energy density (Fig. [3.3b]) is harder near T_c, showing a significantly lessened tendency to bend down. This could indicate a difference in the latent heat determined by the two methods. Fig. [3.3c] shows the continuum extrapolated results for C_s^2. At temperatures of $2T_c$ and above, the speed of sound is consistent with the ideal gas value within 95% confidence limits. It is seen that C_s^2 decreases sharply near T_c. Below T_c there is again a fall in C_s^2, the numerical values being very close 10% below and above T_c. The behaviour of C_V/T^3, shown in Fig. [3.3 d], is the most interesting. At $2T_c$ and above it disagrees strongly with the ideal gas value, but is quite consistent with the prediction in conformal theories that $C_V/T^3 = 4\epsilon/T^4$. Closer to T_c, however, this simplification vanishes. The specific heat peaks at T_c. This is expected as the pure gauge theory has a first order transition. Below T_c the specific heat is very small.

In view of the rise in C_V/T^3 near T_c, we studied the contributions of the terms containing different covariances of the plaquettes. As can be seen from the Eq. [3.10] among all the terms containing covariances, the term $(\sigma_{ss} + \sigma_{\tau\tau} - 2\sigma_{s\tau})/g^4$

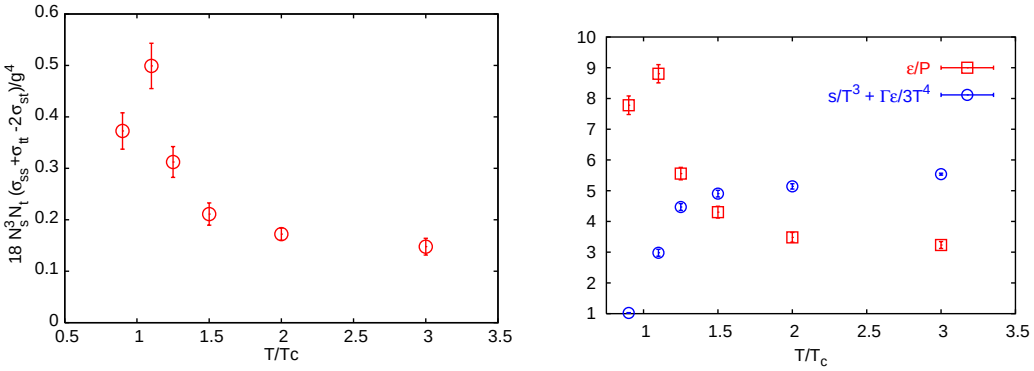

(a) (b)

Figure 3.4: (a) We show the temperature dependence of the contribution of one of the covariance terms in C_V/T^3. (b) We show the the individual contribution of the two factors in Eq. [2.11] for C_V/T^3. See the text for a detailed discussion.

will have the largest contribution to C_V/T^3. All the other terms containing the covariances are multiplied either by one of the c_i', or by $B(\alpha_s)/2\pi\alpha_s^2$ and hence become at least one order of magnitude smaller than this term. In Fig. [3.4a] we show the contribution of the above term, as a function of T in the continuum limit. However, the contribution of this term is very small: comparable to the errors in C_V. The origin of the peak in C_V therefore lies elsewhere. In Fig. [3.4b] we separately plot the two factors, ϵ/P and $s/T^3 + \Gamma\epsilon/3T^4$, in the the expression for C_V in Eq. [2.11]. The factor $s/T^3+\Gamma\epsilon/3T^4$ is smooth in the whole temperature range, and it is the first factor ϵ/P, which has a peak near T_c. Rewriting this as $3/(1-\mathcal{C})$, we can recognize that the peak in C_V is related to that in Δ.

It has been argued in Chapter [2] that the conformal measure $\mathcal{C} = \Delta/\epsilon$ parametrizes the departure from the conformal invariance at the long distance scale. In Fig. [3.3f] we plot $\mathcal{C}$ and the modulus of the β-function, which quantifies the breaking of conformal invariance at short distances. It is clear that at high temperature, 2–3T_c, conformal invariance is better respected in the finite temperature effective long-distance theory than at the microscopic scale. Closer to T_c conformal symmetry is badly broken even in the thermal effective theory. It is interesting to note that the t-favoured differential method yields marginally smaller values of $\mathcal{C}$ than the integral method.

T/T_c	g^2N_c	ϵ/T^4	P/T^4	s/T^3	C_V/T^3	C_s^2
0.9	11.5(3)	1.09(4)	0.14(1)	1.23(5)	8.0(5)	0.162(7)
1.1	10.4(2)	4.31(9)	0.49(1)	4.80(6)	26(2)	0.18(1)
1.25	9.8(2)	4.6(1)	0.82(2)	5.4(1)	25(1)	0.21(1)
1.5	9.0(1)	4.5(1)	1.06(4)	5.6(2)	22.8(7)	0.25(1)
2.0	8.1(1)	4.4(1)	1.26(4)	5.7(2)	17.9(7)	0.31(1)
3.0	7.0(1)	4.4(1)	1.37(3)	5.8(1)	17.9(8)	0.32(1)

Table 3.2: Continuum values of some quantities at all temperatures we have explored. The numbers in brackets are the error on the least significant digit. For the convenience of the readers here we also list the numerical values of these quantities for an ideal gas : $\epsilon/T^4 \approx 5.26$, $P/T^4 \approx 1.75$, $s/T^3 \approx 7.02$, $C_V/T^3 \approx 21.06$ and $C_s^2 = 1/3$. The value of the t'Hooft coupling g^2N_c is computed at the scale $2\pi T$ using the $T_c/\Lambda_{\overline{MS}}$ quoted in [51].

The continuum extrapolations of our measurements are collected in Table [3.2].

3.5 Discussion

In view of the fact the perturbation theory fails to reproduce the lattice data on EoS (see Chapter [1] for details), specially close to T_c, it is interesting to compare our t-favoured scheme results with that of the perturbation theory. In Fig. [3.5a] we compare the pressure obtained in the t-favoured scheme with that from a dimensionally reduced theory, matched with the 4-d theory perturbatively upto order $g^6 \ln(1/g)$ [23]. Writing P_{SB} for the ideal gas (Stefan-Boltzmann) value of the pressure, the ratio for P/P_{SB} found in the dimensionally reduced theory [23] has an undetermined adjustable constant, c. Surprisingly, the pressure determined through dimensional reduction agrees with our results almost all the way down to T_c, for that value of the constant ($c = 0.7$) for which it matches

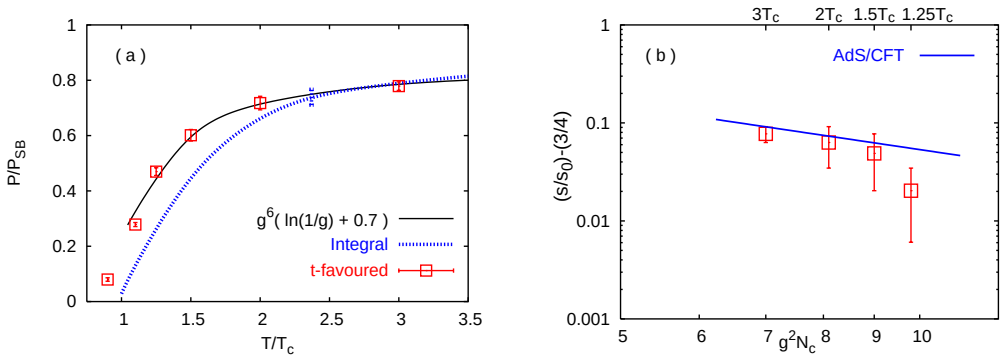

(a) (b)

Figure 3.5: (a) We compare the pressures obtained by t-favoured method (boxes), integral method (dotted line) and the $g^6 \ln(1/g)$ order perturbative expansion (solid line). The data for the integral method and the perturbative expansion are taken from Ref. [55] and Ref. [23] respectively. The values of the $T/\Lambda_{\overline{MS}}$ in Ref. [23] has been converted to T/T_c using the $T_c/\Lambda_{\overline{MS}}$ quoted in Ref. [51]. (b) We show the deviation of s/s_0 from 3/4 (boxes) as a function of the t'Hooft coupling. We also show the prediction of Eq. [3.18] (solid line).

with the integral method in the high temperature range. It would be interesting to check whether an equally good description is available in this approach for the full entropy. This would be a non-trivial extension because perturbation theory misses Δ completely. The question, therefore, addresses the non-perturbative dynamics of the dimensionally reduced theory.

A recent suggestion is that an effective theory which reproduces the results of thermal QCD at long-distance scales may somehow be close to a conformal theory. The result of Ref. [93] for the entropy density s, in a Yang-Mills theory with four supersymmetry charges ($\mathcal{N} = 4$ SYM) and large number of colours N_c, at strong coupling, is

$$\begin{aligned} \frac{s}{s_0} &= f(g^2 N_c), \quad \text{where} \\ f(x) &= \frac{3}{4} + \frac{45}{32}\zeta(3) x^{-3/2} + \cdots, \quad \text{and} \quad s_0 = \frac{2}{3}\pi^2 N_c^2 T^3. \end{aligned} \tag{3.18}$$

Here, g is the Yang-Mills coupling. (In some early literature the factor $x^{-3/2}$, in the right hand side of Eq. [3.18], appear as $(2x)^{-3/2}$, due to the use of some different normalization.) For the $N_c = 3$ case at hand, the well-known result for

the ideal gas, $s_0 = 4(N_c^2 - 1)\pi^2 T^3/45$ takes into account the difference between a $SU(N_c)$ and an $U(N_c)$ theory. Since in the present case the theory we are dealing with is definitely strongly coupled (see Table [3.2]) and also close to its conformal symmetric limit at relatively high temperature, one can attempt a comparison between our results and that of Eq. [3.18]. This has to be done in an appropriate window of T where the 't Hooft coupling $g^2 N_c$ is large and the conformal measure $\mathcal{C}$ is small. The strong coupling series is an expansion in $(g^2 N_c)^{-1/2}$. For $\mathcal{N} = 4$ SYM, the first term vanishes due to a delicate cancellation and the series starts with the $(g^2 N_c)^{-3/2}$ term [93]. When some of the supersymmetry is broken, this cancellation need not occur and the series could start with a term in $(g^2 N_c)^{-1/2}$. Needless to say, the theory we are studying here, pure QCD, lacks supersymmetry. In Fig. [3.5b] we show the deviation of s/s_0 from 3/4 as a function of the 't Hooft coupling (s and $g^2 N_c$ are listed in Table [3.2]). Also shown is the prediction of Eq. [3.18]. Very interestingly, comparison of our data with the latter shows that the AdS/CFT based theory agrees with our data for $g^2 N_c < 9$, or in other words for $\mathcal{C} < 0.3$.

3.6 Summary

In this chapter we have proposed the t-favoured differential method for computation of the QCD EoS. We have shown that this method gives positive pressure for all temperatures, even when the older s-favoured differential method gives negative pressure. Note that this is so in spite of the use of the same one-loop order perturbative values for the Karsch coefficients in both cases. Using this method we have found the continuum limit of energy density and pressure for a pure gluon theory in the temperature range $0.9 \leq T/T_c \leq 3$. These differ from their respective ideal gas values by about 20% at $3T_c$, and by much more as one approaches T_c. On comparing our results with those of the integral method, we found that ours are larger for $T < 2T_c$. Possible reasons for this difference have also been discussed. We have also extended the t-favoured scheme to compute the continuum limit of the specific heat at constant volume and the speed of sound. We found that C_V peaks near T_c where, in addition, C_s becomes small. One of the most interesting feature seen in all lattice computations of EoS is the

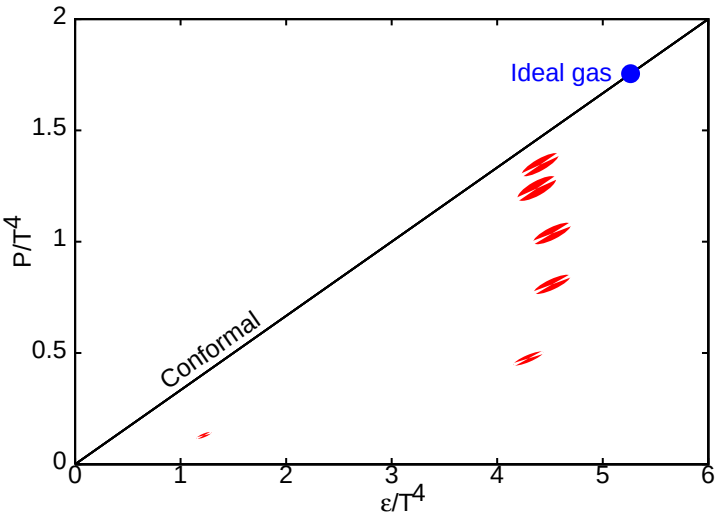

Figure 3.6: The equation of state of QCD matter. The diagonal line denotes possible EoS for theories with conformal symmetry. The circle on the diagonal denotes the ideal gluon gas, whose EoS in this form is temperature independent. The ellipses denote 66% error bounds on the measured EoS. The ratio of the axes is a measure of the covariance in the measurements of ϵ/T^4 and P/T^4. The wedges piercing these ellipses have average slope C_s^2, and the opening half-angle of these wedges indicate the error in C_s^2.

peak in Δ just above T_c. Apart from influencing the EoS, it manifests itself as a peak in C_V. Since C_V could be directly measurable through energy or effective temperature fluctuations in heavy-ion collisions, understanding Δ should be one of the prime goals of theory. We have also compared our data with the predictions of the perturbation theory and the AdS/CFT correspondence, and found reasonable agreements in certain temperature ranges.

A partial summary of our results is shown in Fig. [3.6], by making a similar plot as that of Fig. [2.8]. Pure gauge QCD lies close to the conformal line at high temperature, as shown, but deviates strongly nearer T_c. The slope of the wedges piercing the ellipses indicates the speed of sound— when these are parallel to the conformal line then $C_s^2 = 1/3$. This is clearly the case at high temperature. However, there is an increasing flattening of the axis, denoting a drop in C_s^2 as one approaches T_c. Two other physically important effects can be read off the figure. First, the softening of the equation of state just above T_c is shown by the rapid

drop in pressure at roughly constant ϵ/T^4. Second, a large latent heat is indicated by the jump between the last two points, at almost the same pressure but very different energy densities. A final piece of physics can be deduced from the fact that the low temperature phase shows a very small P/T^4 at a significantly large value of $\epsilon/T^4 > 1$ just below T_c. This is an indication that there are very massive modes in the hadron (glueball) gas which contribute large amounts to ϵ without contributing to P. The small value of C_v/T^3 at the same T also indicates that the energy required to excite the next state is rather large.

Chapter 4

Robustness of baryon-strangeness correlation and related ratios of susceptibilities

4.1 Introduction

Results of Chapter [2] and Chapter [3] show that for the gluonic plasma thermodynamic quantities like pressure, energy density, specific heat *etc.* deviate form there respective ideal gas values by about 20% even at temperature $T = 3T_c$. Similar LQCD results also exist for the full QCD plasma [94, 95]. Also the recent results from the RHIC [13] suggest the formation of a thermalized medium endowed with large collective flow and very low viscosity [96]. On the other hand, other lattice studies indicate the smallness of the viscous forces in QGP [97]. All these findings suggest that close to T_c nature of QGP is far from a gas of free quarks and gluons, rather it is a strongly interacting system. In view of this situation, it is very important to find out more about the degrees of freedom of such a strongly coupled QGP.

If the relevant degrees of freedom of a strongly coupled QGP are quasi-quarks then different conserved charges, *e.g.* baryon number (B), electric charge (Q), third component of isospin (I) *etc.*, are carried by different flavours (u, d, s) of quarks. Thus in the conventional quasi-particle models conserved charges come in strict proportion to number of u, d, s quarks. Hence conserved charges are

strongly correlated with the flavours and the flavours have no correlations among themselves. Based on the above arguments, in Ref. [98] it has been suggested that the baryon-strangeness correlation

$$C_{BS} = -3\frac{\langle BS\rangle - \langle B\rangle\langle S\rangle}{\langle S^2\rangle - \langle S\rangle^2}, \tag{4.1}$$

can be used to probe the degrees of freedom of QGP. Here $B = (U + D - S)/3$ is the net baryon number and U, D, S are the numbers of net (quarks minus anti-quarks) up-quarks, down-quarks and strange-quarks respectively. The quantity C_{BS} probes the linkages of the strangeness carrying excitations to baryon number and hence give an idea about the average baryon number of all the excitations carrying the s flavour. The ratio is normalized such that for an ideal gas of quarks, *i.e.* where unit strangeness is carried by excitations having $B = -1/3$, $C_{BS} = 1$. A value of C_{BS} significantly different from 1 will indicate that the QGP phase may contain some other degrees of freedom apart form the quasi-quarks.

In order to uncover the nature of QGP in the vicinity of T_c many different suggestions have been made over the last decade. Descriptions in terms of various quasi-particles [99, 100, 101], resummed perturbation theories (see Chapter [1] for details), effective models [102, 103] *etc.* are few among many such attempts. Apart from all these, the newly proposed model of Shuryak and Zahed [104] has generated considerable amount of interest in the recent years. Motivated by the lattice results for the continued existence of charmonium in QGP [105] till $T \sim 2T_c$, this model proposed a strongly interacting chromodynamic system of quasi-particles (with large thermal masses) of quarks, anti-quarks and gluons along with their numerous bound states (which also include colour non-singlet states). In the model of Ref. [104], presence of bound states demand correlations among different flavours. Hence correlations between conserved charges and flavours depend on the mass-spectrum of the bound states and the strong correlations among them are lost. For this model $C_{BS} = 0.62$ at $T = 1.5T_c$ [98], while for a gas of hadron resonances $C_{BS} = 0.66$ around T_c [98].

By extending the idea of Ref. [98], recently in Ref. [106], many ratios like

$$C_{(KL)/L} = \frac{\langle KL\rangle - \langle K\rangle\langle L\rangle}{\langle L^2\rangle - \langle L\rangle^2} \equiv \frac{\chi_{KL}}{\chi_L}. \tag{4.2}$$

have been proposed to study the properties of QGP. Here χ_L and χ_{KL} denote the diagonal and off-diagonal susceptibilities corresponding to conserved charge L and correlation among conserved charges K and L, respectively. The physical meaning of the ratios like $C_{(KL)/L}$ can be interpreted as follows [106]— Create an excitation with quantum number L and then observe the value of a different quantum number K associated with this excitation. Thus these ratios identify the quantum numbers corresponding to different excitations and hence provide information about the degrees of freedom. The ratios $C_{(KL)/L}$ can be expressed [106] in terms of Flavour Diagonal Quark Number Susceptibilities (FDQNS) and Flavour Off-Diagonal Quark Number Susceptibilities (FODQNS) (defined in Eq. [1.36]), which are computable on the lattice. For example, the baryon-strangeness correlation and the electric charge-strangeness correlation can be written as [106]—

$$C_{BS} \equiv -3C_{(BS)/S} = -3\frac{\chi_{BS}}{\chi_S} = \frac{\chi_s + 2\chi_{us}}{\chi_s} = 1 + \frac{2\chi_{us}}{\chi_s}, \quad \text{and} \tag{4.3a}$$

$$C_{QS} \equiv 3C_{(QS)/S} = 3\frac{\chi_{QS}}{\chi_S} = \frac{\chi_s - \chi_{us}}{\chi_s} = 1 - \frac{\chi_{us}}{\chi_s}. \tag{4.3b}$$

Using this fact many $C_{(KL)/L}$'s have been computed [106] using LQCD simulations with two flavours of dynamical light quarks and three flavours (two light and one heavy) of valance quarks. These calculations found no evidence for the existence of bound states [104] even at temperatures very close to T_c. These finding are consistent with the results of Ref. [107], where the hypothesis of Ref. [104] has been tested by investigating the ratios of higher order baryon number susceptibilities obtained from lattice simulations.

As these lattice studies [106] involved simulations with dynamical quarks, they were done using small lattices having temporal lattice size $N_\tau = 4$. By comparing with the results from quenched [108] simulations it has been shown [106] that the ratios of the diagonal susceptibilities do not depend on N_τ for temperature $T = 2T_c$. It is clearly important to verify whether the same conclusion holds even for the ratios of the off-diagonal to diagonal susceptibilities, like C_{BS}, specially close to T_c. Furthermore, it is known that in the case of quenched QCD with standard staggered quarks the FDQNS have strong dependence on the lattice spacing even for the free theory [108, 109]. On the other hand, the FODQNS are

identically zero for an ideal gas and acquire non-zero value only in the presence of interactions. So the lattice spacing dependence of the FODQNS may be more complicated, as opposed to that for the FDQNS where these corrections are dominated by the lattice artifacts of the naive staggered action. Thus if these two QNS become comparable the ratios mentioned in Eq. [4.2] can have non-trivial dependence on the lattice spacing a and hence the continuum limit of these ratios can be different from that obtained using small lattices. Since the perturbative expressions for FDQNS and FODQNS (for vanishingly small quark mass and chemical potential) are respectively [66]—

$$\frac{\chi_{ff}}{T^2} \simeq 1 + \mathcal{O}(g^2), \qquad \text{and} \qquad \frac{\chi_{ff'}}{T^2} \simeq -\frac{5}{144\pi^6}\, g^6 \ln g^{-1}, \tag{4.4}$$

it is reasonable to expect that the FODQNS may not be negligible at the vicinity of T_c where the coupling g is large. Since the contributions of the bound states in the QNS become more and more important as one approaches T_c [112], on the lattice it is necessary to investigate the continuum limit of the these ratios in order to check whether C_{BS} *etc.* can have values close to the predictions of the bound state QGP model [104]. At present a continuum extrapolation of this kind can only be performed using quenched approximation [110, 111] due to the limitations of present day computational resources. A quenched result for these ratios will also provide an idea about the dependence of these ratios on the sea quark mass. Since the present day dynamical lattice calculations are performed with bare quark masses heavier than the physical quark masses, such information is very important for estimating the systematic effects in these computations.

The aim of this chapter is to make careful investigation of the continuum limit of the ratios of the kind $C_{(KL)/L}$ for temperatures $T_c < T \leq 2T_c$ using quenched LQCD simulations [70]. By doing so we will gain knowledge about the degrees of freedom which gave rise to the bulk thermodynamic behavior of QGP, investigated in the previous two chapters.

4.2 Simulation details

The partition function of QCD for N_f flavours, each with quark chemical potential μ_f and mass m_f, at temperature T has the form

$$\mathcal{Z}\left(T,\{\mu_f\},\{m_f\}\right) = \int \mathcal{D}U\ e^{-S_G[U]} \prod_f \det M_f(T,\mu_f,m_f), \tag{4.5}$$

where S_G is the gauge part of the action and M_f is the Dirac operator. We have used standard Wilson action for S_G and staggered fermions to define M (see Chapter [1] for details). Using this partition function and the definitions of FDQNS and FODQNS in Eq. [1.36] one can easily see that

$$\begin{aligned}
\chi_{ff} &= \left(\frac{T}{V}\right) \left.\frac{\partial^2 \ln \mathcal{Z}}{\partial \mu_f^2}\right|_{\{\mu_f\}=0} \\
&= \left(\frac{T}{V}\right) \left[\left\langle \mathrm{Tr}\ \left(M_f^{-1}M_f'' - M_f^{-1}M_f'M_f^{-1}M_f'\right)\right\rangle + \left\langle \left\{\mathrm{Tr}\ \left(M_f^{-1}M_f'\right)\right\}^2\right\rangle\right], \qquad (4.6a)\\
\chi_{ff'} &= \left(\frac{T}{V}\right) \left.\frac{\partial^2 \ln \mathcal{Z}}{\partial \mu_f \partial \mu_{f'}}\right|_{\{\mu_f\}=0} = \left(\frac{T}{V}\right) \left\langle \mathrm{Tr}\ \left(M_f^{-1}M_f'\right) \mathrm{Tr}\ \left(M_{f'}^{-1}M_{f'}'\right)\right\rangle. \qquad (4.6b)
\end{aligned}$$

Here the single and double primes denote first and second derivatives with respect to the corresponding μ_f and the angular brackets denote averages over the gauge configurations.

We have investigated these susceptibilities on lattices with $N_\tau = 4,\ 8,\ 10$ and 12, for the temperatures $1.1T_c \leq T \leq 2T_c$, chemical potential $\mu_f = 0$ and using quenched approximation [110, 111]. The gauge configurations were generated in using exactly the same procedure mentioned in Chapter [2]. Since for $m_q/T_c \leq 0.1$ QNS are almost independent of the bare valance quark mass (m_q) [108], we have used $m_q/T_c = 0.1$ for the light u and d flavours. Motivated by the fact that for the full theory $m_s/T_c \sim 1$ we have used $m_q/T_c = 1$ for the heavier s flavour. Since we use degenerate u and d flavours the following relations hold— $\chi_u = \chi_d$, $\chi_{ud} = \chi_{du}$ and $\chi_{us} = \chi_{ds}$.

As can be seen from Eq. [4.6], in order to obtain χ_f, $\chi_{ff'}$ one requires inverse of the fermion matrix M_f. These fermion matrix inversions were done by using

conjugate gradient method [84] with the stopping criterion $|r_n|^2 < \epsilon |r_0|^2$, r_n being the residual after the n-th step and $\epsilon = 10^{-4}$ (see Ref. [65] for details).

The traces have been estimated by using the stochastic estimator for traces [60]. In this method the trace of any matrix A is given by

$$\text{Tr } A = \frac{1}{2N_v} \sum_{i=1}^{N_v} R_i^\dagger A R_i, \tag{4.7}$$

where R_i is a complex vector whose components have been drawn independently from a Gaussian ensemble with unit variance. The square of a trace has been calculated by dividing N_v vectors into L non-overlapping sets and then using the relation

$$(\text{Tr } A)^2 = \frac{2}{L(L-1)} \sum_{i>j=1}^{L} (\text{Tr } A)_i (\text{Tr } A)_j. \tag{4.8}$$

We have observed that as one approaches T_c from above these products, and hence $\chi_{ff'}$, become more and more noisy for larger volumes and smaller quark masses. So in order to reduce the errors on $\chi_{ff'}$ number of vectors N_v have been increased for the larger lattices and the smaller quark masses with decreasing temperature.

Details of all our runs are provided in Table [4.1].

4.3 Results

4.3.1 Susceptibilities

In order to understand the cut-off dependence of $C_{(KL)/L}$ let us start by examining the same for the FDQNS and FODQNS. We found that for all temperatures the FDQNS (χ_u and χ_s) depend linearly on $a^2 \propto 1/N_\tau^2$, *i.e.* the finite lattice spacing corrections to the FDQNS have the form $\chi_{ff}(a, m_f, T) = \chi_{ff}(0, m_f, T) + b(m_f, T)a^2 + \cdots$. As an illustration of this we show our data for $1.1T_c$ and $1.25T_c$ in Fig. [4.1]. Similar variations were found for the other temperatures also. We have made continuum extrapolations of the FDQNS by making linear fits in $1/N_\tau^2$. Our continuum extrapolated results match, within errors, with the available data

T/T_c	β	Lattice size	N_{stat}	N_v	
				$m_q/T_c = 0.1$	$m_q/T_c = 1$
	5.7000	4×10^3	44	250	100
		$\times 16^3$	50	250	100
		$\times 20^3$	30	250	100
1.1	6.1250	8×18^3	48	250	100
	6.2750	10×22^3	38	250	100
	6.4200	12×26^3	41	250	100
	5.7880	4×10^3	52	100	100
1.25	6.2100	8×18^3	49	200	100
	6.3600	10×22^3	46	200	100
	6.5050	12×26^3	45	200	100
	5.8941	4×10^3	51	100	100
1.5	6.3384	8×18^3	49	150	100
	6.5250	10×22^3	49	150	100
	6.6500	12×26^3	48	150	100
	6.0625	4×10^3	51	100	100
2.0	6.5500	8×18^3	50	100	100
	6.7500	10×22^3	46	100	100
	6.9000	12×26^3	49	100	100

Table 4.1: The couplings (β), lattice sizes ($N_\tau \times N_s^3$), number of independent gauge configurations (N_{stat}) and number of vectors (N_v) that have been used for our simulations are given for each temperature. The gauge configurations were separated by 100 sweeps.

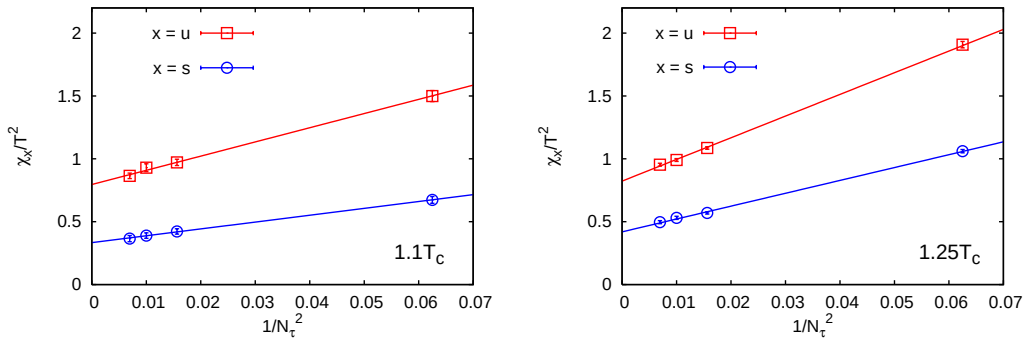

(a) (b)

Figure 4.1: We show the N_τ ($\propto 1/a$) dependence of χ_u/T^2 (squares) and χ_s/T^2 (circles) for $1.1T_c$ (a) and for $1.25T_c$ (b). The continuum extrapolations (linear fits in $1/N_\tau^2$) are shown by the lines.

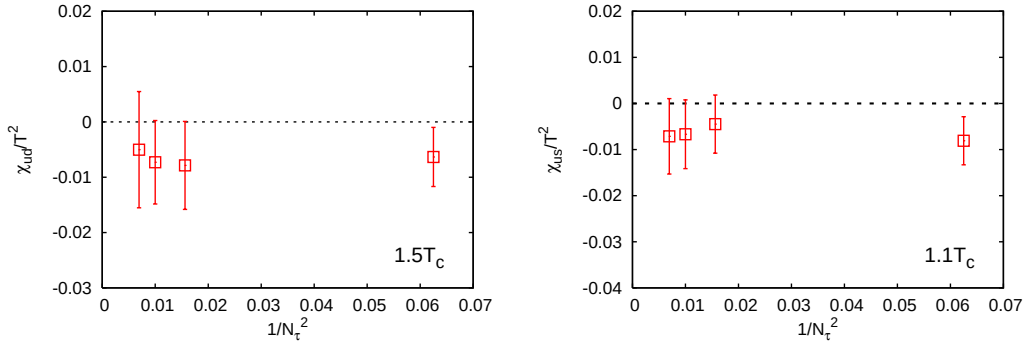

(a) (b)

Figure 4.2: N_τ dependence of the FODQNS χ_{ud}/T^2 at $1.5T_c$ (a) and χ_{us}/T^2 at $1.1T_c$ (b) have been shown.

of [108] at $1.5T_c$ and $2T_c$. Results of our continuum extrapolations for the FDQNS are listed in Table [4.2].

In Fig. [4.2] we present some of our typical results for the FODQNS. Note that here the scales are ~ 100 magnified as compared to Fig. [4.1]. The sign of our FODQNS is consistent with the perturbative predictions of Ref. [66], as well as with the lattice results of Refs. [64, 65]. The order of magnitude of our FODQNS matches with the results of Ref. [65] which uses the same staggered fermion action as in the present case. As can be seen from Fig. [4.2] we have not found any perceptible dependence of $\chi_{ff'}$ on the lattice spacing a within errors.

T/T_c	χ_u/T^2			χ_s/T^2		
	a	b	$\chi^2_{d.o.f}$	a	b	$\chi^2_{d.o.f}$
1.1	0.79(1)	11.3(5)	0.3	0.33(1)	5.4(1)	0.1
1.25	0.84(1)	15(1)	0.5	0.45(1)	10(1)	0.8
1.5	0.83(1)	17.3(3)	0.5	0.55(1)	12.5(5)	0.9
2.0	0.86(2)	19.7(2)	0.7	0.70(2)	17(2)	0.8

Table 4.2: Parameters for the continuum extrapolations of the FDQNS (χ_u, χ_s). Continuum extrapolations are made by fitting $a + b/N_\tau^2$ to our data for the three largest lattice sizes. Numbers in the bracket denote the errors on the fitting parameters and $\chi^2_{d.o.f}$ refers to the value of the chi-square per degrees of freedom for that particular fit.

T/T_c	χ_{ud}/T^2		χ_{us}/T^2	
	$c \times 10^3$	$\chi^2_{d.o.f}$	$c \times 10^3$	$\chi^2_{d.o.f}$
1.1	-4(4)	0.5	-6(4)	0.1
1.25	-0.2(1.0)	0.1	-0.7(1.0)	0.6
1.5	-7(5)	0.1	2(2)	0.6
2.0	2(3)	0.5	-0.1(1.0)	0.8

Table 4.3: Parameters for the continuum extrapolations of the FODQNS (χ_{ud}, χ_{us}). Continuum extrapolations are made by fitting our data to a constant c. Numbers in the bracket denote the errors on the fitting parameters and $\chi^2_{d.o.f}$ refers to the value of the chi-square per degrees of freedom for that particular fit.

Hence to good approximation $\chi_{ff'}(a, m_f, m_{f'}, T) \approx \chi_{ff'}(0, m_f, m_{f'}, T)$. Also for the other temperatures, which are not shown in Fig. [4.2], similar behaviour was found. Results of our continuum extrapolations for the FODQNS are listed in Table [4.3].

We also present our continuum extrapolated results for the two very important

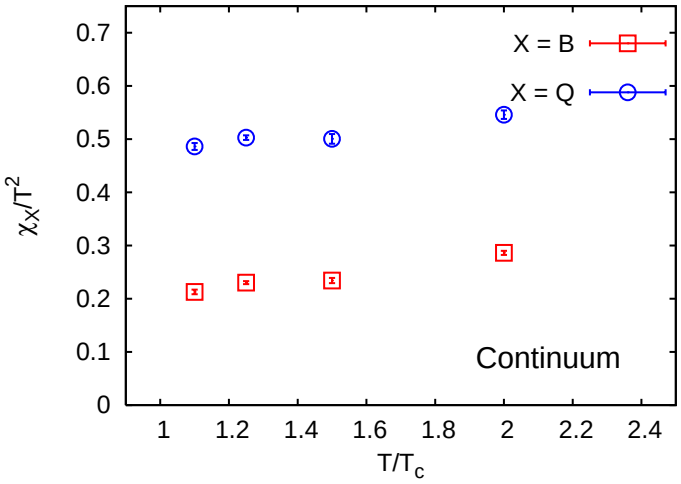

Figure 4.3: The continuum results for χ_B/T^2 (squares) and χ_Q/T^2 (circles) have been shown.

quantities, the baryon number susceptibility (χ_B) and the electric charge susceptibility (χ_Q). These quantities are related to the event-by-event fluctuations of baryon number and electric charge [113] which have already been measured at RHIC [114]. The definitions that we use for χ_B and χ_Q are [106]

$$\chi_B = \frac{1}{9}\left(2\chi_u + \chi_s + 2\chi_{ud} + 4\chi_{us}\right), \qquad \text{and} \tag{4.9a}$$

$$\chi_Q = \frac{1}{9}\left(5\chi_u + \chi_s - 4\chi_{ud} - 2\chi_{us}\right). \tag{4.9b}$$

In Fig. [4.3] we show the continuum results for χ_B/T^2 and χ_Q/T^2. Continuum extrapolations have been performed by making linear fits in $a^2 \propto 1/N_\tau^2$. Continuum limit of these quantities were also obtained in Ref. [108] for $T \geq 1.5T_c$, though using different definitions for these quantities. Nevertheless, given the compatibility of our FDQNS with that of Ref. [108] and the smallness of the FODQNS for $T \geq 1.5T_c$ our continuum results for χ_B and χ_Q are compatible with that of Ref. [108].

4.3.2 Ratios

Wroblewski parameter (λ_s) [115] is a quantity of extreme interest due to its relation to the enhancement of strangeness production in QGP [116]. The rate of

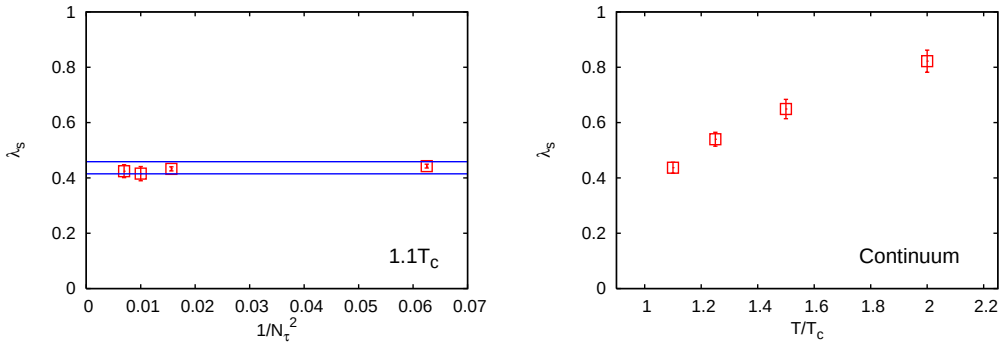

(a) (b)

Figure 4.4: (a) Robustness of the Wroblewski parameter (λ_s) with changing lattice spacings has been shown for $1.1T_c$. The lines indicate the 5% error band of a constant fit to this data. (b) We show our continuum results for λ_s (see text for details).

production of quark pairs in an equilibrated plasma is related to the imaginary part of the complex QNS by fluctuation-dissipation theorem. If one assumes that the plasma is in chemical (and thermal) equilibrium and the typical energy scales for the production of u, d and s quarks are well separated from the inverse of the characteristic time scale of the QCD plasma, then using Kramers-Kronig relation one can relate λ_s to the ratio of QNS [117]—

$$\lambda_s = \frac{2\langle s\bar{s}\rangle}{\langle u\bar{u} + d\bar{d}\rangle} = \frac{\chi_s}{\chi_u}. \tag{4.10}$$

In the above equation $\langle f\bar{f}\rangle$ denotes the number of quark pairs $f\bar{f}$.

We have found that λ_s, which is a ratio of two FDQNS, remains constant (within $\sim 5\%$) with varying lattice spacings for all temperatures in $1 < T/T_c \leq 2$. We have illustrated this in Fig. [4.4a] by plotting λ_s with $1/N_\tau^2$ for the temperature $1.1T_c$. These results are somewhat surprising since the order a^2 corrections are not negligible for the individual FDQNS. But for the ratio of the FDQNS for two different bare valance quark masses these order a^2 corrections happen to be negligible and thus seems to be quark mass independent. This indicates that the finite lattice spacing corrections to the FDQNS is constrained to have the form $\chi_{ff}(a, m_f, T) \approx \chi_{ff}(0, m_f, T)[1 + b(T)a^2 + \cdots]$, as opposed to the more general form $\chi_{ff}(a, m_f, T) = \chi_{ff}(0, m_f, T) + b(m_f, T)a^2 + \cdots$.

Our continuum results for the Wroblewski parameter have been shown in Fig. [4.4b]. In view of the constancy of λ_s we have made the continuum extrapolations by making a constant fit to $a^2 \propto 1/N_\tau^2$. Our Continuum limit for λ_s are consistent with the previously reported [108] continuum values for $T \geq 1.5T_c$. Our continuum results for λ_s are very close to the results of Ref. [106] for the whole temperature range of $T_c < T \leq 2T_c$. Closeness of our quenched results with the results from the dynamical simulations of Ref. [106] suggest that the Wroblewski parameter has practically no dependence on the mass of the sea quarks. This observation, along with the fact that λ_s has very mild dependence on the valance quark mass [108, 118], shows that the present day LQCD results for the Wroblewski parameter are very reliable. The robustness of the Wroblewski parameter is very encouraging specially since in the vicinity of T_c the lattice results for this quantity almost coincides with the value ($\lambda_s \approx 0.43$) extracted by fitting the experimental data of RHIC with a hadron gas fireball model [119], as first noted in Ref. [108].

Given our results for the FDQNS and FODQNS it is clear that the ratio of FODQNS to FDQNS will have the form— $\chi_{ff'}(a, m_f, m_{f'}, T)/\chi_{ff}(a, m_f, T) \approx [\chi_{ff'}(0, m_f, m_{f'}, T)/\chi_{ff}(0, m_f, T)][1 - b(T)a^2]$. Since $b(T)$ is positive, *i.e.* χ_{ff} decreases with decreasing lattice spacing, this ratio is expected to decrease (as $\chi_{ff'}$ is negative) and move away from zero. However, due smallness of these ratios itself, within our numerical accuracies, we were unable to identify any such effect. This has been exemplified in Fig. [4.5] where χ_{ud}/χ_u at $1.5T_c$ (a) and χ_{us}/χ_s at $1.1T_c$ (b) have been shown.

Ratios, like C_{BS} and C_{QS} (see Eq. [4.3]), can also be formed for the light quark sector [106], *e.g.* for the u flavour the ratios

$$C_{BU} \equiv 3C_{(BU)/U} = 3\frac{\chi_{BU}}{\chi_U} = \frac{\chi_u + \chi_{ud} + \chi_{us}}{\chi_u} = 1 + \frac{\chi_{ud}}{\chi_u} + \frac{\chi_{us}}{\chi_u}, \quad \text{and} \quad (4.11a)$$

$$C_{QU} \equiv 3C_{(QU)/U} = \frac{3\chi_{QU}}{\chi_U} = \frac{2\chi_u - \chi_{ud} - \chi_{us}}{\chi_u} = 2 - \frac{\chi_{ud}}{\chi_u} - \frac{\chi_{us}}{\chi_u} \quad (4.11b)$$

quantify the average baryon number (C_{BU}) and and the average electric charge (C_{QU}) of all the excitations carrying u quarks. For a medium of pure quarks, *i.e.* where the u flavours are carried by excitations with baryon number 1/3 and

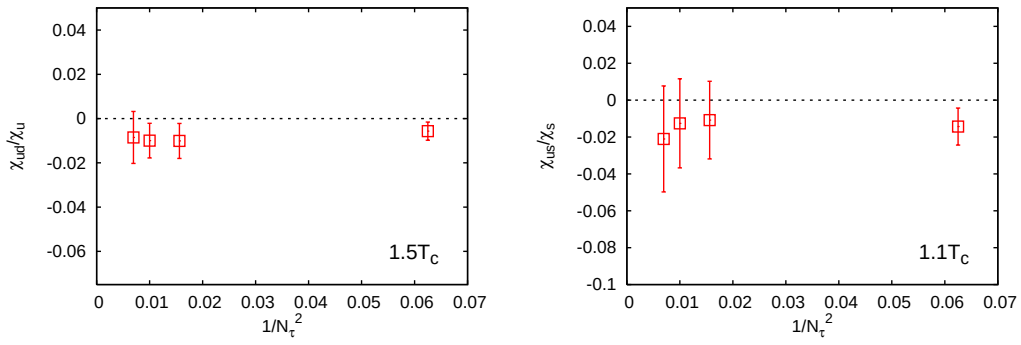

(a) (b)

Figure 4.5: (a) N_τ dependence of χ_{ud}/χ_u at $1.5T_c$. (b) Shows the same for χ_{us}/χ_s at $1.1T_c$

electric charge 2/3, $C_{BU} = 1$ and $C_{QU} = 2$. Similar ratios can also be formed for the d quarks [106].

As can be seen seen from Eqs. [4.3, 4.11] the lattice spacing dependence of C_{BS} *etc.* is governed by the cut-off dependence of the ratios $\chi_{ff'}/\chi_{ff}$. Since we have already emphasized that, within our numerical accuracies, the ratios $\chi_{ff'}/\chi_{ff}$ are almost independent of lattice spacings it is expected that the same will also happen for the ratios $C_{(KL)/L}$. In accordance with this expectation we found that for temperatures $1.1T_c \leq T \leq 2T_c$ these ratios are independent of lattice spacings within $\sim 5\%$ errors, see Fig. [4.6]. Note that these ratios are not only independent of the lattice spacings but also acquire values which are very close to their respective ideal gas limits.

Fig. [4.7] shows our continuum results for C_{XS} (b) and C_{XU} (a), where $X = B, Q$. Since these ratios remain almost constant with changing $1/N_\tau^2$ (see Fig. [4.6]) we have made continuum extrapolations by making constant fits of our data to $1/N_\tau^2$. For the whole temperature range of interests ($T_c < T \leq 2T_c$) these ratios have values which are compatible with that for a gas of pure quarks. This is exactly what has been found in Ref. [106] using dynamical simulations with smaller lattices. For the d quarks also we have found similar results.

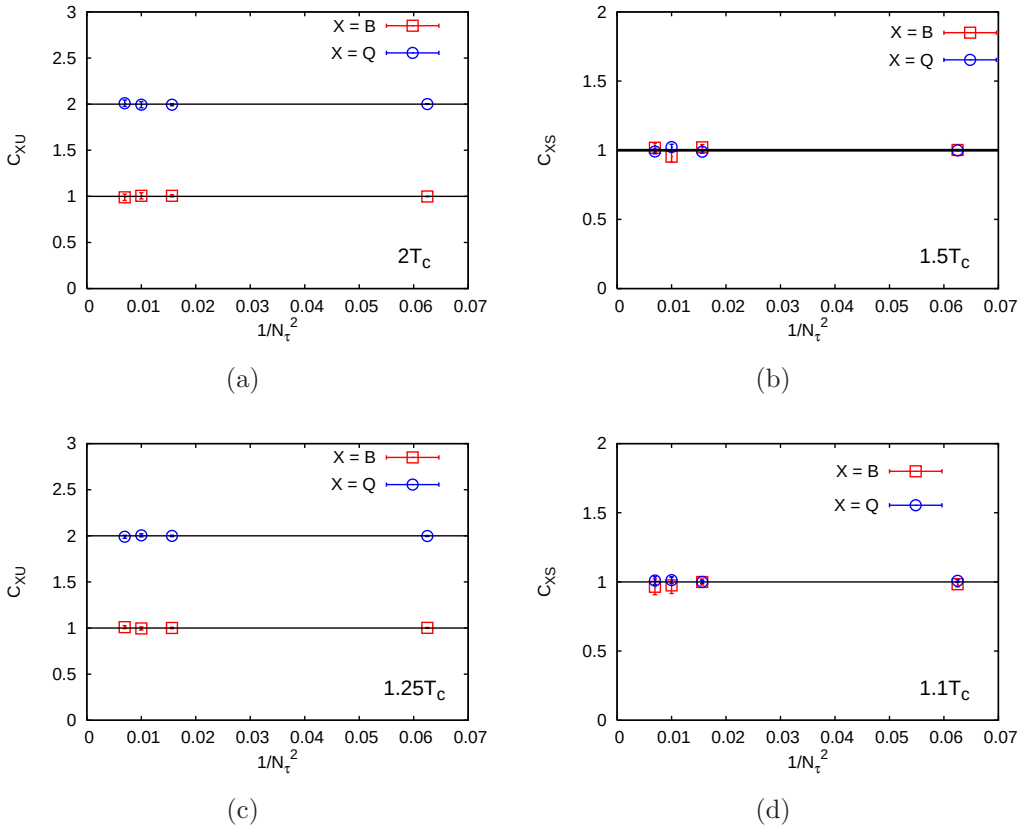

Figure 4.6: Lattice spacing dependence of C_{XU} and C_{XS} are shown for temperatures $2T_c$ [panel (a)], $1.5T_c$ [panel (b)], $1.25T_c$ [panel (c)] and $1.1T_c$ [panel (d)] by plotting these quantities as a function of $1/N_\tau^2$ ($\propto a^2$), for $N_\tau = 4, 8, 10, 12$. The lines indicate the ideal gas values for these ratios.

4.4 Discussion

For all our computations we have used spatial lattice sizes $N_s = 2N_\tau+2$, *i.e.* aspect ratios $N_s/N_\tau = 2.5-2.17$. In view of the fact that quenched QCD has a first order phase transition it is important to have some idea about the volume dependence of our results, specially in the vicinity of the transition temperature T_c. To check this dependence we have performed simulations using lattices having aspect ratios $N_s/N_\tau = 2.5-5$, for our smallest temporal lattice $N_\tau = 4$, at temperature $1.1T_c$. In these simulations we have not found any significant volume dependence of

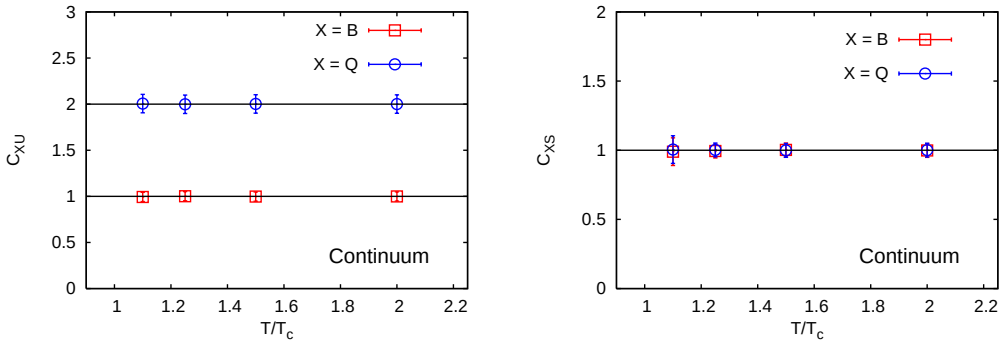

(a) (b)

Figure 4.7: Continuum results for C_{XU} (a) and C_{XS} (b). The lines indicate the ideal gas values for these quantities. See text for details.

any relevant quantity. As an illustration, in Fig. [4.8], we show the dependence of χ_{us}/χ_s on the aspect ratio, for $N_\tau = 4$ at $1.1T_c$. The volume dependence is expected to be even smaller as one goes further away from first order phase transition point. Also the agreement of our results with that of [106], where an aspect ratio of 4 have been used, shows that the these ratios have almost no volume dependence for $N_s \geq N_\tau + 2$.

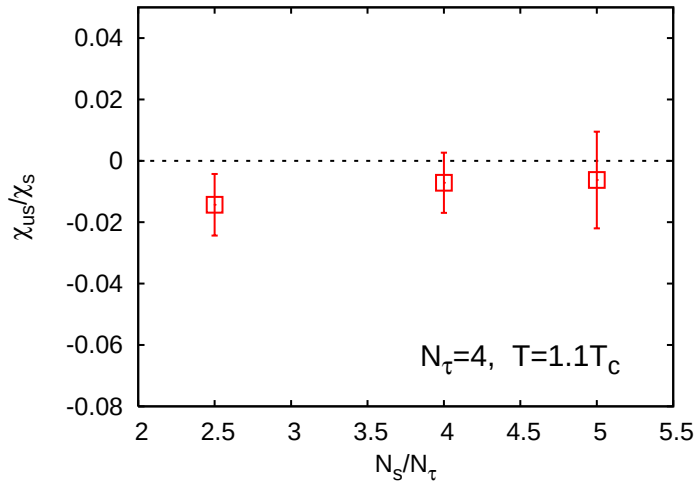

Figure 4.8: Dependence of the ratio χ_{us}/χ_s on the aspect ratio has been shown for $N_\tau = 4$ at temperature $1.1T_c$.

Also it is very important to have some idea about how unquenching may

change our results. It has been found Ref. [120] that in the temperature range $T \geq 1.25T_c$ there is only $5-10\%$ change in the QNS in going from quenched to $N_f = 2$ dynamical QCD. On the other hand, since the order of the phase transition depends strongly on the number of dynamical flavours the change in QNS is likely to be much larger in the vicinity of the transition temperature for the quenched theory which has a first order phase transition. Though this may be true for the individual QNS, their ratios may have very mild dependence on the sea quark content of the theory. Given the good compatibility of our results with that of Ref. [106] it is clear that indeed these ratios have very mild dependence on the sea quark content of the theory. It is also known [108] that for bare valance quark mass of $m_q/T_c \leq 0.1$ the dependence of the QNS on the valance quarks mass is very small. Hence our results show that the ratios like $C_{(KL)/L}$ are not only independent on the lattice spacings but also they have very mild dependence on the quark masses.

While the closeness of C_{XU} and C_{XS} $(X = B, Q)$ to their respective ideal gas values do support the notion of quasi-particle like excitations in QGP, a significant deviation of these ratios from their ideal gas values neither rule out the quasi-particle picture nor confirms the existence of the bound states proposed in Ref. [104]. Large contributions from the chemical potential dependence of the quasi-particle masses may lead to significant deviation of these ratios, especially in the vicinity of T_c. It has already been pointed out [101, 112] that, near T_c, the chemical potential dependence of the quasi-particle masses becomes crucial for the baryonic susceptibilities. Nevertheless, it may be interesting to compare our results with the predictions of the bound state model of Ref. [104]. Based on the model of Ref. [104] (and assuming that the mass formulae given in Ref. [104] hold right down to T_c) the predicted values of C_{BS} are approximately 0.62 at $1.5T_c$ [98], 0.11 at $1.25T_c$ and almost zero at $1.1T_c$ [121]. Clearly, as can be seen form Fig. [4.7b], these values are very much different from our continuum results. However, it has been argued in Ref. [112] that apart from all the bound states mentioned in Ref. [104], baryon like bound states may also exist in QGP. These baryons make large contributions to the baryonic susceptibilities, especially close to T_c [112]. Taking account of the contributions from the strange baryons may increase the value of C_{BS}. In Ref. [112] it has also been argued that for two

light flavours if one considers the contributions of the baryons only then close to T_c the ratio of 2-nd order isospin susceptibility c_2^I to the 2-nd order baryonic susceptibility c_2 (see Eq. [1.40]) is $c_2^I/c_2 = (\chi_u - \chi_{ud})/(\chi_u + \chi_{ud}) = 0.467$. Clearly this is inconsistent with our results since a value of $c_2^I/c_2 = 0.467$ gives a positive χ_{ud}/χ_u $(= 0.363)$. Whereas, the lattice results for χ_{ud}/χ_u are negative and much smaller in magnitudes. This suggest that the contribution of the mesons (also possibly of the quarks, diquarks and qg-states) are definitely important in the isospin susceptibility c_2^I. If one takes into account of the contributions from the mesons (pions and rhos) and assumes that the Boltzmann weight of the mesons are equal to that of the baryon one gets a lower bound for c_2^I/c_2, namely $c_2^I/c_2 \geq 0.644$ [122]. But this lower bound gives $\chi_{ud}/\chi_u \leq 0.217$ and hence very far from our results. Moreover, very recently it has been argued [123] that one can carefully tune the densities of the baryon and meson like bound states in the model of Refs. [104, 112] to reproduce the lattice results for FODQNS. But even those carefully tuned values fail to reproduce [123] the lattice results for higher order susceptibilities. In view of all these, the lattice results of Ref. [106] favour a quasi-particle like picture of QGP, as opposed to the bound state model of Ref. [104, 112]. The results of this chapter show that these lattice results are really robust in the sense that they have very mild dependence on the lattice spacing and on the sea quark content of the theory [70].

4.5 Summary

In this chapter we have made a careful investigation of the continuum limit of FODQNS, FDQNS and their different ratios in quenched QCD at vanishing chemical potentials. We have performed continuum extrapolations using lattices with large temporal extents, $N_\tau = 12, 10, 8, 4$, and in the temperature range $T_c < T \leq 2T_c$, where QGP is likely to be strongly coupled. Using these results we have looked at the continuum limits of different conserved charge-flavour correlations. These observables are helpful in identifying the degrees of freedom of the strongly interacting QGP. Our study shows that the LQCD estimates of these quantities are robust— (i) they are almost independent of the lattice spacing, (ii) they have very mild dependence on the sea quark content of the theory. We

have also investigated the volume dependence of these ratios and found that the finite volume effects are under control. Finally, we have found that all these quantities acquire values very close to their respective ideal gas limits, even for temperatures just above T_c. All these results indicate that the degrees of freedom of the strongly coupled QGP are quasi-quark like. We have also confirmed the robustness of the Wroblewski parameter, which is of interest to the experiments in RHIC and LHC.

Chapter 5

PNJL model and lattice results

5.1 Introduction

Our LQCD studies of previous chapters indicate that in the vicinity of T_c QGP is a strongly interacting system with quasi-particle like degrees of freedom. As mentioned earlier, similar indications have been found in numerous other LQCD studies, as well as from the experimental results of RHIC. While lattice studies are based on the first principles, in view of their numerical nature it is important to understand the underlying physics of these lattice results in terms of QCD inspired effective models. Apart from the understanding of the underlying physics, an added advantage of such models is that they can be used to investigate the properties of QCD in the parameter region inaccessible to LQCD studies, *e.g.* in the region of large chemical potentials. But in order to make those predictions, first, these models must reproduce the known LQCD results to verify that they capture the correct physics. Hence it is necessary to put these effective models to stringent tests against the available LQCD data.

Out of many such effective models which have been proposed (*e.g.* see Refs. [99, 100, 101, 102, 104]), we concentrate on one such model, *viz.* the Polyakov loop coupled Nambu-Jona-Lasinio (PNJL) model [124, 125, 103], in this chapter. QCD exhibits dynamical chiral symmetry breaking and confinement properties. Both these features of QCD are related to two different global symmetries of the QCD Lagrangian in appropriate limits. However, the relation between the spontaneous chiral symmetry breaking and confinement still remains an open

issue. The primary aim of the PNJL model is to provide a unified picture of these two features of QCD.

In the limit of infinite quark mass, the thermal average of the Polyakov loop (*i.e.* the Wilson line) can be considered as the order parameter for the confinement-deconfinement transition [126]. Though in presence of dynamical quarks the Polyakov loop is not a rigorous order parameter for this transition, it still serves as an indicator of a rapid quark-hadron crossover. Motivated by this observation, Polyakov loop based effective theories have been suggested [127, 128, 129] to capture the underlying physics of the confinement-deconfinement transition. The essential ingredient of these models is an effective potential constructed out of the Polyakov loop (and its complex conjugate). More recently, the parameters in these effective theories have been fixed [130, 131] using the data from LQCD simulations.

In the limit of vanishing quark masses the QCD Lagrangian has a global chiral symmetry, which is however broken spontaneously at low temperatures (and hence the absence of chiral partners of low-lying hadrons). This symmetry is expected to be restored at higher temperatures and chemical potentials. The chiral condensate is considered to be the order parameter in this case. Various effective chiral models exist for the study of physics related to the chiral dynamics. One such oft-used model is the Nambu-Jona-Lasinio (NJL) model [132, 133]. The parameters of this model are fixed from the phenomenology of the hadronic sector at zero temperature.

In the PNJL model one is able to couple the chiral and deconfinement order parameters within a single framework. This is done by extending the NJL Lagrangian through the introduction of a Polyakov loop based effective Lagrangian and by replacing the ordinary derivatives of the NJL Lagrangian by covariant derivatives, which takes care of the interactions of quarks with effective gluon fields. While the NJL part is supposed to give the correct chiral properties, the Polyakov loop part captures the deconfinement physics. Thus, such a model can be considered as a testing ground to study the phase structure and critical phenomena related with deconfinement and chiral phase transitions.

The initial motivation to couple the Polyakov loop to the NJL model was to provide some understanding of the coincidence of chiral symmetry restoration and

deconfinement transitions observed in LQCD simulations [134, 135] . (A somewhat different claim has been made in Ref. [136]). Indeed the PNJL model worked well to obtain the coincidence of onset of chiral restoration and deconfinement [124, 125]. Recently the introduction of the Polyakov loop potential has made it possible to extract estimates of various thermodynamic quantities [103]. In Ref. [103] it was found that the QCD EoS, at $\mu_0 = 0$ (for the definition of μ_0 see Eq. [1.37]), calculated from the PNJL model agrees with the LQCD data. However, though the PNJL model reproduces the qualitative features of LQCD data for the quark number density $n_0 = \partial \ln \mathcal{Z}/\partial\mu_0$, quantitative deviations are significant for larger values of μ_0. Later in Ref. [137] c_n 's (see Eq. [1.40]) were analyzed within the PNJL model. It was found that while both the lattice and PNJL model have the same qualitative features for c_n, the quantitative agreements are not so good.

In view of these results it is very important to perform more stringent tests on the PNJL model, specially in presence of non-zero chemical potentials. In Chapter [4] we have seen that the Flavour Off-Diagonal Quark Number Susceptibilities (FODQNS) play a crucial role in capturing the underlying physics of the lattice results. Hence the main aim of this chapter is to calculate the FODQNS within the framework of the PNJL model and compare them against the available LQCD data. In order to do so, we extend [71] the PNJL model for non-zero isospin chemical potential μ_I (see Eq. [1.37] for the definition) to calculate the coefficients c_n^I 's (see Eq. [1.40]). Once both c_n and c_n^I are known the FDQNS and FODQNS are given by the relations [64]—

$$\frac{\chi_u}{T^2} = \frac{c_2^I + c_2}{2}, \qquad \text{and} \qquad \frac{\chi_{ud}}{T^2} = \frac{c_2^I - c_2}{2}. \tag{5.1}$$

So by making this extension to the PNJL model one will be able to compute the FODQNS, as well as the FDQNS.

As discussed in Chapter [4], the FODQNS can be thought of as a measure of the correlations among different flavours. In order to have a closer look at the FODQNS we, further, modify the NJL part of the PNJL model by using the NJL Lagrangian proposed in [138]. This Lagrangian has a term that can be interpreted as an interaction induced by instantons and reflects the $U_A(1)$-anomaly of QCD. It has the structure of a 't-Hooft determinant in the flavour space [139], leading to flavour-mixing. By adjusting the relative strength of this

term one can explicitly control the amount of flavour-mixing in the NJL sector. This modified NJL Lagrangian reduces to the standard NJL Lagrangian [132, 133] in some particular limit. This modification of the PNJL model will allow us to study the effects of such flavour-mixing on various susceptibilities, specially on the FODQNS which measures the u-d flavour correlation (for a $N_f = 2$ theory).

Such flavour-mixing effect is also related to an important issue regarding the NJL-type models. Within the framework of an NJL model it has been found [140] that for $\mu_I = 0$, in the $T - \mu_0$ plane, there is a single first order phase transition line (which ends at a critical endpoint) at low temperatures. But for $\mu_I \neq 0$ this single line separates into two first order phase transition lines because of the different behaviour of the u and d quark condensates [141]. Thus there is a possibility of having two critical end-points in the QCD phase diagram [141]. This has also been observed in Random Matrix models [142], in ladder QCD models [143] as well as in hadron resonance gas models [144]. It was then argued in Ref. [138] that the flavour-mixing through the instanton effects [145, 146] may wipe out this splitting. By comparing various susceptibilities for different amount of flavour-mixing one may have some idea about the amount of the flavour-mixing favoured by the LQCD simulations. This in turn may shed some light on the phase structure of the NJL model itself.

5.2 Formalism

5.2.1 The model

Following Refs. [140, 138] we chose the two flavour (u and d) NJL part of the Lagrangian to be

$$\begin{aligned}
\mathcal{L}_{NJL} &= \mathcal{L}_0 + \mathcal{L}_1 + \mathcal{L}_2, \qquad \text{with} && \text{(5.2a)}\\
\mathcal{L}_0 &= \bar{\psi}(i\partial\!\!\!/ - m)\psi, && \text{(5.2b)}\\
\mathcal{L}_1 &= G_1\left[\left(\bar{\psi}\psi\right)^2 + \left(\bar{\psi}\vec{\tau}\psi\right)^2 + \left(\bar{\psi}i\gamma_5\psi\right)^2 + \left(\bar{\psi}i\gamma_5\vec{\tau}\psi\right)^2\right], && \text{(5.2c)}\\
\mathcal{L}_2 &= G_2\left[\left(\bar{\psi}\psi\right)^2 - \left(\bar{\psi}\vec{\tau}\psi\right)^2 - \left(\bar{\psi}i\gamma_5\psi\right)^2 + \left(\bar{\psi}i\gamma_5\vec{\tau}\psi\right)^2\right]. && \text{(5.2d)}
\end{aligned}$$

Here,

$$\psi = (u, d)^T, \qquad \text{and} \qquad m = diag(m_u, m_d). \tag{5.3}$$

G_1 and G_2 are two coupling constants with dimensions $[G_1] = [G_2] = [\text{energy}]^{-2}$. We will also assume flavour degeneracy, *i.e.* $m_u = m_d = m_0$. For $m_0 = 0$ different parts of the Lagrangian $\mathcal{L}_{NJL}$ have the following global symmetries—

$$\mathcal{L}_0 \;:\; SU_V(2) \times SU_A(2) \times U_V(1) \times U_A(1), \tag{5.4a}$$

$$\mathcal{L}_1 \;:\; SU_V(2) \times SU_A(2) \times U_V(1) \times U_A(1), \tag{5.4b}$$

$$\mathcal{L}_2 \;:\; SU_V(2) \times SU_A(2) \times U_V(1), \tag{5.4c}$$

where $SU_V(2)$ is the isospin symmetry, $U_V(1)$ is the baryonic symmetry, $SU_A(2)$ is the chiral symmetry and $U_A(1)$ is the axial symmetry. $\mathcal{L}_2$ has the structure of a 't-Hooft determinant, $\det\left[\bar{\psi}(1+\gamma_5)\psi\right] + \det\left[\bar{\psi}(1-\gamma_5)\psi\right]$ [133, 139], and breaks $U_A(1)$ axial symmetry. This interaction can be interpreted as induced by instantons and reflects the $U_A(1)$-anomaly of QCD [139].

Once the NJL part of the Lagrangian is chosen one can then introduce the Polyakov loop part (at non-zero quark chemical potentials μ_f) [125, 103]—

$$\begin{aligned} \mathcal{L}_{PNJL} &= \mathcal{L}'_{NJL} + \bar{\psi}\mu\gamma_0\psi - \mathcal{U}\left(\Phi[A], \bar{\Phi}[A], T\right) \\ &= \mathcal{L}'_0 + \mathcal{L}_1 + \mathcal{L}_2 + \bar{\psi}\mu\gamma_0\psi - \mathcal{U}\left(\Phi[A], \bar{\Phi}[A], T\right), \end{aligned} \tag{5.5}$$

where $\mu = diag(\mu_u, \mu_d)$. The difference between the kinetic terms $\mathcal{L}_0$ and $\mathcal{L}'_0$ is that one has replaced the partial derivative of $\mathcal{L}_0$ by a covariant derivative, *i.e.*

$$\mathcal{L}'_0 = \bar{\psi}\left(i\not{D} - m\right)\psi. \tag{5.6}$$

Here,

$$D_\mu = \partial_\mu - iA_\mu, \qquad A_\mu = \delta_{\mu 0}A^0, \qquad \text{and} \qquad A_\mu(x) = g\mathcal{A}^{(a)}_\mu(x)\lambda_a/2. \tag{5.7}$$

$\mathcal{A}^{(a)}_\mu(x)$ are $SU(3)$ gauge fields, λ_a are Gell-Mann matrices and g denotes the QCD coupling.

$\mathcal{U}\left(\Phi[A], \bar{\Phi}[A], T\right)$ is an effective potential expressed in terms of the traced (over color) Polyakov loop (L), with periodic boundary conditions, and its charge conjugate—

$$L(\vec{x}) = \mathcal{P}\exp\left[i\int_0^\beta d\tau\ A_4(\vec{x}, \tau)\right], \qquad \Phi = \frac{\text{Tr } L}{N_c}, \qquad \bar{\Phi} = \frac{\text{Tr } L^\dagger}{N_c}. \tag{5.8}$$

Here the notation $\mathcal{P}$ denotes the path order product, β is the inverse temperature and $A_4 = iA_0$. Following Ref. [103] the gauge part of the Lagrangian is chosen to be

$$\frac{\mathcal{U}(\Phi,\bar{\Phi},T)}{T^4} = -\frac{b_2(T)}{2}\Phi\bar{\Phi} - \frac{b_3}{6}\left(\Phi^3+\bar{\Phi}^3\right) + \frac{b_4}{4}\left(\bar{\Phi}\Phi\right)^2, \qquad \text{with} \tag{5.9a}$$

$$b_2(T) = a_0 + a_1\left(\frac{T_0}{T}\right) + a_2\left(\frac{T_0}{T}\right)^2 + a_3\left(\frac{T_0}{T}\right)^3. \tag{5.9b}$$

The effective Lagrangian $\mathcal{U}$ for the gauge field has a global $Z(3)$ symmetry, corresponding to the center symmetry of QCD's $SU(3)$ gauge symmetry. At low temperatures $\mathcal{U}$ has a single minimum at $\Phi = 0$, while at high temperatures it develops a second one which turns into the absolute minimum above a critical temperature T_0. Φ and $\bar{\Phi}$ are treated as independent classical fields.

One can proceed along the standard way [133] to perform a mean field analysis of the NJL part of the PNJL action, by expanding $\mathcal{L}'_{NJL}$ around the independent u and d quarks condensates $\sigma_u \equiv \langle\bar{u}u\rangle$ and $\sigma_d \equiv \langle\bar{d}d\rangle$ [138, 103], to obtain the thermodynamic potential ($\Omega = -T\ln\mathcal{Z}/V$)

$$\Omega(T,\mu_u,\mu_d) = \mathcal{U}\left(\Phi,\bar{\Phi},T\right) + \sum_{f=u,d}\Omega_0(T,\mu_f;M_f) + 2G_1\left(\sigma_u^2+\sigma_d^2\right) + 4G_2\sigma_u\sigma_d, \quad \text{where} \tag{5.10a}$$

$$\begin{aligned}\Omega_0(T,\mu_f;M_f) &= -2N_c\int\frac{d^3p}{(2\pi)^3}E_f\theta(\Lambda^2-\vec{p}^{\,2}) \\ &- 2T\int\frac{d^3p}{(2\pi)^3}\mathrm{Tr}\,\ln\left[1+Le^{-(E_f-\mu_f)/T}\right] \\ &- 2T\int\frac{d^3p}{(2\pi)^3}\mathrm{Tr}\,\ln\left[1+L^\dagger e^{-(E_f+\mu_f)/T}\right].\end{aligned} \tag{5.10b}$$

Here the effective energies (E_f) and the effective masses (m_f) of the quarks are given by

$$E_{u,d} = \sqrt{m_{u,d}^2+p^2}, \qquad \text{and} \qquad m_{u,d} = m_0 - 4G_1\sigma_{u,d} - 4G_2\sigma_{d,u}. \tag{5.11}$$

The momentum integral has an ultraviolet cut-off Λ. This is because the NJL model contains four-fermion interactions, which are non-renormalizable operators in $3+1$ dimensions.

For an $SU(3)$ gauge theory the Polyakov loop L satisfies the conditions $LL^\dagger = 1$, $\det L = 1$ and hence can be diagonalized as $L = diag(e^{i\psi}, e^{i\psi'}, e^{-i(\psi+\psi')})$. Using this fact and the identity $\mathrm{Tr}\ \ln X = \ln\det X$ one can easily see that

$$\begin{aligned} & \ln\det\left[1 + Le^{-(E_f-\mu_f)/T}\right] + \ln\det\left[1 + L^\dagger e^{-(E_f+\mu_f)/T}\right] \\ = \;& \ln\left[1 + 3\left(\Phi + \bar{\Phi}e^{-(E_f-\mu_f)/T}\right)e^{-(E_f-\mu_f)/T} + e^{-3(E_f-\mu_f)/T}\right] \\ + \;& \ln\left[1 + 3\left(\bar{\Phi} + \Phi e^{-(E_f+\mu_f)/T}\right)e^{-(E_f+\mu_f)/T} + e^{-3(E_f+\mu_f)/T}\right]. \end{aligned} \tag{5.12}$$

With the help of the above relation one arrives at the final form of the thermodynamic potential

$$\begin{aligned} \Omega(T,\mu_u,\mu_d) &= \mathcal{U}\left(\Phi,\bar{\Phi},T\right) \\ &+ \sum_{f=u,d}\Omega_0(T,\mu_f;M_f) + 2G_1\left(\sigma_u^2+\sigma_d^2\right) + 4G_2\sigma_u\sigma_d, \end{aligned} \tag{5.13}$$

where

$$\begin{aligned} & \Omega_0(T,\mu_f;M_f) = -2N_c\int\frac{d^3p}{(2\pi)^3}E_f\theta(\Lambda^2-\vec{p}^{\,2}) \\ - \;& 2T\int\frac{d^3p}{(2\pi)^3}\ln\left[1+3\left(\Phi+\bar{\Phi}e^{-(E_f-\mu_f)/T}\right)e^{-(E_f-\mu_f)/T}+e^{-3(E_f-\mu_f)/T}\right] \\ - \;& 2T\int\frac{d^3p}{(2\pi)^3}\ln\left[1+3\left(\bar{\Phi}+\Phi e^{-(E_f+\mu_f)/T}\right)e^{-(E_f+\mu_f)/T}+e^{-3(E_f+\mu_f)/T}\right]. \end{aligned} \tag{5.14}$$

The equations of motion for the mean field variables (σ_u, σ_d, Φ, $\bar{\Phi}$) are obtained by minimizing the thermodynamic potential Ω with respect to those variables—

$$\frac{\partial\Omega}{\partial\sigma_u}=0, \qquad \frac{\partial\Omega}{\partial\sigma_d}=0, \qquad \frac{\partial\Omega}{\partial\Phi}=0, \qquad \frac{\partial\Omega}{\partial\bar{\Phi}}=0. \tag{5.15}$$

These coupled equations can then be simplified to obtain

$$\sigma_f = -6\int\frac{d^3p}{(2\pi)^3}\frac{m_f}{E_f}\left[\theta(\Lambda^2-p^2) - \mathcal{N}(E_f)\mathcal{M}(E_f) - \bar{\mathcal{N}}(E_f)\bar{\mathcal{M}}(E_f)\right], \tag{5.16a}$$

$$\frac{\partial\mathcal{U}}{\partial\Phi} = 6T\sum_{f=u,d}\int\frac{d^3p}{(2\pi)^3}\left[\mathcal{N}(E_f)e^{-(E_f-\mu_f)/T} + \bar{\mathcal{N}}(E_f)e^{-2(E_f+\mu_f)/T}\right], \tag{5.16b}$$

$$\frac{\partial\mathcal{U}}{\partial\bar{\Phi}} = 6T\sum_{f=u,d}\int\frac{d^3p}{(2\pi)^3}\left[\mathcal{N}(E_f)e^{-2(E_f-\mu_f)/T} + \bar{\mathcal{N}}(E_f)e^{-(E_f+\mu_f)/T}\right], \tag{5.16c}$$

where

$$\mathcal{N}(E_f) = \left[1+3\left(\Phi+\bar{\Phi}e^{-(E_f-\mu_f)/T}\right)e^{-(E_f-\mu_f)/T}+e^{-3(E_f-\mu_f)/T}\right]^{-1}, \quad (5.17a)$$

$$\bar{\mathcal{N}}(E_f) = \left[1+3\left(\bar{\Phi}+\Phi e^{-(E_f+\mu_f)/T}\right)e^{-(E_f+\mu_f)/T}+e^{-3(E_f+\mu_f)/T}\right]^{-1}, \quad (5.17b)$$

$$\mathcal{M}(E_f) = \left(\Phi+2\bar{\Phi}e^{-(E_f-\mu_f)/T}\right)e^{-(E_f-\mu_f)/T}+e^{-3(E_f-\mu_f)/T}, \quad (5.17c)$$

$$\bar{\mathcal{M}}(E_f) = \left(\bar{\Phi}+2\Phi e^{-(E_f+\mu_f)/T}\right)e^{-(E_f+\mu_f)/T}+e^{-3(E_f+\mu_f)/T}, \quad (5.17d)$$

and $f \in \{u, d\}$.

For convenience, following Ref. [138], we parametrize the two couplings G_1 and G_2 —

$$G_1 = (1-\alpha)G_0, \qquad \text{and} \qquad G_2 = \alpha G_0. \quad (5.18)$$

Before proceeding further we note some important features of this model:

- Since the gluons in this model are contained only in a static background field, the model would be suitable to study the physics below $T = 2.5T_c$. It has been argued in Ref. [147] that above this temperature the transverse degrees of freedom become important.

- In general, pion condensation takes place in NJL model for $\mu_I > m_\pi/2$, m_π being the pion mass. Also there is a chiral transition for $\mu_0 \sim 340\ MeV$ (at small T), above which diquark physics becomes important. For simplicity we have neglected both the pion condensates and diquarks in our mean field analysis. This will restrict us in the parameter range $\mu_I < 70\ MeV$ and $\mu_0 < 200\ MeV$.

- The NJL part of our PNJL model is a generalization of the standard NJL model. It can be easily seen form Eqs. [5.13, 5.14] that for $\alpha = 1/2$ (*i.e.* for $G_1 = G_2$) and $\mu_u = \mu_d$ (*i.e.* for $\sigma_u = \sigma_d$) our thermodynamic potential reduces exactly to that of Ref. [103], where standard NJL Lagrangian have been used to formulate the PNJL model, if one puts G_0 equals to half the four-point coupling G of that reference.

  As discussed earlier, for $G_2 = 0$, in the chiral limit ($m_0 = 0$), the full symmetry of the Lagrangian is $SU_V(2) \times SU_A(2) \times U_V(1) \times U_A(1)$. The

coefficient G_2 is inducing the instanton effects, as it breaks the $U_A(1)$ symmetry explicitly by mixing the quark flavours. This flavour-mixing is very clearly seen from Eqs. [5.13, 5.11], where $G_2 = 0$ makes u and d flavours independent. Thus for $\alpha = 0$ there is no instanton induced flavour-mixing. On the other hand, for $\alpha = 1$ the $U_A(1)$ preserving $\mathcal{L}_1$ vanishes and the Lagrangian only contains the $U_A(1)$ breaking $\mathcal{L}_2$. Hence in this limit the flavour-mixing becomes maximal.

- For the NJL sector, without coupling to the Polyakov loop (i.e. setting $\Phi = \bar{\Phi} = 1$), one can easily see that the expression for Ω in Eqs. [5.13, 5.14] is invariant under the transformations $\mu_u \to -\mu_u$ and/or $\mu_d \to -\mu_d$. This implies that the physics along the directions of $\mu_0 = 0$ and $\mu_I = 0$ at any given temperature are equivalent. However, inclusion of the Polyakov loop makes Ω invariant only under the simultaneous transformations $\Phi \to \bar{\Phi}$ and $\mu_{u,d} \to -\mu_{u,d}$ and vice-verse. This is a manifestation of the CP symmetry. Thus coefficients of Φ and $\bar{\Phi}$ are found to be equal when $\mu_0 = 0$, and different when $\mu_I = 0$. So in the $T - \mu_I$ plane one is expected to have $\Phi = \bar{\Phi}$, and everywhere else $\Phi \neq \bar{\Phi}$. This feature is reminiscent of the complex fermion determinant of LQCD at $\mu_0 \neq 0$.

- Quark condensates σ_u and σ_d are equal to each other whenever $\mu_0 = 0$ or $\mu_I = 0$ (see Eqs. [5.16, 5.17]) in the NJL as well as PNJL model. It is clear from Eq. [5.13] that whenever $\sigma_u = \sigma_d$, the couplings G_1 and G_2 come in the combination $G_1 + G_2 = G_0 = \textit{constant}$. This means that the physics is completely independent of the relative strength of these couplings whenever either $\mu_0 = 0$ or $\mu_I = 0$.

5.2.2 Taylor expansion of pressure in chemical potentials

Once the thermodynamic potential is known the pressure, as function of T, μ_0 and μ_I, can be easily computed using the relation

$$P(T, \mu_0, \mu_I) = -\Omega(T, \mu_0, \mu_I). \tag{5.19}$$

The above relation assumes the system to be homogeneous. One can, further, expand the pressure in a Taylor series of the two chemical potentials μ_0 and μ_I, around $\mu_0 = \mu_I = 0$ —

$$\frac{P\left(T,\mu_0,\mu_I\right)}{T^4} = \sum_{n=0}^{\infty}\sum_{j=0}^{n} \frac{n!}{j!\ k!}\ c_n^{jk}(T)\left(\frac{\mu_0}{T}\right)^j\left(\frac{\mu_I}{T}\right)^k, \tag{5.20}$$

where

$$c_n^{jk}(T) = \left.\frac{\partial^n\left(P/T^4\right)}{\partial\left(\frac{\mu_0}{T}\right)^j\partial\left(\frac{\mu_I}{T}\right)^k}\right|_{\mu_0=\mu_I=0}, \qquad \text{and} \qquad k = n-j. \tag{5.21}$$

The n = odd terms vanish due to CP symmetry. Even for the n = even terms, all the coefficients c_n^{jk} with j and k both odd vanish identically due to flavour degeneracy.

These coefficients can easily be related to c_n and c_n^I, defined in Eq. [1.40]—

$$c_n = c_n^{n0}, \qquad \text{and} \qquad c_n^I = c_n^{(n-2)2} \quad (n \geq 2). \tag{5.22}$$

Flavour diagonal (c_n^{uu}) and flavour off-diagonal (c_n^{ud}) susceptibilities can also be defined in terms of these coefficients [64]

$$c_n^{uu} = \frac{c_n^{n0} + c_n^{(n-2)2}}{4}, \qquad \text{and} \qquad c_n^{ud} = \frac{c_n^{n0} - c_n^{(n-2)2}}{4}. \tag{5.23}$$

For $n = 2$ these relations give the FDQNS and FODQNS (see Eqs. [1.36])—

$$\frac{\chi_u}{T^2} = 2c_2^{uu}, \qquad \text{and} \qquad \frac{\chi_{ud}}{T^2} = 2c_2^{ud}. \tag{5.24}$$

5.2.3 Specific heat and speed of sound

Given the thermodynamic potential Ω, the energy density ϵ is obtained from the relation

$$\epsilon = -T^2\left.\frac{\partial(\Omega/T)}{\partial T}\right|_V = -T\left.\frac{\partial\Omega}{\partial T}\right|_V + \Omega. \tag{5.25}$$

While the specific at constant volume (C_V) is given by

$$C_V = \left.\frac{\partial\epsilon}{\partial T}\right|_V = -T\left.\frac{\partial^2\Omega}{\partial T^2}\right|_V, \tag{5.26}$$

the speed of sound (C_s) can be computed using the relation—

$$C_s^2 = \left.\frac{\partial P}{\partial\epsilon}\right|_S = \left.\frac{\partial P}{\partial T}\right|_V \Big/ \left.\frac{\partial\epsilon}{\partial T}\right|_V = \left.\frac{\partial\Omega}{\partial T}\right|_V \Big/ T\left.\frac{\partial^2\Omega}{\partial T^2}\right|_V. \tag{5.27}$$

5.3 Results

The NJL sector of the PNJL model has three parameters, *viz.* the four-fermion coupling G_0, the ultraviolet cut-off Λ and the bare quark mass m_0 (we will keep α as a free parameter to tune the amount of flavour-mixing). These three parameters are usually chosen by demanding that the NJL sector reproduces the three physical quantities in the hadronic sector (at $T = 0$), *viz.* the pion mass m_π, the pion decay constant f_π and quark condensates $\sigma_u = \sigma_d$ at zero temperature. On the other hand, the gauge potential $\mathcal{U}$ has seven parameters, *viz.* T_0, a_i $(i = 0, \cdots, 3)$, b_3 and b_4. These parameters are fixed by demanding that $\mathcal{U}$ reproduces the LQCD data on the EoS of a pure $SU(3)$ gauge theory. Using these criteria, all these ten parameters have been fixed in Ref. [103]. Except for T_0, values of all the other parameters of the PNJL model have been chosen to be the same as in Ref. [103].

The parameter T_0 is precisely the transition temperature for this theory. Motivated by LQCD data for the pure $SU(3)$ gauge theory [55, 148] its value was chosen to be 270 MeV [137, 71]. With the coupling to NJL model the transition does not remain first order, as opposed to the pure gauge theory. In this case from the peak in $d\Phi/dT$ the transition (or crossover) temperature T_c comes around 230 MeV [103, 137, 71]. Due to this the authors of Ref. [103] have chosen $T_0 = 190$ MeV such that the T_c becomes about 180 MeV, commensurate with lattice data with two flavours of dynamical fermions [94, 134]. However, following Ref. [137], we shall keep using $T_0 = 270$ MeV, since for $T_0 = 190$ MeV there is about 25 MeV shift in the chiral and deconfinement transitions with all other model parameters remaining fixed. Whereas, for $T_0 = 270$ MeV this shift is less than 5 MeV. We have checked that for both the values of T_0 the susceptibilities we compute, when plotted against T/T_c, show very little dependence on T_0.

Values that we use for all the parameters are listed in Table [5.1] and Table [5.2].

5.3.1 Taylor expansion of pressure

In general, to obtain the Taylor coefficients of pressure one can use either of the two methods— (i) obtain the expressions for c_n^{jk} by taking derivatives of pressure

Inputs		Parameters	
$m_\pi =$	139.3 MeV	$\Lambda =$	0.651 GeV
$f_\pi =$	92.3 MeV	$G_0 =$	5.04 GeV^{-2}
$\mid \langle \bar{u}u \rangle \mid^{1/3} = \mid \langle \bar{d}d \rangle \mid^{1/3} =$	251 MeV	$m_0 =$	5.5 MeV

Table 5.1: Parameters for the NJL sector, taken form Ref. [103].

T_0 (MeV)	a_0	a_1	a_2	a_3	b_3	b_4
270	6.75	-1.95	2.625	-7.44	0.75	7.5

Table 5.2: Parameters of the Polyakov loop potential $\mathcal{U}$, fixed by fitting the LQCD data on EoS of Ref. [55]. Values of these parameters have been from Ref. [103]

with respect to μ_0 and μ_I and then use the values of σ_u, σ_d, Φ and $\bar{\Phi}$ at zero chemical potentials into those expressions; (ii) compute the pressure as a function of μ_0 and μ_I for each value of T, and then fit that pressure to a polynomial in μ_0 and μ_I. In that case the c_n^{jk} will be the coefficients (*i.e.* the fitting parameters) of that fitted polynomial. In any exact computation, these two methods should yield identical results. LQCD, however, at present cannot use method (ii) due to the complex determinant problem. On the other hand, since we are using the mean field analysis, the method (i) may give us wrong results as the mean fields used would be insensitive to μ_0 and μ_I. In this work we have computed the c_n^{jk} using method (ii).

We extract the Taylor expansion coefficients of Eq. [2.9] by fitting, with a polynomial 6-th order in both μ_0 and μ_I, the pressure as a function of μ_0 and μ_I at each temperature. Data for pressure was obtained in the range $0 < \mu_0 < 50\ MeV$ and $0 < \mu_I < 50\ MeV$ at all the temperatures. Spacing between consecutive data was kept at $0.1\ MeV$. We obtain all possible coefficients upto 6-th order. We have checked the reliability of our fits by changing the order of the fitting polynomial, ranges of μ_0 and μ_I and value of m_0. We have done satisfactory reproduction all the coefficients computed in Ref. [137]. In this section we, first, present the results for the standard flavour-mixing in the NJL model parametrization (*i.e.* with $G_1 = G_2$), and then present the results for minimal ($G_2 = 0$) and maximal

($G_1 = 0$) flavour-mixing.

5.3.1.1 $G_1 = G_2$

In this section we present our results for the PNJL model with the standard NJL Lagrangian with $G_1 = G_2 = G_0/2$ (*i.e.* $\alpha = 1/2$). Note that this case has been studied earlier in Refs. [125, 103, 137], but without the isospin chemical potential.

In Fig. [5.1] we show our results for c_n and c_n^I. We have also plotted the LQCD data from Ref. [64] for quantitative comparison. At the second order of Taylor expansion we find (also observed earlier in Ref. [137]) that c_2 compares well with the LQCD data. But c_2^I quickly reaches its ideal gas value above T_c (around $2T_c$) in our model calculations, whereas the LQCD values are lower and match with the value of c_2. At the 4-th order we see that the values of c_4 (also observed in Ref. [137]) in the PNJL model matches closely with those of LQCD data for upto $T \sim 1.05T_c$ and deviates significantly thereafter. The coefficient c_4^I is close to the LQCD data for the full range of T upto $2T_c$. The 6-th order coefficients c_6 and c_6^I are quite consistent with the LQCD results.

In order to investigate these discrepancies between the the PNJL model results and the LQCD data more closely, we have calculated the flavour diagonal (c_n^{uu}) and off-diagonal (c_n^{ud}) susceptibilities, defined in Eq. [5.23], upto 6-th order. The diagonal flavour susceptibilities c_n^{uu} are shown in Fig. [5.2]. Except for c_2^{uu}, all the other LQCD results for flavour diagonal susceptibilities are close to their respective ideal gas values from around $1.2T_c$ onwards. While c_2^{uu} and c_6^{uu} are more or less consistent with the LQCD data, c_4^{uu} deviate significantly from $T \sim 1.05T_c$ onwards.

The flavour off-diagonal susceptibilities c_n^{ud} for the PNJL model are shown, and compared with the LQCD data, in Fig. [5.3]. The LQCD values for all the c_n^{ud} are close to their respective ideal values for $T \gtrsim 1.2T_c$. While c_6^{ud} from the PNJL model follows the LQCD data quite nicely, c_4^{ud} starts deviating for $\gtrsim 1.05T_c$. However, the most striking discrepancy with the LQCD data shows up in the 2-nd order flavour off-diagonal susceptibility c_2^{ud}. The PNJL result for this quantity is very far away form the corresponding LQCD data for the whole temperature range. While for $T > T_c$ the PNJL results do not even start approaching the

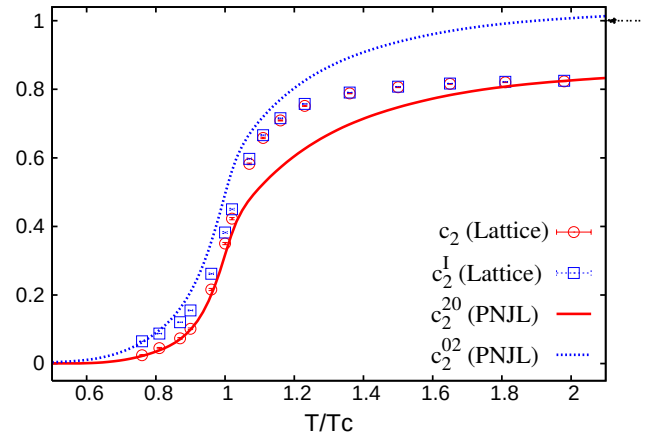

(a)

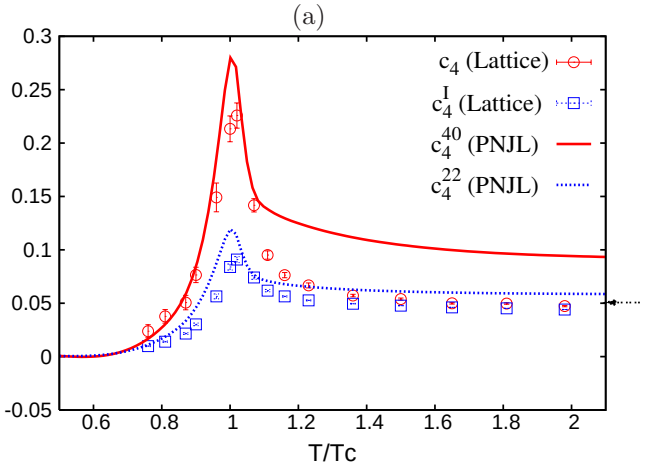

(b)

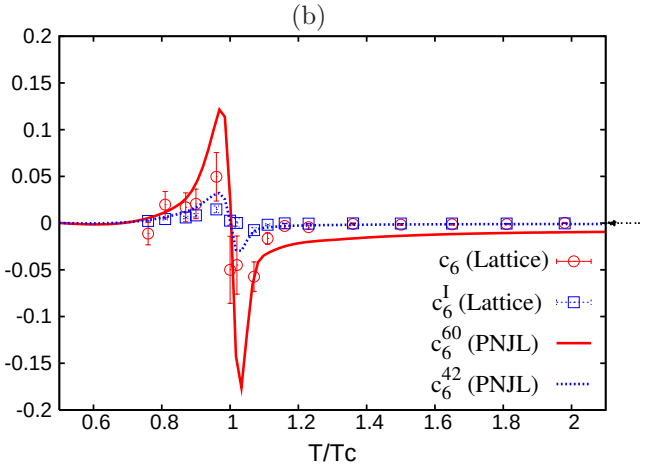

(c)

Figure 5.1: c_n and c_n^I as functions of T/T_c. Symbols are LQCD data [64]. Arrows on the right indicate the corresponding ideal gas values.

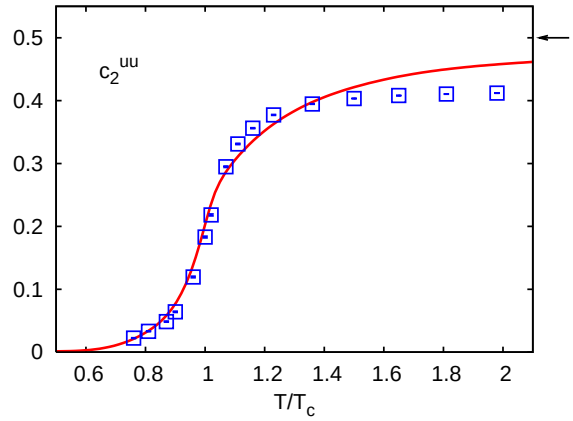

(a)

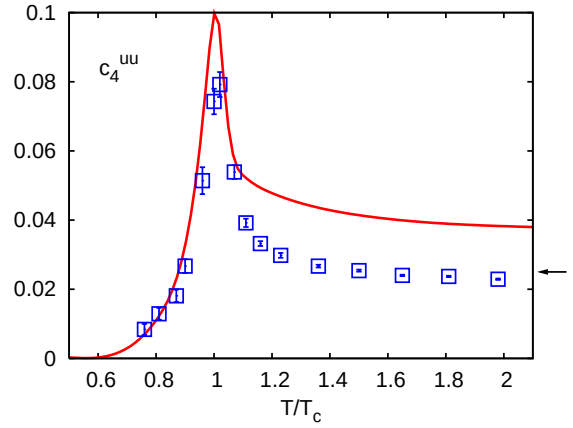

(b)

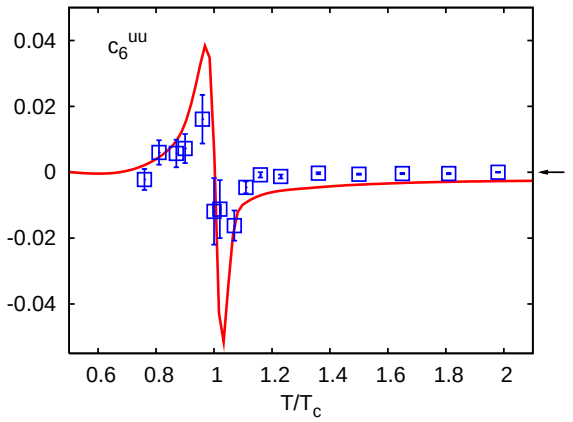

(c)

Figure 5.2: The flavour diagonal susceptibilities, for $n = 2$, 4 and 6, as functions of T/T_c. Symbols are LQCD data [64]. The arrows on the right indicate the respective ideal gas values.

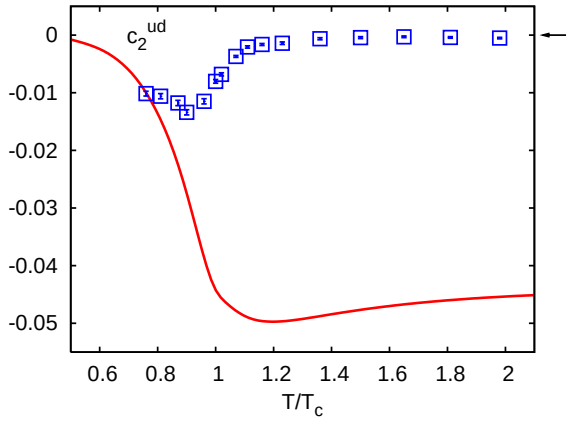

(a)

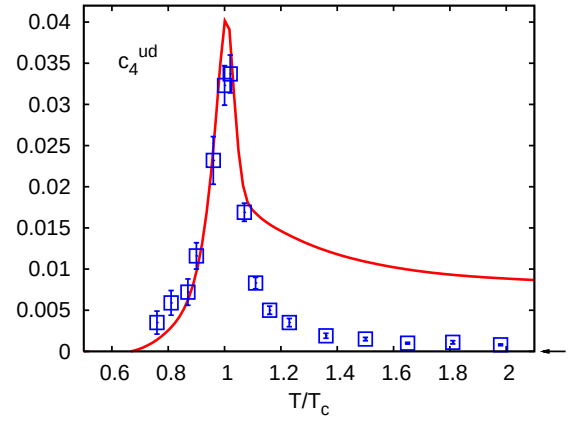

(b)

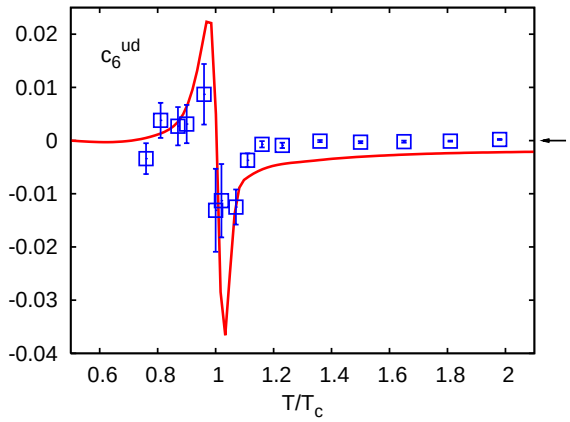

(c)

Figure 5.3: The flavour off- diagonal susceptibilities, for $n = 2$, 4 and 6, as functions of T/T_c. Symbols are LQCD data [64]. The arrows on the right indicate the respective ideal gas values.

corresponding ideal gas value and seems to saturate for $T \sim 1.8T_c$, the LQCD results are very close to the ideal gas value even for temperatures just above T_c.

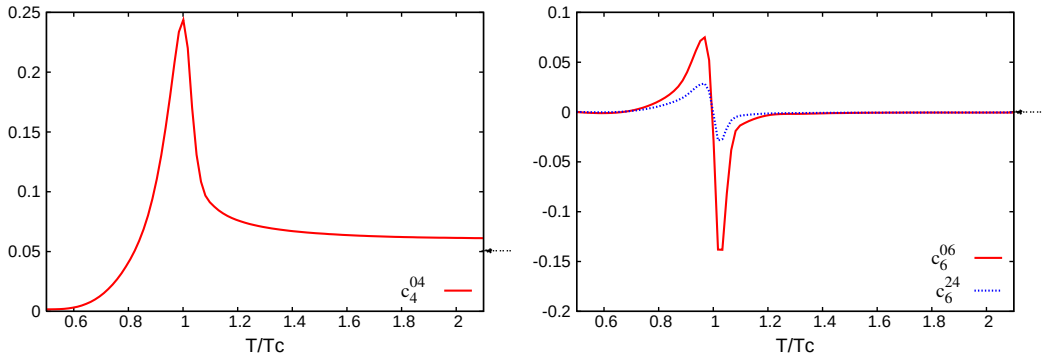

(a) (b)

Figure 5.4: c_4^{04}, c_6^{06} and c_6^{24} as functions of T/T_c. Arrows on the right indicate the respective ideal gas values.

We also present the temperature dependence of the remaining nonzero coefficients (Fig. [5.4]), for which the LQCD data are not available. c_4^{04} is the 4-th order diagonal coefficient in the isospin direction. In contrast to c_4^{40} we see that c_4^{04} approaches the ideal gas value quite fast above T_c. The behaviour of c_6^{06} is quite similar to its counterpart c_6^{60}. Same is also true for the coefficient c_6^{24}.

5.3.1.2 $G_1 \neq G_2$

As can be seen from Eq. [5.24] c_2^{ud} is very closely related to the FODQNS, which is a measure of the flavour-flavour correlation (see Chapter [4] for detail discussion). The fact that the PNJL model has problem in reproducing the LQCD data for c_2^{ud} motivates us to have a closer look at the effects of flavour-mixing on different susceptibilities. As discussed earlier, the instanton induced flavour-mixing can be tuned by varying the value of α between $0-1$. Here we discuss the two extreme cases of $\alpha = 1$ (maximal mixing) and $\alpha = 0$ (zero mixing). We have re-calculated all c_n and c_n^I, upto $n = 6$, for $\alpha = 0,$ and 1. We found that all the diagonal coefficients, including c_2^I and c_4 whose behaviour are the most drastically different in the PNJL model and in LQCD, are independent of the values of α. As a consequence, the FODQNS $[\chi^{ud}/T^2 = (c_2^I - c_2)/2]$ is also unaffected by the instanton induced flavour-mixing effects (see Fig. [5.5a]). This fact can be

understood from the following reasoning. In Section [5.2] we have discussed that the physics is completely independent on the value of α whenever either $\mu_0 = 0$ or $\mu_I = 0$. This in turn implies that all the diagonal coefficients (*i.e.* with no mixed derivatives in μ_0 and μ_I) are expected to be unaffected by amount of flavour-mixing.

However, the mixed derivatives in μ_0 and μ_I can have dependence on α. This is because the values of σ_u and σ_d can be different when both μ_0 and μ_I are together nonzero. This was observed in Ref. [138] for NJL model. But those authors also found that there is a critical value of $\alpha_c \approx 0.11$ above which the condensates σ_u and σ_d become equal even for both μ_0 and μ_I being nonzero. Here, for the PNJL model we have found that all the mixed derivatives upto 6-th order are exactly equal for the two cases $\alpha = 0.5$ (standard mixing used in NJL and PNJL models) and $\alpha = 1$ (maximal mixing), which is in accordance to the results of the above reference. For $\alpha = 0$ all the off-diagonal coefficients were found to differ from those at $\alpha = 0.5$. The dependence of the mixed susceptibilities on the flavour-mixing have been illustrated in Fig. [5.5b] and Fig. [5.5c] by showing one representative coefficient each for $n = 4$, and 6. As can be seen, the instanton effects significantly suppress the temperature variation of these coefficients near T_c. Also it can be observed from Fig. [5.5], that the LQCD data favours larger amount of instanton induced flavour-mixing.

5.3.2 Specific heat and speed of sound

We have also investigated the chemical potential dependence of specific heat C_V and the speed of sound C_s. As discussed in Section [5.2], in order to compute C_V and C_s one requires temperature derivatives of Ω. These derivatives were obtained using the standard finite difference method. To get points close enough we have used cubic spline interpolations. The range of the three representative values of μ_0 and μ_I are such that neither the diquark physics nor the pion condensation become important.

In the ideal gas limit the expression for C_V as a function of temperature T and either of the chemical potentials μ_0 or μ_I is given by, $C_V/T^3 = (74\pi^2/15) + 6(\mu_{0,I}^2/T^2)$. Thus, for large temperatures and not so large chemical potentials, it

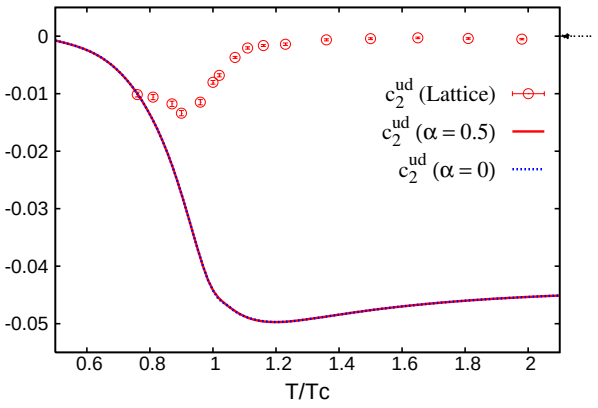

(a)

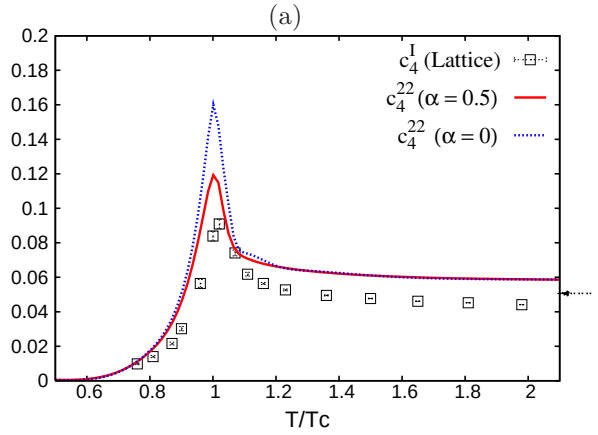

(b)

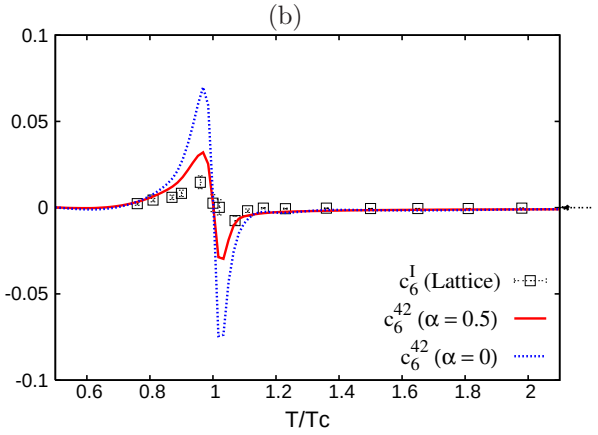

(c)

Figure 5.5: (a) c_2^{ud} is independent of α. (b) & (c) Dependence of some off-diagonal coefficients on the flavour mixing parameter α. Symbols are lattice data [64]. Arrows on the right indicate the corresponding ideal gas values.

is expected that the C_V is more or less independent of $\mu_{0,I}$'s. This is borne out in the PNJL model as seen in Fig. [5.6]. At low temperatures, however, there can be non-trivial contributions from chemical potentials. As illustrated in Fig. [5.6a], at low temperatures there is significant dependence of C_V on μ_0. In the range of μ_I considered, even for $T < T_c$ there seems to be no significant isospin effect. Another interesting feature is that with increasing μ_0 the peak of C_V shifts towards lower temperatures. This signifies that the transition temperature may decrease and also the nature of transition may change as the chemical potentials increase. A decrease of T_c with increasing μ_0 and μ_I is consistent with what have been found in LQCD studies [149, 150].

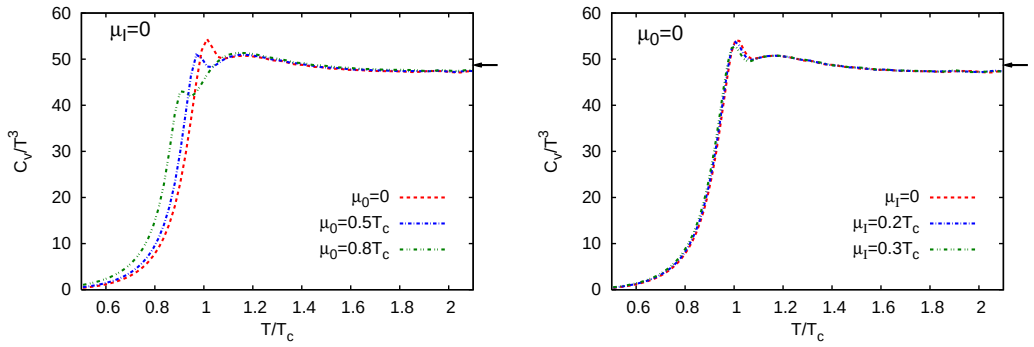

(a) (b)

Figure 5.6: C_V as a function of T/T_c. (a) Shows the variation with μ_0. (b) Shows the variation with μ_I. Arrows on the right indicate the ideal gas value for $\mu_0 = \mu_I = 0$.

The speed of sound in the ideal gas limit is the same $\sqrt{3}$ for any given temperature and chemical potential. As shown in Fig. [5.7] the C_s^2 for different μ_0 and μ_I merge towards the ideal gas value at large temperatures. However, even just above T_c, there is significant increase in C_s^2 for increase in μ_0. So for nonzero quark matter density the speed of sound is higher near T_c and this may have important contribution to thermalization of the matter created in relativistic heavy-ion collision experiments. There seems to be negligible isospin dependence of C_s in the range of temperatures studied here.

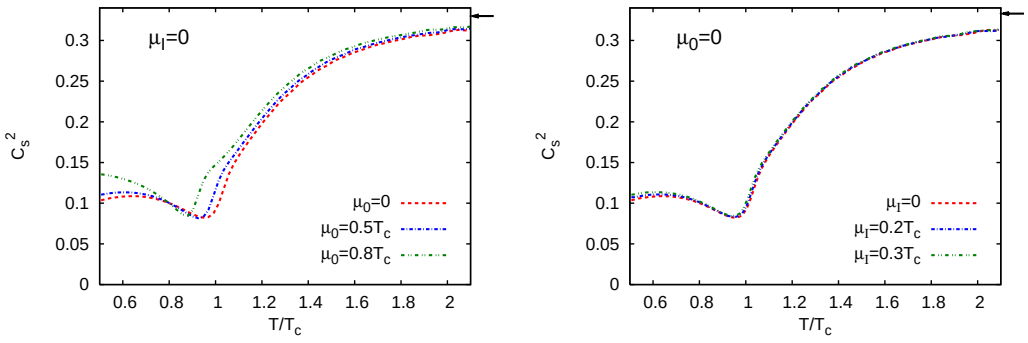

(a) (b)

Figure 5.7: C_s as a function of T/T_c. (a) Shows the variation with μ_0. (b) Shows the variation with μ_I. Arrows on the right indicate the ideal gas value for $\mu_0 = \mu_I = 0$.

5.4 Discussion

Earlier expectation of Refs. [137, 151] was that the mean field analysis may not be adequate and hence the higher order coefficient c_4 in the PNJL model shows significant departure from lattice results. This should have also meant that the c_2^I should be more closer to LQCD data than c_4^I. However, our results show that the c_2^I is significantly different from the LQCD data above T_c, but c_4^I is quite consistent (see Fig. [5.1]). Further, as can be seen from Fig. [5.1] that both the 6-th order coefficients c_6 and c_6^I are quite consistent with the LQCD results. Here we try to present a qualitative explanation of the above mentioned facts.

As pointed out in Section [5.2], in the thermodynamic potential of Eqs. [5.13, 5.14] Φ couples to μ_0 and its conjugate $\bar{\Phi}$ couples to $-\mu_0$ due to CP symmetry. As observed in Refs. [103, 137], in the PNJL model this difference in coupling leads to splitting of Φ and $\bar{\Phi}$ for any nonzero μ_0. (Note that this same phenomenon has also been observed in $SU(N)$ matrix model [152].) Thus even at high temperatures when Φ is close to 1, it decreases with increasing μ_0 and its conjugate $\bar{\Phi}$ increases with increasing μ_0 (see Fig. [5.8a]). This means that the μ_0 dependence of pressure is not the same as that for an ideal gas. Hence the coefficients c_2 and c_4 are both away from their respective ideal gas values. Also note that though c_6 is close enough, it is still distinctly different from zero. On the other hand, for $\mu_0 = 0$, Φ as well as $\bar{\Phi}$ couples to both the μ_I and $-\mu_I$. They are, thus, equal

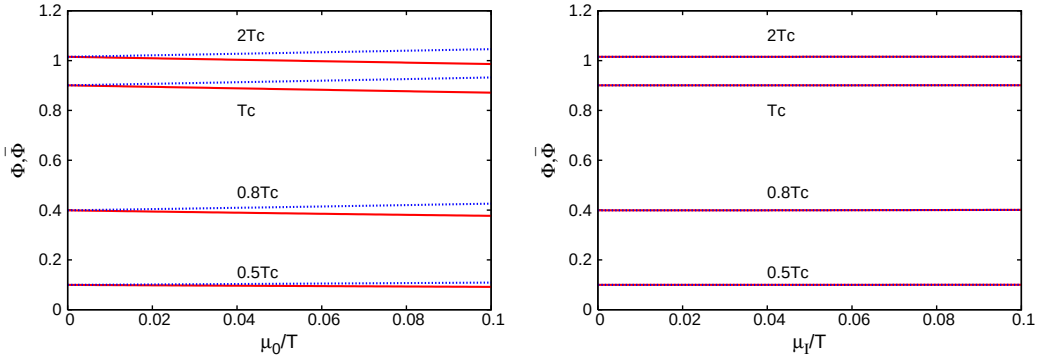

(a) (b)

Figure 5.8: (a) Φ (solid lines) decreases and $\bar{\Phi}$ (dotted lines) increases as a function of μ_0/T ($\mu_I = 0$). (b) Φ (solid lines) and $\bar{\Phi}$ (dotted lines) are equal and almost constant as a function of μ_I/T (for $\mu_0 = 0$).

for all temperatures (see Fig. [5.8b]). Also, both of them remain almost constant with changing μ_I. So the temperature dependence of the c_2^I and its μ_I derivatives are expected to reach the ideal gas behaviour above T_c. Indeed this is exactly what we have found in our studies, see Fig. [5.1a] and Fig. [5.4].

We have seen that the PNJL model fails to reproduce the LQCD results for the FODQNS. As observed in Chapter [4], the correlation among the flavours in FODQNS is largely governed by the interaction of the quarks with the gauge fields and is almost independent of the presence of the quarks loops. This, along with our discussion in the above paragraph, indicates that a modification of the gauge potential in the PNJL model may improve the agreement. (Very recently, in Refs. [154, 155] some studies along this line have been made.) Also, the negativity of c_2^{ud} (see Fig. [5.3a]) indicates that the dominant correlation is between u and $\bar{d}$ and vice-verse, *i.e.* pion-like. Hence inclusion of dynamical pion condensate may also improve the agreement between PNJL model results and LQCD data on FODQNS . (Recently some studies along this line have been made in Refs. [153])

Finally, we have found that a larger amount of instanton induced flavour-mixing is favoured by the LQCD data (see Figs. [5.5b, 5.5b]). We note that value of α which is favoured by the LQCD results is larger than $\alpha_c \approx 0.11$ [138], above which the u and d quark condensates become equal in the NJL model at large μ_0 (but small T and $\mu_I \neq 0$). This observation implies that the NJL model may

have only one first order transition at large values of μ_0, as opposed to the case of two when the flavour-mixing is negligible (see the discussion in Section [5.1] for references).

5.5 Summary

We have extended the PNJL model of Ref. [103] by the introduction of isospin chemical potential. Using this we have studied, within the framework of mean field approximation, the behaviour of strongly interacting matter with two degenerate quark flavours in the phase space of T, μ_0 and μ_I, for small values of the chemical potentials. We have extracted 10 coefficients of Taylor expansion of pressure in the two chemical potentials (μ_0 and μ_I) upto 6-th order. Some of these coefficients were compared with available LQCD data. Since (see Chapter [4]) the FODQNS plays an important role in capturing the underlying physics of the lattice results , we have also computed the FDQNS and FODQNS using the above mentioned coefficients. We found that although the PNJL model reproduces the LQCD data on FDQNS satisfactorily, it fails to do so for FODQNS. We have argued that this discrepancy is probably not due to the limitation of our mean field approximation and use of a modified gauge potential may improve the agreement with the LQCD data. Motivated by the fact that the FODQNS is a measure of flavour-flavour correlations we have, further, extended the model to study the effects of instanton induced flavour-mixing. Unfortunately, we found no effect of flavour-mixing on any diagonal susceptibilities of μ_0 and μ_I, and hence on the FODQNS. However, flavour-mixing effects on the mixed susceptibilities of quark and isospin chemical potentials indicate that large flavour-mixing is favoured by the LQCD data. This may have important consequences [138] on the phase diagram of the NJL model at low temperatures and large chemical potentials. We have also investigated chemical potential dependence of specific heat and speed of sound. Consistent with LQCD findings [149, 150], the peak in specific heat shifts towards lower temperatures with increasing chemical potentials indicating a decrease in the transition temperature.

Chapter 6

Summary and conclusion

Recent experimental results from RHIC indicate the formation of a thermalized medium endowed with large collective flow and very low viscosity. These findings suggest that close to the transition temperature (T_c) nature of Quark Gluon Plasma (QGP) is far from a gas of free quarks and gluons, rather it is a strongly interacting system. Since at these temperatures the QCD coupling is rather large, perturbative studies are not suitable for studying the strongly coupled QGP and non-perturbative techniques are called for. At present, Lattice QCD (LQCD) is the most viable and successful non-perturbative technique for studying such a system. Moreover, numerical simulations of LQCD have the advantage of obtaining almost parameter free predictions for the theory from first principles. This approach has been very successful in providing detail information about the thermodynamic properties of QCD at finite temperature. In this thesis we have studied different thermodynamic properties of QGP using LQCD.

Specific heat at constant volume (C_V) is directly related to the event-by-event transverse momentum fluctuations, which are measurable in heavy ion collision experiments. The speed of sound (C_s), on the other hand, controls the expansion rate of the fire-ball produced in the heavy-ion collisions. Thus the value of C_s is an important input parameter for hydrodynamic studies. Moreover, these quantities provide further tests of all the models and perturbative expansions which try to explain the lattice data on the equation of state (EoS) of QGP. In Chapter [2] we have determined of the continuum limit of C_V and C_s in pure $SU(3)$ gauge theory, for relatively high temperatures ($T \geq 2T_c$). Such a lattice determination

of C_V and C_s needs the appropriate lattice expressions for these quantities. In Chapter [2] we have shown that a naive application of the lattice temperature derivative on the corresponding energy density (ϵ) leads to incorrect expression for C_V, since C_V/T^3 does not give the correct ideal gas value ($4\epsilon/T^4$) in the high temperature ($T \to \infty$ or $g \to 0$). We then derived the correct expressions for C_V and C_s by employing a dimensionless quantity $\mathcal{C} = \Delta/\epsilon$, $\Delta = \epsilon - 3P$ being the so-called interaction measure. Using those expressions we made a precise (with errors $\sim 5\%$) determination of the continuum limit of C_V and C_s in the high temperature ($T = 2T_c$ and $3T_c$) phase of the gluonic plasma. In the process we also recomputed the EoS by a method which has not been used earlier to obtain the continuum limit. While we found that ϵ, P and C_V deviate from there respective ideal gas values by about 20% even at $3T_c$, the the speed of sound C_s is very close to its ideal gas value at these temperatures. More surprisingly, the ideal gas relation $C_V/T^3 = 4\epsilon/T^4$ seems to hold in spite of the non-ideal behaviour of these quantities. We argued that these apparently contradictory behaviour of the gluonic plasma follows from the smallness of the quantity $\mathcal{C}$. Furthermore, we have argued that the quantity $\mathcal{C}$ gives a measure of the breaking of conformal symmetry in QCD at the long distance scales. Hence our results indicate that, at these temperatures the pure $SU(3)$ gauge theory is close to its conformal symmetric limit. Since the formalism presented in Chapter [2] can easily be extended for the case of fermions, it would be very interesting to recalculate C_V and C_s for the full theory and check whether the above conclusion also holds in that case.

The method (known as the differential method) which we used in Chapter [2] to compute C_V and C_s produces negative pressure in the vicinity of T_c. This restricted us to investigate only the high temperature region. But more interesting physics is expected around the phase transition region. Hence a precise computation of these quantities close to T_c is necessary. The alternative technique which solves this negative pressure problem is known as the integral method. But within the framework of the integral method a quantity like C_V can only be computed using numerical differentiations, which are prone to larger errors. In view of this situation, in Chapter [3] we proposed an improvement for the differential method. In contrast to the choice of the spatial lattice spacing in the previous approach of

the differential method, we chose the temporal lattice spacing to set the scale of the theory. We have shown that this improved method gives positive pressure for all temperatures and lattice spacings that we have studied, even when the earlier method gave negative pressure. Note that this is so in spite of the use of the same perturbative values for the couplings (Karsch coefficients), which was thought to be the cause behind the negative pressure. Moreover, being a differential method, this method can be easily extended for the calculations of C_V and C_s. Using this improved differential method we determined the continuum limit of P, ϵ, C_V and C_s for a pure $SU(3)$ gauge theory in the temperature range $0.9Tc \leq T \leq 3T_c$. A comparison with the integral method showed that both the methods agree for $T \geq 2T_c$. Around T_c pressure and energy density obtained by our method rise more sharply than those for the integral method. We discussed possible sources for these differences. These include coarser lattices, higher order Karsch coefficients, subtraction constant in the integral method *etc.* . Our continuum results showed that for $T \geq 2T_c$, C_V/T^3 and ϵ/T^4 are far from its ideal gas value but are consistent with the prediction in conformal theories that $C_V/T^3 = 4\epsilon/T^4$. At these temperatures we have found that C_s is also quite close to its ideal gas limit, supporting the hypothesis that the pure $SU(3)$ gauge theory is close to its conformal symmetric limit for these temperatures. We also compared our data with the predictions of the perturbation theory and the AdS/CFT correspondence, and found reasonable agreements in certain temperature ranges. A more detailed study regarding the systematic difference between the integral method and our improved differential method is clearly desirable before applying our improved method to the full theory including the quarks.

As mentioned earlier, the results form RHIC experiments as well as different LQCD studies indicate that the QGP is a strongly interacting system in the vicinity of the transition region. In view of this situation, it is very important to identify the degrees of freedom of a strongly coupled QGP. In Chapter [4] we have studied different correlations among the conserved charges and flavours, *viz.* the baryon-strangeness correlation (C_{BS}), electric charge-strangeness correlation (C_{QS}) *etc.* , to do so. Previously it was argued [98, 106] that these correlations help in the identification of the degrees of freedom of QGP. If the relevant degrees of freedom of QGP are quasi-quarks then these quantities will have values close

to their respective ideal gas limit. These quantities can be expressed as ratios of Flavour Off-Diagonal Quark Number Susceptibilities (FODQNS) to Flavour Diagonal Quark Number Susceptibilities (FDQNS), which are computable on the lattice. In Chapter [4] we argued that in general these ratios can depend on the lattice cut-off, and hence their continuum values can be different form those obtained [106] for full QCD but on coarser lattices. In order to have a closer look at these correlations in Chapter [4] we made a careful investigation of the continuum limits of the FDQNS and FODQNS. For these studies we employed the quenched approximation, *i.e.* we neglected the quark loops, due the limitation of present day computer resources. We performed these continuum extrapolations using lattices with large temporal extents, up to temporal lattice size of 12, and in the temperature range $T_c < T \leq 2T_c$, where QGP is likely to be strongly coupled. Using continuum results for FODQNS and FDQNS we studied their ratios, and hence the correlations like C_{BS}, C_{QS} *etc.* . We found that these quantities are almost independent (within 5%) of the lattice spacing over the whole temperature range that we studied. Furthermore, a comparison of our results with that of the previous dynamical simulations [106] also showed that these correlations have very mild dependence on the sea quark content of the theory. We checked the volume dependence of these quantities and found that the finite-volume effects are under control. Hence we conclude that these observables are robust, in the sense that they are almost independent on the lattice spacing and have very mild dependence on the sea quark content of the theory. Moreover, our results showed that all these correlations acquire values very close their respective ideal gas limits, even when the temperature is just above T_c. All these results indicate that the excitations in the strongly coupled QGP are quasi-quark like. In this chapter we have also confirmed the robustness of the Wroblewski parameter, which is related to the strangeness enhancement in QGP and hence relevant for the experiments of RHIC and LHC.

While the LQCD studies have the advantage of being based on first principles, in view of their numerical nature it is important to understand the LQCD results in terms of some QCD inspired effective models. These models have an advantage that they can be used to study the region of the phase space where lattice studies are currently not possible, *e.g.* in the region of large chemical potentials. For

better acceptance, these models should reproduce the known lattice results in order to prove that they capture the correct physics. In Chapter [5] we focus on one such QCD inspired effective model, *viz.* the Polyakov loop coupled Nambu Jona-Lasinio (PNJL) model. In Chapter [4] we found that the FODQNS plays an important role in capturing the underlying physics of the LQCD results. Hence, our aim in Chapter [5] was to calculate this quantity within the framework of the PNJL model and perform a stringent test of the model by comparing those results with that obtained from the LQCD simulations. The primary goal of the PNJL model is to provide a unified picture of the spontaneous chiral symmetry breaking and the confinement phenomenon of QCD. These two features of QCD are related to two different global symmetry of the QCD Lagrangian, *viz.* the approximate chiral symmetry (exact in the limit of vanishing bare quark masses) and the $Z(3)$ center symmetry of the $SU(3)$ gauge symmetry. The PNJL model tries to provide a unified framework for these two phenomena by the coupling a Polyakov loop based effective Lagrangian (which has $Z(3)$ global symmetry) for the gauge fields to the Lagrangian of Nambu Jona-Lasinio (NJL) model (which has the global chiral symmetry for vanishing bare quark masses). The coupling of these two part is done by replacing the ordinary derivatives in the kinetic term of the NJL Lagrangian by covariant derivatives. This takes care of the interactions of quarks with effective gluon fields. In order to compute the FODQNS, we extended the PNJL model (with two degenerate quark flavours) to non-zero isospin chemical potential (μ_I). This enabled us to study, within the framework of mean field approximation, the Taylor expansion of the pressure in the average quark chemical potential (μ_0) and in the isospin chemical potential, around $\mu_0 = \mu_I = 0$. We extracted 10 coefficients of Taylor expansion of pressure upto 6-th order in μ_0 and μ_I. We compared some of these coefficients with available lattice results. Using these coefficients we have calculated the FODQNS, as well as the FDQNS. Although the FDQNS showed reasonably good agreement with the lattice data, the PNJL model failed to reproduce the LQCD results for the FODQNS. While the lattice results on the FODQNS are very close to zero starting from just above T_c, the PNJL model results are far from zero even for temperature as high as $2T_c$. In Chapter [5] we have also argued that this disagreement is probably not due the mean field approximation. We have also provided a qualitative explanation

that these discrepancies are probably caused by the gauge part of the PNJL model. This, along with the fact that the LQCD results for the FODQNS are largely governed by the interactions between the quarks and the gauge fields (as found in Chapter [4]), motivated us to conclude that a modified form of the gauge part of the PNJL Lagrangian may improve its agreement with the lattice results. As the FODQNS is a measure of the flavour-flavour correlation, in order to look at this quantity more closely we modified the NJL part of the PNJL Lagrangian such that it can incorporate the effects of instanton induced flavour-mixing. Unfortunately, we did not find any effect of instanton induced flavour-mixing on the FODQNS. However, comparison of other susceptibilities with the lattice results showed that a larger amount of flavour-mixing is favoured by the LQCD results. This may have an important consequence on the phase structure of NJL-type models, *i.e.* for large μ_0, small T and non-zero μ_I the NJL-type models may have only one first order phase transition line as opposed to two for the case of small flavour-mixing. In future it would be very interesting to perform these analyses using an improved form the gauge Lagrangian (and also possibly including the dynamical pion condensates) in the PNJL model. If these modifications reproduce the LQCD results satisfactorily, one can then employ this model to make predictions for QCD at large chemical potentials.

References

[1] T. Padmanabhan, *Theoretical Astrophysics, Volume III: Galaxies and Cosmology*, Cambridge University Press (2002). 1

[2] For a review see : M. L. Perl, E. R. Lee and D. Loomba, *Mod. Phys. Lett.* A 19, 2595 (2004); L. Lyons, *Phys. Rept.* 129, 225 (1985). 1

[3] For recent reviews see : J. Greensite, *Prog. Part. Nucl. Phys.* 51, 1 (2003); R. Alkofer and L. V. Smeka, *Phys. Rept.* 353, 281 (2001). 1

[4] J. C. Collins and M. J. Perry, *Phys. Rev. Lett.* 34, 1353 (1975). 1, 2

[5] D. J. Gross and F. Wilczek, *Phys. Rev. Lett.* 30, 1343 (1973); H. D. Politzer, *Phys. Rev. Lett.* 30, 1346 (1973). 1, 2

[6] For a review see : L. McLerran, *Rev. Mod. Phys.* 58, 1021 (1986); H. Meyer-Ortmanns, *Rev. Mod. Phys.* 68, 473 (1996); J. Cleymans, R. V. Gavai and E. Suhonen, *Phys. Rept.* 130, 217 (1986); J. Letessier and J. Rafelski, *Hadrons and quark-gluon plasma*, Cambridge University Press (2002). 2

[7] For a review see : D. J. Schwarz, *Annalen Phys.* 12, 220 (2003). 2

[8] For a review see : F. Weber, *Pulsars as astrophysical laboratories for nuclear and particle physics*, Institute of Physics Publishing (1999); K. Rajagopal, *Acta Phys. Polon.* B 31, 3021 (2000). 2

[9] R. Anishetty, P. Koehler and L. D. McLerran, *Phys. Rev.* D 22, 2793 (1980); E. V. Shuryak, *Phys. Rept.* 61, 71 (1980). 2

[10] For a review see : J. W. Harris and B. Muller, *Ann. Rev. Nucl. Part. Sci.* 46, 71 (1996); S. A. Bass, M. Gyulassy, H. Stoecker and W. Greiner, *J. Phys.* G 25, R1 (1999). 2

[11] For a review see : C. A. Ogilvie, *Nucl. Phys.* A 698, 3 (2002). 2

[12] For a review see : H. Satz, *Phys. Rept.* 403-404, 33 (2004). 2

[13] For a review see : K. Adcox *et al.* [PHENIX Collaboration], *Nucl. Phys.* , A 757 (2005) 184; I. Arsene *et al.* [BRAHMS collaboration], *Nucl. Phys.* , A 757 (2005) 1; B. B. Back *et al.* [PHOBOS collaboration], *Nucl. Phys.* , A 757 (2005) 28; J. Adams *et al.* [STAR Collaboration], *Nucl. Phys.* , A 757 (2005) 102. 2, 57

[14] For a review see : F. Carminati *et al.* [ALICE collaboration], *J. Phys.* G 30, 1517 (2004). 2

[15] For a review see : R. Brock *et al.* [CTEQ Collaboration], *Rev. Mod. Phys.* 67, 157 (1995); S. Bethke and J. E. Pilcher, *Ann. Rev. Nucl. Part. Sci.* 42, 251 (1992); J. Engelen and P. Kooijman, *Prog. Part. Nucl. Phys.* 41, 1 (1998); R. Blair, G. Grindhammer, M. Klasen and M. Kramer, hep-ph/0008154. 2

[16] For a review see : J. P. Blaizot, E. Iancu and A. Rebhan, R. C. Hwa (*ed.*) *Quark gluon plasma*, 60 (hep-ph/0303185); J. P. Blaizot and E. Iancu, *Phys. Rept.* 359, 355 (2002); D. F. Litim and C. Manuel, *Phys. Rept.* 364, 451 (2002). 3, 4

[17] E. V. Shuryak, *Sov. Phys. J. E. T. P* 47, 212 (1978). 3

[18] J. Kapusta, *Nucl. Phys.* B 148, 461 (1979). 3

[19] T. Toimela, *Phys. Lett.* B 124, 407 (1983). 3

[20] P. Arnold and C. X. Zhai, *Phys. Rev.* 50, 7603 (1994); *Phys. Rev.* D 51, 1906 (1995). 3

[21] C. X. Zhai and B. M. Kastening, *Phys. Rev.* D 52, 7232 (1995). 3

[22] E. Braaten and A. Nieto, *Phys. Rev. Lett.* 76, 1417 (1996). 3

[23] K. Kajantie, M. Laine, K. Rummukainen and Y. Schroder, *Phys. Rev.* D 67, 105008 (2003); *J. H. E. P.* 0304, 036 (2003). 3, 4, 51, 52

[24] A. D. Linde, *Phys. Lett.* B 96, 289 (1980). 3

[25] B. A. Freedman and L. D. McLerran, *Phys. Rev.* D 16, 1169 (1977). 3

[26] V. Baluni, *Phys. Rev.* D 17, 2092 (1978). 3

[27] T. Toimela, *Int. J. Theor. Phys.* 24, 901 (1985); Erratum *ibid* . 26, 1021 (1987). 3

[28] A. Vuorinen, *Phys. Rev.* D 68, 054017 (2003). 3

[29] A. Ipp, K. Kajantie, A. Rebhan and A. Vuorinen, *Phys. Rev.* D 74, 045016 (2006). 3

[30] K. Kajantie, M. Laine, K. Rummukainen and Y. Schroder, *Phys. Rev. Lett.* 86, 10 (2001). 4

[31] J. O. Andersen, E. Braaten and M. Strickland, *Phys. Rev.* D 61, 074016 (2000); A. Peshier, *Phys. Rev.* D 63, 105004 (2001). 4

[32] J. P. Blaizot, E. Iancu and A. Rebhan, *Phys. Rev. Lett.* 83, 2906 (1999); *Phys. Lett.* B 470, 181 (1999); *Phys. Rev.* D 63, 065003 (2001). 4

[33] K. Wilson, *Phys. Rev.* D 10, 2445 (1970). 4, 7

[34] M. Creutz, Quarks, *Gluon and Lattices*, Cambridge University Press (1985); I. Montvay and G. Münster, *Quantum Fields on a Lattice*, Cambridge University Press (1997); H. J. Rothe, *Lattice Gauge Theories: An Introduction*, World Scientific (1998); F. Karsch, *Lect. Notes Phys.* 583, 209 (2002); E. Laermann and O. Philipsen, *Ann. Rev. Nucl. Part. Sci.* 53, 163 (2003). 4, 5, 7, 8

[35] J. Engels, F. Karsch and H. Satz, *Nucl. Phys.* B 205, 239 (1982). 7

[36] J. Engels, F. Karsch, H. Satz and I. Montvay, *Nucl. Phys.* B 205, 545 (1982). 7, 11, 12, 13, 38, 39

[37] F. Karsch, *Nucl. Phys.* B 205, 285 (1982). 7, 13, 24, 25, 27, 43, 44

[38] K. Symanzik, *Nucl. Phys.* B 226, 187 (1983); *Nucl. Phys.* B 226, 205 (1983). 7

[39] P. Hasenfratz and F. Niedermayer, *Nucl. Phys.* B 414, 785 (1994). 7

[40] H. B. Nielsen and M. Ninomiya, *Phys. Lett.* B 105, 219 (1981); *Nucl. Phys.* B 185, 20 (1981), Erratum *ibid* B 195, 541 (1982); *Nucl. Phys.* B 193, 173 (1981). 8

[41] L. Susskind, *Phys. Rev.* D 16, 3031 (1977). 8

[42] For a recent review see : S. R. Sharpe, *PoS* LAT2006, 022 (2006); hep-lat/0610094. 8

[43] H. Kluberg-Stern, A. Morel, O. Napoly and B. Petersson, *Nucl. Phys.* B 220, 447 (1983) 9

[44] P. Mitra and P. Weisz, *Phys. Lett.* B 126, 355 (1983). 9

[45] M. F. L. Golterman and J. Smit, *Phys. Lett.* B 140, 392 (1984). 9

[46] M. Göckeler, *Phys. Lett.* B 142, 197 (1984). 9

[47] F. Gliozzi, *Nucl. Phys.* B 204, 419 (1982). 9

[48] F. Karsch and I. Stamatescu, *Phys. Lett.* B 227, 153 (1989). 9

[49] P. Hasenfratz and F. Karsch, *Phys. Lett.* B 125, 308 (1983). 9, 15

[50] R. V. Gavai, *Phys. Rev.* D 32, 519 (1985). 9, 15

[51] S. Gupta, *Phys. Rev.* D 64, 034507 (2001). 10, 28, 51, 52

[52] G. P. Lepage and P. B. Mackenzie, *Phys. Rev.* D 48, 2250 (1993). 10

[53] R. G. Edwards, U. M. Heller and T. R. Klassen, *Nucl. Phys.* B 517, 377 (1998). 10

[54] J. Engels, J. Fingberg, F. Karsch, D. Miller and M. Weber, *Phys. Lett.* B 252, 625 (1990). 11, 13

[55] G. Boyd, J. Engels, F. Karsch, E. Laermann, C. Legeland, M. Lutgemeier and B. Petersson, *Phys. Rev. Lett.* , 75 (1995) 4169, *Nucl. Phys.* , B 469 (1996) 419. 13, 14, 19, 27, 28, 47, 48, 49, 52, 85, 86

[56] A. Hasenfratz and P. Hasenfratz, *Nucl. Phys.* B 193, 210 (1981). 12, 42

[57] Y. Deng, *Nucl. Phys.* B (*Proc. Suppl.*) 9, 334 (1989). 13, 37

[58] For a review see : S. Muroya, A. Nakamura, C. Nonaka and T. Takaishi, *Prog. Theor. Phys.* 110, 615 (2003). 15

[59] For a recent review see : C. Schmidt, PoS LAT2006, 021 (2006); hep-lat/0610116. 15

[60] S. A. Gottlieb, W. Liu, D. Toussaint, R. L. Renken and R. L. Sugar, *Phys. Rev.* D 38, 2888 (1988). 15, 62

[61] R. V. Gavai and S. Gupta, *Phys. Rev.* D 68, 034506 (2003). 15

[62] C. R. Allton, S. Ejiri, S. J. Hands, O. Kaczmarek, F. Karsch, E. Laermann and C. Schmidt, *Phys. Rev.* D 68, 014507 (2003). 15

[63] R. V. Gavai and S. Gupta, *Phys. Rev.* D 64, 074506 (2001). 15

[64] C. R. Allton, M. Doring, S. Ejiri, S. J. Hands, O. Kaczmarek, F. Karsch, E. Laermann and K. Redlich, *Phys. Rev.* D 71, 054508 (2005). 16, 64, 77, 84, 87, 88, 89, 90, 93

[65] R. V. Gavai and S. Gupta, *Phys. Rev.* D 71, 114014 (2005). 16, 62, 64

[66] J. P. Blaizot, E. Iancu and A. Rebhan, *Phys. Lett.* B 523, 143 (2001). 16, 60, 64

[67] A. Vuorinen, *Phys. Rev.* D 67, 074032 (2003). 16

[68] R. V. Gavai, S. Gupta and S. Mukherjee, *Phys. Rev.* D 71, 074013 (2005) 16, 21, 24, 38, 43, 44

[69] R. V. Gavai, S. Gupta and S. Mukherjee, *PoS* LAT2005, 173 (2006); hep-lat/0506015. 16, 37, 38

[70] S. Mukherjee; *Phys. Rev.* D 74, 054508 (2006). 17, 60, 73

[71] S. Mukherjee, M. G. Mustafa and R. Ray, *Phys. Rev.* D 75, 094015 (2007). 17, 77, 85

[72] L. Stodolsky, *Phys. Rev. Lett.* 75, 1044 (1995). 19

[73] R. Korus, S. Mrowczynski, M. Rybczynski and Z. Wlodarczyk, *Phys. Rev.* C 64, 054908 (2001). 19

[74] M. J. Tannenbaum [PHENIX Collaboration], nucl-ex/0512004. 19

[75] J. Y. Ollitrault, *Phys. Rev.* D 46, 229 (1992). 20

[76] H. Sorge, *Phys. Rev. Lett.* 82, 2048 (1999). 20

[77] P. F. Kolb, J. Sollfrank and U. Heinz, *Phys. Lett.* , B 459 (1999) 667; P. F. Kolb, J. Sollfrank, P. V. Ruuskanen and U. Heinz, *Nucl. Phys.* A 661, 349 (1999). 20

[78] D. Teaney, J. Lauret and E. V. Shuryak, *Phys. Rev. Lett.* 86, 4783 (2001); nucl-th/0110037. 20

[79] R. S. Bhalerao, J. P. Blaizot, N. Borghini and J. Y. Ollitrault, *Phys. Lett.* B 627, 49 (2005). 20

[80] B. Mohanty, J. Alam and T. K. Nayak, *Phys. Rev.* C 67, 024904 (2003). 20

[81] M. Gaździcki, M. I. Gorenstein and St. Mrówczyński, *Phys. Lett.* , B 585, 115 (2004). 20

[82] J. Casalderrey-Solana, E. V. Shuryak and D. Teaney, *Nucl. Phys.* A 774, 577 (2006); J. Adams *et al.* [STAR Collaboration], *Phys. Rev. Lett.* 95, 152301 (2005); S. S. Adler *et al.* [PHENIX Collaboration], *Phys. Rev. Lett.* 97, 052301 (2006). 20

[83] U. M. Heller and F. Karsch, *Nucl. Phys.* B 251, 254 (1985). 22, 41

[84] W. H. Press, S. A. Teukolsky, W. T. Vetterling and B. P. Flannery, *Numerical Recipes*, Cambridge University Press (1986). 27, 62

[85] N. Cabibbo and E. Marinari, *Phys. Lett.* B 119, 387 (1982). 28, 44

[86] A. D. Kennedy and B. J. Pendleton, *Phys. Lett.* B 156, 393 (1985). 28, 44

[87] S. Datta and S. Gupta, *Phys. Lett.* B 471, 382 (2000). 31

[88] S. Datta and R. V. Gavai, *Phys. Rev.* D 60, 034505 (1999). 32

[89] S. Ejiri, Y. Iwasaki and K. Kanaya, *Phys. Rev.* D 58, 094505 (1998). 38, 44

[90] See for example : S. Aoki *et al.* , *Nucl. Phys. Proc. Suppl.* 106, 477 (2002). 39

[91] J. Engels, F. Karsch and T. Scheideler, *Nucl. Phys.* B 564, 303 (2000). 44

[92] S. Datta and S. Gupta, *Phys. Rev.* D 67, 054503 (2003). 46

[93] S. S. Gubser, I. R. Klebanov and A. A. Tseytlin, *Nucl. Phys.* B 534, 202 (1998); I. R. Klebanov, hep-th/0009139. 52, 53

[94] F. Karsch, E. Laermann and A. Peikert, *Phys. Lett.* B 478, 447 (2000). 57, 85

[95] Y. Aoki, Z. Fodor, S. D. Katz and S. S. Szabo, *J. H. E. P.* 0601, 89 (2006). 57

[96] D. Teaney, *Phys. Rev.* C 68, 034913 (2003). 57

[97] A. Nakamura and S. Sakai, *Phys. Rev. Lett.* 94, 072305 (2005). 57

[98] V. Koch, A. Majumder and J. Randrup, *Phys. Rev. Lett.* 95, 182301 (2005). 58, 72, 101

[99] P. Levai and U. Heinz, *Phys. Rev.* C 57, 1879 (1998). 58, 75

[100] A. Peshier, *Nucl. Phys.* A 702, 128 (2002). 58, 75

[101] M. Bluhm, B. Kampfer and G. Soff, *Phys. Lett.* B 620, 131 (2005). 58, 72, 75

[102] A. Dumitru, J. Lenaghan and R. D. Pisarski, *Phys. Rev.* D 71, 074004 (2005). 58, 75

[103] C. Ratti, M. A. Thaler and W. Weise, *Phys. Rev.* D 73, 014019 (2006). 58, 75, 77, 79, 80, 82, 85, 86, 87, 95, 97

[104] E. Shuryak and I. Zahed, *Phys. Rev.* D 70, 054507 (2004); *Phys. Rev.* C 70, 021901 (2004). 58, 59, 60, 72, 73, 75

[105] M. Asakawa and T. Hatsuda, *Phys. Rev. Lett.* 92, 012001 (2004); S. Datta, F. Karsch, P. Petreczky and I. Wetzorke, *Phys. Rev.* D 69, 094507 (2004). 58

[106] R. V. Gavai and S. Gupta, *Phys. Rev.* D 73, 014004 (2006). 58, 59, 66, 68, 69, 71, 72, 73, 101, 102

[107] S. Ejiri, F. Karsch and K. Redlich, *Phys. Lett.* B 633, 275 (2006). 59

[108] R. V. Gavai and S. Gupta, *Phys. Rev.* D 67, 034501 (2003). 59, 61, 64, 66, 68, 72

[109] R. V. Gavai, *Nucl. Phys. Proc. Suppl.* 119, 529 (2003). 59

[110] F. Fucito, E. Marinari, G. Parisi and C. Rebbi, *Nucl. Phys.* B 180, 369 (1981). 60, 61

[111] E. Marinari, G. Parisi and C. Rebbi, *Nucl. Phys.* B 190, 734 (1981). 60, 61

[112] J. Liao and E. Shuryak, *Phys. Rev.* D 73, 014509 (2006). 60, 72, 73

[113] M. Asakawa, U. Heinz and B. Muller, *Phys. Rev. Lett.* 85, 2072 (2000); S. Jeon and V. Koch, *Phys. Rev. Lett.* 85, 2076 (2000). 66

[114] K. Adcox *et al.* [PHENIX Collaboration], *Phys. Rev. Lett.* 89, 082301 (2002); J. Adams *et al.* [STAR Collaboration], *Phys. Rev.* C 68, 044905 (2003). 66

[115] A. Wroblewski, *Acta. Phys. Polon.* B 16, 379 (1985). 66

[116] J. Rafelski and B. Muller, *Phys. Rev. Lett.* 48, 1066 (1982); Erratum *ibid* 56, 2334 (1986). 66

[117] R. V. Gavai and S. Gupta, *Phys. Rev.* D 65, 094515 (2002). 67

[118] S. Gupta and R. Ray, *Phys. Rev.* D 70, 114015 (2004). 68

[119] J. Cleymans, *J. Phys.* G 28, 1575 (2002). 68

[120] R. V. Gavai, S. Gupta and P. Majumdar, *Phys. Rev.* D 65, 054506 (2002). 72

[121] Abhijit Majumder, private communication. 72

[122] Jinfeng Liao, private communication. 73

[123] A. Majumder and B. Muller, nucl-th/0605079. 73

[124] P. N. Meisinger and M. C. Ogilvie, *Phys. Lett.* B 379, 163 (1996) 75, 77

[125] K. Fukushima, *Phys. Lett.* B 591, 277 (2004). 75, 77, 79, 87

[126] For a review see : B. Svetitsky, *Phys. Rept.* 132, 1 (1986). 76

[127] R. D. Pisarski, *Phys. Rev.* D 62, 111501 (2000). 76

[128] E. Megias, E. R. Arriola and L. L. Salcedo, *Phys. Rev.* D 69, 116003 (2004). 76

[129] D. Diakonov and M. Oswald, *Phys. Rev.* D 70, 105016 (2004). 76

[130] A. Dumitru and R. D. Pisarski, *Phys. Lett.* B 504, 282 (2001); *Phys. Rev.* D 66, 096003 (2002); *Nucl. Phys.* A 698, 444 (2002). 76

[131] O. Scavenius, A. Dumitru and J. T. Lenaghan, *Phys. Rev.* C 66, 034903 (2002). 76

[132] Y. Nambu and G. Jona-Lasinio, *Phys. Rev.* 122, 345 (1961); *Phys. Rev.* 124, 246 (1961). 76, 78

[133] For a review see : U. Vogl and W. Weise, *Prog. Part. Nucl. Phys.* 27, 195 (1991); S. P. Klevansky, *Rev. Mod. Phys.* 64, 649 (1992); T. Hatsuda and T. Kunihiro, *Phys. Rept.* 247, 221 (1994); M. Buballa, *Phys. Rept.* 407, 205 (2005). 76, 78, 79, 80

[134] F. Karsch and E. Laermann, *Phys. Rev.* D 50, 6954 (1994). 77, 85

[135] M. Cheng *et al.* , *Phys. Rev.* D 74, 054507 (2006). 77

[136] Y. Aoki, Z. Fodor, S. D. Katz and K. K. Szabo, hep-lat/0609068. 77

[137] S. K. Ghosh, T. K. Mukherjee, M. G. Mustafa and R. Ray, *Phys. Rev.* D 73, 114007 (2006). 77, 85, 86, 87, 95

[138] M. Frank, M. Buballa and M. Oertel, *Phys. Lett.* B 564, 212 (2003). 77, 78, 80, 82, 92, 96, 97

[139] G. 't Hooft, *Phys. Rev.* D 14, 3432 (1976); Erratum *ibid* D 18, 2199 (1978); *Phys. Rept.* 142, 357 (1986). 77, 79

[140] M. Asakawa and K. Yazaki, *Nucl. Phys.* A 504, 668 (1989). 78

[141] D. Toublan and J. B. Kogut, *Phys. Lett.* B 564, 212 (2003). 78

[142] B. Klein, D. Toublan and J. J. M. Verbaarschot, *Phys. Rev.* D 68, 014009 (2003). 78

[143] A. Barducci, G. Pettini, L. Ravagli and R. Casalbuoni, *Phys. Lett.* B 564, 217 (2003). 78

[144] D. Toublan and J. B. Kogut, *Phys. Lett.* B 605, 129 (2005). 78

[145] H. Reinhardt and R. Alkofer, *Phys. Lett.* B 207, 482 (1988). 78

[146] V. Bernard, R. L. Jaffe and U. G. Meissner, *Nucl. Phys.* B 308, 753 (1988). 78

[147] P. N. Meisinger, M. C. Ogilvie and T. R. Miller, *Phys. Lett.* B 585, 149 (2004). 82

[148] Y. Iwasaki *et al. Phys. Rev.* D 56, 151 (1997); B. Beinlich *et al.* , *Eur. Phys.* C 6, 133 (1999); M. Okamoto *et al.* , *Phys. Rev.* D 60, 094510 (1999); P. de Forcrand *et al.* , *Nucl. Phys.* B 577, 263 (2000); Y. Namekawa *et al.* , *Phys. Rev.* D 64, 074507 (2001). 85

[149] C. R. Allton *et al.* , *Phys. Rev.* D 66, 074507 (2002). 94, 97

[150] J. B. Kogut and D. K. Sinclair, *Phys. Rev.* D 70, 094501 (2004). 94, 97

[151] C. Ratti, M.A. Thaler and W. Weise, nucl-th/0604025. 95

[152] A. Dumitru, R. D. Pisarski and D. Zschiesche, *Phys. Rev.* D 72, 065008 (2005). 95

[153] Z. Zhang and Y. X. Liu, hep-ph/0610221. 96

[154] S. Roessner, C. Ratti and W. Weise, hep-ph/0609281. 96

[155] C. Sasaki, B. Friman and K. Redlich, hep-ph/0611147. 96